Solar Sails: Modeling, Estimation, and Trajectory Control

by

Leonel Rios-Reyes

A dissertation submitted in partial fulfillment
of the requirements for the degree of
Doctor of Philosophy
(Aerospace Engineering)
in The University of Michigan
2006

Doctoral Committee:

Professor Daniel J. Scheeres, Chair
Professor N. Harris McClamroch
Professor Pierre T. Kabamba
Professor Thomas H. Zurbuchen
Dr. Michael E. Lisano, Jet Propulsion Laboratory

To my parents

ACKNOWLEDGEMENTS

I want to give special recognition to the support of my family throughout all these years, especially my dad, Hector, and my mom, Alicia. Also, I want to thank my sister, Ethel, and brother, Leonardo, for their constant encouragement. Muchas gracias.

Also, I want thank my doctoral committee members for their comments on this dissertation. I am grateful with my advisor, Prof. Scheeres, for his guidance on my research, for his patience, and for given me encouragement.

I also want to express gratitude to all of my professors from elementary school to now, since each of them contributed in part to my education. Some of them are Prof. Joseph Katz, Prof. Allen Plotkin, and Prof. John Conly from San Diego Sate University; Prof. Edgar Rojano, Prof. Horacio Monroy, and Prof. Jose Angel Tovar from CBTIS 237 in Mexico.

I want to thank my close friends Nalin Chaturvedi, Matthew McNenly, Fu-Yuen Hsiao, Ryan Park, Stephen Broschart, Fabio Riviera, Amit Sanyal, Angie Krebs, Dennis Crespo, David Tello, Rosaicela Roman, Chad Berman, Leonel Flores, Rodrigo Zuñiga, Abel Sanchez Tellez, Armando Rodriguez, Luis Fernando Martinez, Luis Alberto Cueto, Juan Carlos Arredondo, and Moises Aranda for all the fun times. Special thanks to Margaret Fillion and Denise Phelps.

The work presented in this dissertation was funded in part by the Jet propulsion Laboratory, California Institute of Technology which is under contract with the

National Aeronautics and Space Administration.

TABLE OF CONTENTS

LIST OF FIGURES

Figure

LIST OF TABLES

Table

ABSTRACT

Solar Sails: Modeling, Estimation, and Trajectory Control

by

Leonel Rios-Reyes

Chair: Daniel J. Scheeres

There has been great interest in developing solar sail technology and missions by several international space agencies in recent years. However, at present there is no consensus on how one can mathematically model forces and moments acting on a solar sail. Traditional analytical models and finite element methods are not feasible for integration into a precise navigation system.

This dissertation takes a step toward resolving this issue by developing tools and concepts that can be integrated into a precise solar sail navigation system. These steps are the derivation of a generalized sail model, a linear estimation method for estimating and predicting forces and moments acting on a solar sail, and a new trajectory control methodology for tracking a nominal trajectory when the sail performance exceeds the nominal design performance.

The main contributions of this dissertation follow. First, the generalized sail model (GSM) is defined to analytically describe the forces and moments acting on a solar sail of arbitrary shape. The GSM is derived by performing an integration, of all the differential forces and moments acting on the sail, over the sail surface. Next,

the GSM is applied to several examples to illustrate the use of the GSM's analytic equations. These examples allow comparisons of forces and moments generated by different solar sails, the computation of force derivatives, and the application of the model to orbital mechanics problems. Since it is difficult to model the sail geometry based on ground measurements, errors in the sail model are expected once the sail is deployed in space. Due to this difficulty, a least-squares estimation method for the force and moment coefficients of the GSM is derived. For realistic implementation of a sail trajectory, the deployed sail must have an excess thrust capacity. We develop and implement a control methodology for flying a nominal mission profile with such an excess capacity. Control laws for maintaining a flat, ideal solar sail orbiting an equilibrium point of the circular restricted three-body problem and tracking neighboring halo orbits are provided. The control laws are tested under several conditions including solar sail surface degradation.

CHAPTER I

Introduction

This dissertation makes contributions to solar sail technology. Specifically, it addresses important issues necessary to successfully navigate a solar sail. These include solar sail force and moment modeling, force and moment parameter estimation, and trajectory control. Solar sails use solar radiation pressure to create a propulsive force in order to achieve a mission. The force created is highly correlated to the sail shape. In this thesis we provide a model to capture the exact sail geometry and model the force and moment generated using a set of coefficients. With this analytic result, the assumption of flat solar sails can be relaxed from mission design and detailed shape models can be easily represented. This analytic model blends directly to a methodology to estimate the forces and moments coefficients. Finally, controllers for maintaining a solar sail on a nominal trajectory are provided.

1.1 Brief History of Solar Sails

The concept of flying solar sails originated in the 20th century. Soon after Maxwell theoretically proved that radiation produces pressure, people started thinking about propelling objects using the radiation of the sun [37]. Early in the 1920's Konstantin Tsiolkovsky and Fridickh Tsander, both co-workers and Russian engineers, started

writing about using light to propel ships. The idea of using solar sails for space navigation originated with Tsander [37].

In the 1950's the work on solar sails started in the U.S. In the 1970's NASA started funding studies on solar sails. In 1976 Jerome L. Wright wrote a paper showing that it was possible to rendezvous with the comet Halley in 1986 using a solar sail if launched in 1982 [38]. NASA became interested in this mission called the Halley Rendezvous Mission. Several studies on solar sails arose from this proposal; however, the concept was dropped. Later, Wright wrote one of the first books on solar sails titled "Space Sailing," which was first published in 1992 [37].

The next milestone in the field of solar sails came from Collin R. McInnes in 1999. He wrote a book titled "Solar Sailing: Technology, Dynamics and Mission Applications" [21]. The solar sail community regards this book as the reference book on solar sailing. In this book, McInnes compiled the work available, including his own, for solar sails at the time.

Several of the world space agencies have also become interested in solar sails. 1n 1999 ESA demonstrated the depolyment of a 20m$\times$ 20m sail in a ground test [8]. In 2004 the Japanese Aerospace Exploration Agency, JAXA, successfully deployed two solar sails onboard a sounding rocket [33]. The sails were composed of four segments and were clover shaped. NASA performed several tests on sail deployment. In 2004 NASA along with L'Garde engineers demonstrated the deployment of a solar sail during ground tests [17]; the following year a sail deployment was demonstrated in vacuum conditions [18].

Despite all this effort, none of the space agencies have specific plans to fly a solar sail. The first attempt to fly a solar sail came from a private effort by the Planetary Society, led by Louis Friedman [9]. Cosmos I was built in Russia and launched from a

submarine rocket. The first attempt to demonstrate the deployment of Cosmos I was carried out in July, 2001; however, this attempt was unsuccessful due to a failure in the rockets. In June 2005, Cosmos I was launched again into space. The mission was to demonstrate the feasibility of solar sails by raising its orbit using solar radiation only. A failure in the first stage of the rocket that transported Cosmos I doomed the mission.

In 2002 NASA funded a project, led by Dr. Michael E. Lisano at JPL, in order to create a high fidelity tool that would allow the mission design and analysis for solar sails. This project was completed in 2006. The project is called the Solar Sail Spaceflight Simulation Software or S5. Several organizations were involved in the development of S5. These included JPL, The University of Colorado, The University of Michigan, Ball Aerospace and L'Garde Inc. S5 is composed of several modules that can be used to study all the aspects of a solar sail mission [7].

Currently there are several researchers that focus on aspects that would allow a solar sail mission to be successful. L'Garde Inc. [17, 18, 6] and AEC Able [25] are solar sail manufactures in the U. S. Prof. Bong Wie, at Arizona Sate University, has performed extensive studies on solar sail attitude control [34, 35]. Dr. Dachwald, at the German Aerospace Agency (DLR), has performed research on trajectory optimization [3, 2]. Prof. Dale Lawrence, at the University of Colorado, has worked on solar sail trajectory control [15].

All the previous studies on solar sails were performed using a flat sail model. In order to study sails with billow, or curvature in its surface, finite element models are required. However, these model introduce difficulties as they provide forces and moments computed at specific sail attitudes; hence, it is necessary to interpolate between these attitudes.

Among the contributions made in this thesis, a new methodology is presented to model analytically solar sails of arbitrary shape. The Generalized Sail Model allows us to model solar sails using billow with a series of tensors coefficients. This model is employed in the Solar Radiation Pressure Module of S5.

1.2 Thesis Structure

In Chapter II, the dynamics and equations of motion used throughout this dissertation are briefly discussed. First, in section 2.1 the Two-Body problem is reviewed and some comments are provided. Section 2.2 describes the Circular Restricted Three-Body Problem and the equations of motion are stated. Also, the models for solar radiation pressure are given in Section 2.3. The model for the sun as a point source and as a finite disc are explained. Finally, the traditional flat sail models are derived in Section 4.1.1. The assumptions on the ideal flat sail model are explained in Section 2.4.1. Section 2.4.2 explains how deviations from ideal reflection are captured with the non-ideal flat sail model.

The main contributions of this dissertation build upon the concepts presented in Chapter II to create an analytic generalized sail model, GSM, for modeling solar sails of arbitrary shape, a least-squares estimation algorithm based on force and moment measurements for refinement of the sail model, and a control methodology for tracking a nominal trajectory for sails with performance in excess of the mission requirements. The details of these contributions are presented in Chapters III-VI.

In Chapter III the non-ideal flat sail model is used in order to derive a more precise solar sail model: the generalized sail model. First, it is shown that the differential equations for the force and moment acting on a solar sail can be written in a form where the integration of these equations is not independent of sail attitude. Section

3.2 provides a derivation of the force equation for solar sails of arbitrary shapes. Section 3.3 gives an analytic equation for the moment acting on a solar sail due to its billow. Knowing the force and the moment, it is possible to calculate the sail's center of pressure as shown in section 3.4. In Section 3.5 properties of the generalized sail model tensors are provided. Section 3.5.1 deals specifically with the force tensor coefficients as well as the simplifications that arise when the sail has symmetries. Properties of the moment tensor coefficients as well as simplifications due to sail symmetry are discussed in Section 3.5.2. One conference [29] paper and one journal [27] paper were published from this chapter.

Chapter IV provides applications of the generalized sail model to a number of different examples. In Section 4.1 several sail geometries are studied by computing their force and moment tensors. Section 4.1.1 describes the traditional sail model and recovers the classical flat sail model equation. In Section 4.1.2 a circular sail with billow is studied. The force and moment coefficients are computed analytically. Section 4.1.3 describes the geometry of a square billowed sail. This design is a good approximation to a L'Garde sail and has been constructed and used in mission design examples [17]. In Section 4.1.4 the principles for modeling sails using finite element methods are discussed. This concept is applied to a sinusoid sail with no symmetries by computing its force and moment tensor coefficients. Given the force and moment coefficients for all these sail geometries, their resulting force and moment are compared for several sail attitudes in Section 4.2. In Section 4.3 the GSM force partial derivatives with respect to the sail attitude, optical parameters and control angles are derived. First, the partial derivatives needed throughout the rest of the sections are presented. Section 4.3.1 presents the force partial derivatives with respect to the sail attitude and each of the optical parameters. In Section 4.4 the force second

order partial derivatives are presented with respect to the optical parameters and sail attitude. The first and second order partial derivatives with respect to the sail control angles are given in Sections 4.5 and 4.6, respectively. Finally in Section 4.7 the generalized sail model, applied to the four-quadrant billowed sail, as well as the force partial derivatives are employed to revisit classical orbital mechanics problems where the flat solar sail had been used before. Specifically, Section 4.7.1 discusses a guidance law to optimally increase the sail orbit semi-major axis in order to escape from the solar system. The result is compared with the classical solution for a flat solar sail. In section 4.7.2, the attitude that provides the maximum force for a single quadrant of the four-quadrant billow sail is derived. Two conference [26, 31] papers were presented from this chapter.

Chapter V provides a methodology for refining the sail force and moment models from test data or measured navigation data. The GSM force and moment equations are linear with respect to the GSM tensor coefficients; thus a least-squares estimation method is developed. In Section 5.1 the normalized equations for the force and moments are discussed. In Section 5.2 the force and moment equations are manipulated and presented in linear form, as a product of a matrix, which contains the sail attitude information, and a vector, which contain the force or moment tensor coefficients to facilitate the estimation. The least-squares algorithm for estimating the force and moment tensor coefficients is derived in Section 5.3. Section 5.3.1 provides the covariance for the estimated force and moment based on uncertainties from the measurements used to perform the estimation. In Section 5.4 the normalized force and moment data are generated using the sinusoid sail shape in order to simulate navigation data to test the estimation algorithm. The force estimation results are presented in Section 5.4.1. Four different attitude sampling cases are used for the

force estimation and their results are compared. Section 5.4.2 provides the estimation results for the moment using two different sampling strategies. Section 5.5 is focused on the simplification that occurs for sails that present different types of symmetries. Section 5.5.1 presents the simplified equations for the force estimation, while in Section 5.5.2 the simplified moment equation is stated. One conference paper has been presented from this chapter [30] and a journal paper is under review.

Chapter VI provides control laws for station-keeping an ideal flat sail about a sub-L_1 point and tracking a neighboring halo orbit. In Section 6.1 the equations of motion for the circular restricted three-body are transformed into polar coordinates to facilitate the design of control laws. In Section 6.2 the sail acceleration is provided in the new polar frame. Section 6.3 provides a brief description on the effects of the solar radiation pressure in the equations of motion and how new equilibria and families of halo orbits arise. This sub-L_1 points and corresponding halo orbits are used as references to stabilized a sail. Section 6.3.1 describes how the sub-L_1 points are dependent on the sail characteristics, how to find them, and their inherent instability is explained. Section 6.3.2 provides an explanation on how to find the families of halo orbits about these new equilibrium points. In Section 6.4 the problem of having a solar sail with a performance greater than the mission requirements is discussed. In Section 6.5 control laws are presented to stabilize a solar sail about a given sub-L_1 point. Two independent controllers are necessary to stabilize the sail distance from the sun and the orbit radius about the sub-L_1 point. Section 6.5.1 provides several controller for maintaining the sailcraft distance from the sun at the required sub-L_1 location. Two proportional-derivative controllers and one linear-feedback controller are developed and their performances are discussed. In Section 6.5.2 a controller for stabilizing a sail about a sub-L_1 point is presented. The controller is a feed-

back controller based on the sail kinetic energy. In Section 6.6 the controllers are generalized to track a halo orbit in the vicinity of a sub-L_1 point. The proportional-derivative controller is modified to track the velocity of a moving point in the halo orbit. Then, the energy based controller is extended to account for the energy of the moving point. Sections 6.7 and 6.8 present preliminary work on the control of a solar sail that suffers from surface degradation due to the space environment. A simple adaptive control technique is presented and tested under several conditions. Finally, Section 6.9 discusses a way of implementing these controllers with an attitude control system. The sail rotational dynamics are discussed as well as the torques required to achieve the required rotational rate for a sail using these control strategies. One conference paper [28] has been presented from this chapter and a journal paper is under preparation.

Chapter VII provides a summary of the main contributions of this dissertation and indicates the topics for future research.

CHAPTER II

Dynamical Model and Flat Sail Models

In this chapter the models for the dynamics and flat solar sail models are presented. The much studied restricted two body problem and three body problem are briefly presented. Then, the flat model for solar sails is introduced for both ideal and non-ideal sails. The ideal flat model assumes perfect reflection with no losses. The non-ideal flat model includes parameters to account for optical and thermal sail properties.

2.1 Restricted Two-Body Problem

The two-body problem is the only general problem in astrodynamics with a closed form solution. The orbiting bodies are treated as two point masses under mutual gravitational attraction. The more massive body is called the primary and the less massive one is the secondary and their masses are denoted by m_1 and m_2, respectively. The equations of motion are

$$\ddot{\mathbf{r}} = -\frac{G(m_1 + m_2)}{|\mathbf{r}|^3}\mathbf{r}, \tag{2.1}$$

where G is the universal constant of gravitation and $\mathbf{r}$ is the position of the secondary body with respect to the primary. The restricted two-body problem is a simplification

of the two-body problem, which arises when the mass ratio between the secondary and the primary bodies tends to zero as in the case of a planet and orbiting satellite. Thus, the gravitational μ parameter can be defined as $\mu = m_1 G$ and the equations of motion become

$$\ddot{\mathbf{r}} = -\frac{\mu}{|\mathbf{r}|^3}\mathbf{r}. \tag{2.2}$$

The solution of this problem is obtained by finding integrals of motions, which are derived in Reference [11].

For a spacecraft with its own propulsion unit the equations of motion are

$$\ddot{\mathbf{r}} = -\frac{\mu}{|\mathbf{r}|^3}\mathbf{r} + \mathbf{a}, \tag{2.3}$$

where $\mathbf{a}$ is the acceleration.

2.2 Circular Restricted Three-Body Problem

The equations of motion for a spacecraft under the influence two massive bodies in a mutually circular orbit can be written in a rotating frame as:

$$\ddot{\mathbf{r}} + 2\boldsymbol{\Omega} \times \dot{\mathbf{r}} + \boldsymbol{\Omega} \times (\boldsymbol{\Omega} \times \mathbf{r}) = \mathbf{a} + \nabla U(\mathbf{r}), \tag{2.4}$$

where $\mathbf{r}$ is the spacecraft position vector, $\boldsymbol{\Omega}$ is the angular velocity of the rotating frame, $\mathbf{a}$ is an acceleration from a propulsion unit acting on the spacecraft, and $U(\mathbf{r})$ is the three-body problem gravitational potential given by:

$$U(\mathbf{r}) = \frac{1-\mu}{|\mathbf{r}_1|} + \frac{\mu}{|\mathbf{r}_2|}. \tag{2.5}$$

Here $U(\mathbf{r})$ has been normalized by the the ratio of the masses of the attracting bodies, $\mu = m_2/(m_1 + m_2)$, where $m_1 \geq m_2$. $\mathbf{r}_1$ and $\mathbf{r}_2$ are the position vectors from the primary bodies to the spacecraft given by:

$$\mathbf{r}_1 = (x+\mu)\mathbf{e}_x + y\mathbf{e}_y + z\mathbf{e}_z, \tag{2.6}$$

$$\mathbf{r}_2 = (x-1+\mu)\mathbf{e}_x + y\mathbf{e}_y + z\mathbf{e}_z, \tag{2.7}$$

where the unit vectors $\mathbf{e}_x$, $\mathbf{e}_y$, $\mathbf{e}_z$ denote the x, y, and z directions along the rotating coordinate frame.

The system's angular velocity is perpendicular to the plane in which the primaries orbit and is defined to be the z-direction, i.e., $\mathbf{\Omega} = \Omega\mathbf{e}_z$ as shown in Figure 2.1. Writing the equations of motion in scalar form and normalizing $\Omega = 1$, we obtain

$$\ddot{x} = 2\dot{y} + x - \frac{(1-\mu)(x+\mu)}{|\mathbf{r}_1|^3} - \frac{\mu}{|\mathbf{r}_2|^3}(x+\mu-1) + a_x, \tag{2.8}$$

$$\ddot{y} = -2\dot{x} + y - \frac{(1-\mu)y}{|\mathbf{r}_1|^3} - \frac{\mu y}{|\mathbf{r}_2|^3} + a_y, \tag{2.9}$$

$$\ddot{z} = -\frac{(1-\mu)z}{|\mathbf{r}_1|^3} - \frac{\mu z}{|\mathbf{r}_2|^3} + a_z. \tag{2.10}$$

2.3 Solar Radiation Pressure Model

In Reference [21] the solar pressure due to the sun's finite disk on an ideal sail normal to the sun is derived, which includes the force exerted on the sail due to impinging and reflected photons. The radiation pressure at a distance r from the sun due to a finite solar disk is [21]:

$$P(r) = \frac{1}{c}\int_0^{\infty}\int_0^{2\pi}\int_0^{C_0} I_\nu \cos^2(C)\sin(C) dC d\delta d\nu, \tag{2.11}$$

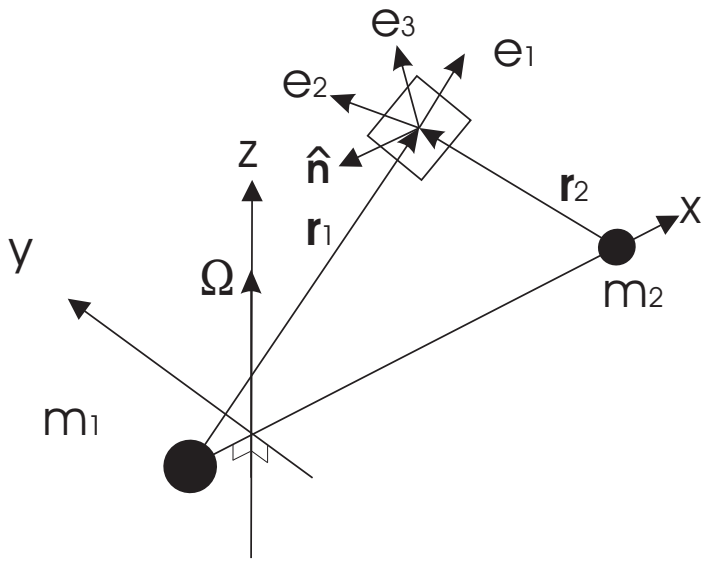

Figure 2.1: Geometry of the Restricted Three Body Problem.

where c is the speed of light, C the sun's apparent angular radius, C_0 the maximum apparent angular radius given by $\arcsin(R_s/r)$, R_s is the sun's radius, r is the distance from the sun, δ the clock angle, ν the radiation wavelength, and I_ν the radiation specific intensity at a wavelength ν. Since I_ν does not depend on r, it can be averaged over the entire spectrum to yield [21]:

$$P(r) = \frac{2\pi I_0}{c} \int_0^{C_0} \cos^2(C) \sin(C) dC, \tag{2.12}$$

where I_0 is the frequency integrated specific intensity. Performing the integration and substituting for C_0, the radiation pressure becomes [21]:

$$P(r) = \frac{2\pi I_0}{3c} \left\{ 1 - \left[1 - \left(\frac{R_s}{r} \right)^2 \right]^{3/2} \right\}. \tag{2.13}$$

Eq. (2.13) can be rearranged as [21]:

$$P(r) = P^*(r) F(r), \tag{2.14}$$

where $P^*(r)$ is the radiation pressure of a point source given by [21]:

$$P^*(r) = \frac{I_0 \pi}{c} \left(\frac{R_s}{r} \right)^2, \tag{2.15}$$

where $I_0 = 2.04 \times 10^7 W/m$ [21] is the sun's specific intensity, $R_s = 6.96 \times 10^8 m$ [11], and

$$F(r) = \frac{2}{3} \left(\frac{r}{R_s} \right)^2 \left\{ 1 - \left[1 - \left(\frac{R_s}{r} \right)^2 \right]^{3/2} \right\}. \tag{2.16}$$

$F(r)$ is a correction function to account for the sun's finite disk. With this formalism we assume the solar radiation travels in parallel rays when it reaches the sail.

The difference between these two models increases with proximity to the sun. As the distance from the sun increases the difference between the models decreases and by 10 solar radii the difference is within one percent [21]. Specifically, expanding Eq. 2.19 in powers of (R_s/r) yields

$$\begin{aligned} F(r) &= \frac{2}{3} \left(\frac{r}{R_s} \right)^2 \left[1 - 1 + \frac{3}{2} \left(\frac{R_s}{r} \right)^2 - O\left(\frac{R_s}{r} \right)^4 \right] \\ &= 1 - O\left(\frac{R_s}{r} \right)^2. \end{aligned} \tag{2.17}$$

2.4 Flat Solar Sail Models

The propulsion on solar sails is generated through the momentum carried by the solar radiation pressure. When photons strike the sail membrane there is a momentum transfer into the sail as well as when they are reflected. This momentum transfer is small; by Newton's second the acceleration and mass are related as $a = F/m$, therefore, in order to generate a useful acceleration, the sailcraft must have a high surface area to intercept as much as the radiation flux as possible and be lightweight at the

same time. The force generated is also dependent on the characteristics of the sail such as its reflective properties and surface shape. Two widely used sail models for initial sail studies are the ideal flat model and the non-ideal flat model for solar sails, which are discussed next.

2.4.1 Ideal Flat Sail Model

The ideal sail model assumes that the solar radiation pressure is perfectly reflected from the sail surface. Therefore the force generated when the photons strike the sail has the same magnitude as when they are reflected off the sail. From Figure 2.2 it can be seen that the force generated from impinging photons is

$$\mathbf{F}_i = P(r)A_e(-\cos\alpha\hat{\mathbf{n}} + \sin\alpha\hat{\mathbf{t}}), \tag{2.18}$$

where A_e is the effective sail area, α is the angle between the incoming solar radiation and the sail normal $\hat{\mathbf{n}}$ pointing from the sail surface into the sun's hemisphere, and $\hat{\mathbf{t}}$ is the transverse vector perpendicular to $\hat{\mathbf{n}}$ and in the plane of the incoming radiation and $\hat{\mathbf{n}}$. The force due to the reflected radiation is

$$\mathbf{F}_r = PA_e(-\cos\alpha\hat{\mathbf{n}} - \sin\alpha\hat{\mathbf{t}}). \tag{2.19}$$

The effective sail area is the projected sail area orthogonal to the solar radiation, $A_e = A\cos\alpha$. Thus adding Eqs. (2.18) and (2.19), the total force acting on an ideal flat sail is

$$\mathbf{F} = -2P(r)A\cos^2\alpha\hat{\mathbf{n}}. \tag{2.20}$$

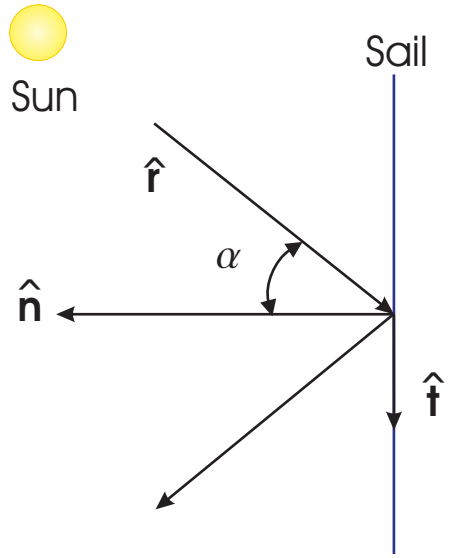

Figure 2.2: Ideal Sail Model.

The angle α can be found from the sail unit position vector $\hat{\mathbf{r}}$ and $\hat{\mathbf{n}}$ through the relation $\cos\alpha = -\hat{\mathbf{r}} \cdot \hat{\mathbf{n}}$. Thus, the force acting on ideal sail can be written as

$$\mathbf{F} = -2P(r)A(\hat{\mathbf{r}} \cdot \hat{\mathbf{n}})^2\hat{\mathbf{n}}. \tag{2.21}$$

The acceleration of the sail is obtained by dividing the force by the sail mass. Introducing the sail lightness number β [21], the sail acceleration can be defined relative to the solar mass. The sail lightness number β is defined as the ratio of the magnitude of the sail acceleration due to the solar radiation pressure and the acceleration caused by the sun's gravitational attraction [21] when the sail is oriented face-on to the sun. Thus, the acceleration due to the propulsion of an ideal sail is given by:

$$\mathbf{a} = -\frac{\beta M_s G}{|\mathbf{r}_1|^4}(\mathbf{r}_1 \cdot \hat{\mathbf{n}})^2\hat{\mathbf{n}}, \tag{2.22}$$

where M_sG is the solar gravitational parameter. $\hat{\mathbf{n}}$ can be described in terms of the control angles α and δ; sun-sail angle and clock angle, respectively. Another

interpretation of the sail lightness can be given in terms of the sail loading σ defined as the ratio of the mass per sail area:

$$\sigma = \frac{m}{A}. \tag{2.23}$$

In Reference [21] it was shown that a critical sail loading σ^* that produces an acceleration on the sail equal to the acceleration due to the sun's gravitational attraction can be found from:

$$\sigma^* = \frac{L_s}{2\pi G M_s c} = 1.53 \frac{g}{m^2}. \tag{2.24}$$

The sail lightness can be defined using the actual sail loading and the critical sail loading as

$$\beta = \frac{\sigma}{\sigma^*}. \tag{2.25}$$

The sail force can also be described using the control angles sun-sail, α, and clock angle, δ. For a given sail area and distance from the sun, α controls the force magnitude and δ controls the force direction. These angles are measured with respect to a local vertical/local horizontal (LVLH) frame as shown in Figures 2.1 and 2.3. The acceleration for an ideal sail is in the opposite direction of $\hat{\mathbf{n}}$, i.e., $\mathbf{a} = -a\hat{\mathbf{n}}$. Thus, the acceleration scalar components in terms of the control angles are:

$$\begin{bmatrix} a_{e_1} \\ a_{e_2} \\ a_{e_3} \end{bmatrix} = \frac{\beta M_s G}{|\mathbf{r}_1|^2} \cos^2 \alpha \begin{bmatrix} \cos \alpha \\ -\sin \alpha \cos \delta \\ -\sin \alpha \sin \delta \end{bmatrix}. \tag{2.26}$$

Note that the acceleration is maximum when $\hat{\mathbf{n}}$ and $\mathbf{r}_1$ are opposite in direction.

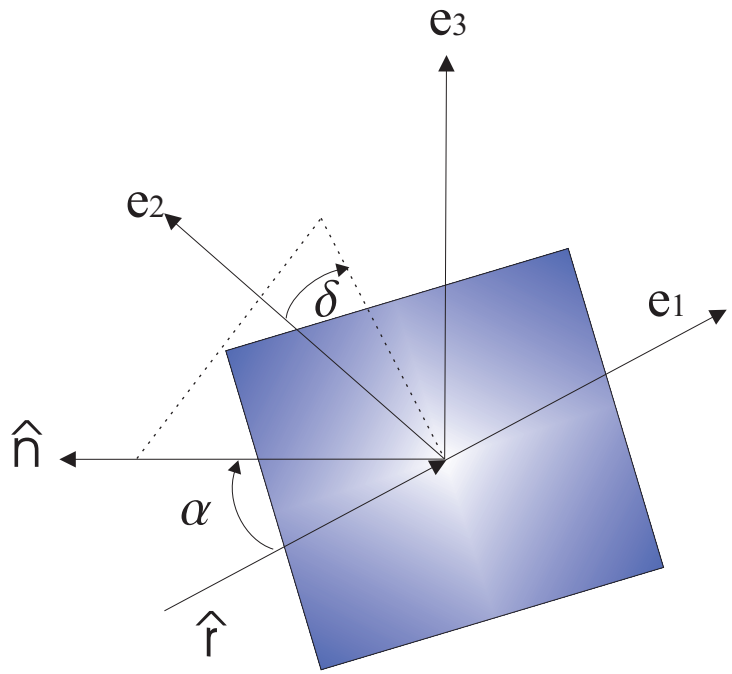

Figure 2.3: Sail Control Angles. α is the angle between $\hat{\mathbf{n}}$ and $-\hat{\mathbf{r}}$, δ is the angle between the projection of $\hat{\mathbf{n}}$ into the (e_2, e_3)-plane and the e_2-axis.

2.4.2 Non-Ideal Flat Sail Model

The total force acting on the solar sail is due to a combination of forces that result from photons impinging on and reflecting from the sail surface, as shown in Figure 2.4. Here, the sail is assumed to be opaque so that the transmissivity is zero. Then, the sum of the reflectivity ρ and the absorptivity a must be unity. Also, it must be noted that ρ and a might be dependent on the angle between the incident light source direction and the surface normal α and the wavelength ν. The force due to reflection $\mathbf{F}_r$ is composed of two components: $\mathbf{F}_{rs}$, a fraction s due to specular reflection acting along the normal and transverse directions, and $\mathbf{F}_{rd}$, a fraction $B_f(1-s)$ due to diffuse or uniform reflection acting along the normal direction. B is a coefficient describing the deviation of the surface from a Lambertian surface while the subscript f denotes the front surface. A Lambertian surface has the same radiance in all directions [23].

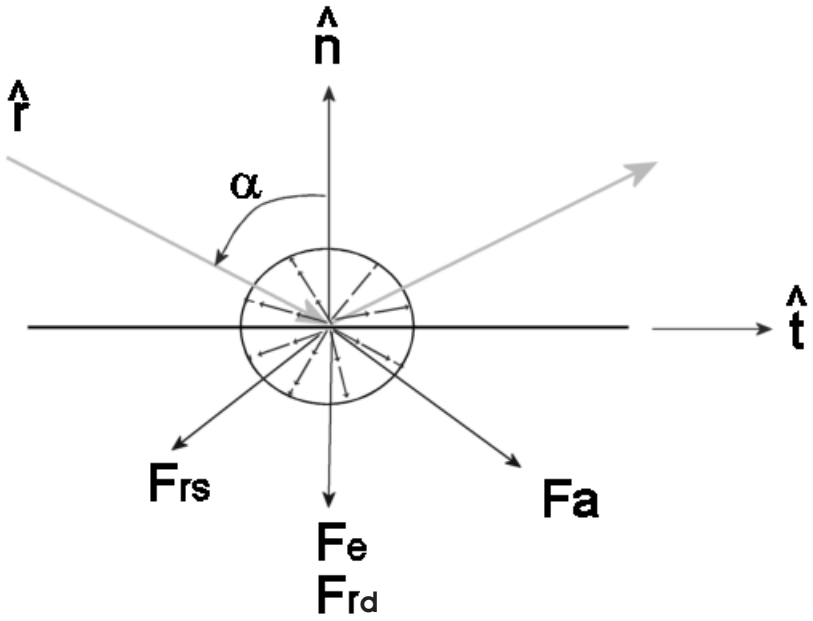

Figure 2.4: Non-ideal force directions. F_{rs} force reflected specularly, F_e force due emission, F_{rd} force reflected diffusively, and F_a force due to absorption.

The force caused by emission $\mathbf{F}_e$ is due to absorbed photons that are now being radiated as heat and acts along the normal direction. When the sail absorbs photons its temperature increases up to an equilibrium temperature at which the absorbed energy is equal to the radiated energy. Performing an energy balance, it can be shown that the equilibrium temperature of the sail is given by [21]:

$$T^4 = \frac{(1-\rho)cP\cos(\alpha)}{\tilde{\sigma}(\epsilon_f + \epsilon_b)} \tag{2.27}$$

where ϵ is the surface emissivity, the subscripts f and b denote the front and back surfaces, respectively, and $\tilde{\sigma}$ is the Stefan-Boltzmann constant.

Defining the unit normal vector $\hat{\mathbf{n}}$ perpendicular to a surface of an area dA and pointing toward the sun's hemisphere and the transverse vector $\hat{\mathbf{t}}$, perpendicular to

$\hat{\mathbf{n}}$ and in the plane of the incident light and the surface normal, the forces acting on the sail area along these directions are given by Eqs. (2.28)-(2.31). They represent the contribution from radiation impacting the sail $\mathbf{F}_a$, reflected specularly $\mathbf{F}_{rs}$ and diffusively $\mathbf{F}_{rd}$ from it, and emitted by radiation from the sail $\mathbf{F}_e$, respectively [21] .

$$\mathbf{F}_a = P(r)\cos\alpha\left[-\cos\alpha\hat{\mathbf{n}} + \sin\alpha\hat{\mathbf{t}}\right]A \tag{2.28}$$

$$\mathbf{F}_{rs} = P(r)\cos\alpha\rho s\left[-\cos\alpha\hat{\mathbf{n}} - \sin\alpha\hat{\mathbf{t}}\right]A \tag{2.29}$$

$$\mathbf{F}_{rd} = -P(r)\cos\alpha B_f\rho(1-s)\hat{\mathbf{n}}A \tag{2.30}$$

$$\mathbf{F}_e = -P(r)\cos\alpha(1-\rho)\frac{\epsilon_f B_f - \epsilon_b B_b}{\epsilon_f + \epsilon_b}\hat{\mathbf{n}}A \tag{2.31}$$

Decomposing the forces into their normal and transverse components, we obtain [21]:

$$F_n = -P(r)\Big[(1+\rho s)\cos^2(\alpha) + B_f(1-s)\rho\cos(\alpha) + (1-\rho)\frac{\epsilon_f B_f - \epsilon_b B_b}{\epsilon_f + \epsilon_b}\cos(\alpha)\Big]A \tag{2.32}$$

$$F_t = P(r)(1-\rho s)\cos(\alpha)\sin(\alpha)A \tag{2.33}$$

where the subscripts n and t denote the force magnitude along the normal and transverse vectors. Grouping the optical sail elements, the force normal to the sail can be expressed as:

$$\mathbf{F}_n = -P(r)[a_1\cos^2\alpha + a_2\cos\alpha]A\hat{\mathbf{n}} \tag{2.34}$$

where $a_1 = 1+\rho s$, $a_2 = B_f(1-s)\rho + (1-\rho)\frac{\epsilon_f B_f - \epsilon_b B_b}{\epsilon_f + \epsilon_b}$. The differential transverse force is given by:

$$\mathbf{F}_t = P(r)a_3\cos\alpha\sin\alpha A\hat{\mathbf{t}} \tag{2.35}$$

where $a_3 = 1 - \rho s$. The sun position unit vector is specified as $\hat{\mathbf{r}}$ and points from the sun to the sail. Thus, the angle α is defined by $\cos\alpha = -\hat{\mathbf{r}} \cdot \hat{\mathbf{n}}$.

For a given flat sail, the total acceleration is then

$$\mathbf{a} = \frac{\mathbf{F}_n + \mathbf{F}_t}{m} \tag{2.36}$$

For an ideal sail ρ and s are unity, hence $a_3 = 0$ and $\mathbf{F}_t = 0$. Thus it reduces to Eq. (2.21).

CHAPTER III

Generalized Sail Model

In this chapter we develop a generalized sail model to describe the force and moment generated by a non-ideal, non-flat sail. It is assumed that the sail shape is fixed and does not change with attitude and can be described as a surface with a normal vector specified at any point $\hat{\mathbf{n}}(x, y)$, where x and y are nominally a coordinate plane parallel to the sail plane. The normal vector can be obtained for either a discrete or an analytical model of the sail surface.

3.1 Sail Surface and Normal Vector

Assume that an analytical sail surface model exists and is given by $z = -S(x, y)$, a function of the position in the sail body-fixed frame. The surface equation can be written as

$$\phi = z + S(x, y). \tag{3.1}$$

Then, the unit normal vector is related to the surface by

$$\hat{\mathbf{n}} = \frac{\nabla\phi}{\|\nabla\phi\|} = \frac{1}{\sqrt{1 + S_x^2 + S_y^2}} \begin{bmatrix} S_x \\ S_y \\ 1 \end{bmatrix}, \tag{3.2}$$

where

$$S_x(x,y) = \frac{\partial}{\partial x}S(x,y), \quad S_y(x,y) \quad = \frac{\partial}{\partial y}S(x,y). \tag{3.3}$$

A sail differential area, dA, can be written in terms of the sail body-fixed coordinates [14]:

$$dA = \left(1 + S_x^2 + S_y^2\right)^{1/2} dxdy. \tag{3.4}$$

We assume that there is a one-to-one correspondence between the coordinates (x, y) and the sail surface. We also make this nominal assumption that the xy-coordinate plane is parallel on average to the sail surface. In all our computations we will take a sail-centric view and map all significant geometries into the frame fixed to the sail.

3.2 Derivation of the Generalized Sail Force Equation

Taking a surface area differential element dA, the differential force can be modeled using the non-ideal force model:

$$d\mathbf{F}_n \quad = \quad -P(r)[a_1 \cos^2\alpha + a_2 \cos\alpha]dA\hat{\mathbf{n}}, \tag{3.5}$$

$$d\mathbf{F}_t \quad = \quad P(r)a_3 \cos\alpha \sin\alpha dA\hat{\mathbf{t}}. \tag{3.6}$$

The total force due to these normal and transverse components are found by integrating these expressions over the sail surface:

$$\mathbf{F} \quad = \quad \int_A (d\mathbf{F}_n + d\mathbf{F}_t). \tag{3.7}$$

We note that Eqs. (3.5) and (3.6) require knowledge of $\cos\alpha$, $\sin\alpha$ and $\hat{\mathbf{t}}$, which can be obtained from:

$$\cos\alpha = -\hat{\mathbf{n}}\cdot\hat{\mathbf{r}}, \tag{3.8}$$

$$\sin\alpha = \sqrt{1-(\hat{\mathbf{n}}\cdot-\hat{\mathbf{r}})^2} = \|\hat{\mathbf{n}}\times(\hat{\mathbf{n}}\times-\hat{\mathbf{r}})\|, \tag{3.9}$$

$$\hat{\mathbf{t}} = \frac{(\hat{\mathbf{n}}\times\hat{\mathbf{r}})\times\hat{\mathbf{n}}}{\|(\hat{\mathbf{n}}\times\hat{\mathbf{r}})\times\hat{\mathbf{n}}\|} = -\frac{\hat{\mathbf{n}}\times(\hat{\mathbf{n}}\times\hat{\mathbf{r}})}{\|\hat{\mathbf{n}}\times(\hat{\mathbf{n}}\times\hat{\mathbf{r}})\|}. \tag{3.10}$$

Here we define $\hat{\mathbf{r}}$ to be the unit vector pointing away from the sun, representing the direction of the incident sun radiation in the sail body-fixed frame.

The force equations stated in this form lead to difficulties when trying to carry out the surface integrations analytically. If the sail surface, and therefore its normal vector, is not simple, analytic solutions cannot be found in general. Also, the integrals are strongly dependent on the sun's position, apparently making it very difficult to generalize to any sail attitude.

We have found that the integration of Eq. (3.7) can be reduced to an integration over the sail, independent of the incident light direction and magnitude (under an assumption where the structure is fixed).

Let $\hat{\mathbf{n}} = [\hat{n}_1 \;\; \hat{n}_2 \;\; \hat{n}_3]^T$ and define the cross product as

$$\hat{\mathbf{n}}\times\hat{\mathbf{r}} = \tilde{\mathbf{n}}\cdot\hat{\mathbf{r}}, \tag{3.11}$$

where

$$\tilde{\mathbf{n}} = \begin{bmatrix} 0 & -\hat{n}_3 & \hat{n}_2 \\ \hat{n}_3 & 0 & -\hat{n}_1 \\ -\hat{n}_2 & \hat{n}_1 & 0 \end{bmatrix}. \tag{3.12}$$

Then, Eqs. (3.9) and (3.10) can be multiplied to obtain:

$$\sin\alpha\hat{\mathbf{t}} = -\hat{\mathbf{n}}\times(\hat{\mathbf{n}}\times\hat{\mathbf{r}}) = -\tilde{\mathbf{n}}\cdot\tilde{\mathbf{n}}\cdot\hat{\mathbf{r}}. \tag{3.13}$$

Applying Eqs. (3.8) and (3.9), Eqs. (3.5) and (3.6) become:

$$d\mathbf{F}_n = -P(r)[a_1(\hat{\mathbf{r}}\cdot\hat{\mathbf{n}})\hat{\mathbf{n}}(\hat{\mathbf{n}}\cdot\hat{\mathbf{r}}) - a_2(\hat{\mathbf{r}}\cdot\hat{\mathbf{n}})\hat{\mathbf{n}}]dA, \tag{3.14}$$

$$d\mathbf{F}_t = -P(r)a_3(\hat{\mathbf{r}}\cdot\hat{\mathbf{n}})\tilde{\mathbf{n}}\cdot\tilde{\mathbf{n}}\cdot\hat{\mathbf{r}}dA. \tag{3.15}$$

Some of the terms in the above expressions can be simplified by the introduction of a dyadic and triadic notation [10]. It is possible to define the dyadic of the normal vector as:

$$\overline{\overline{\mathbf{n}}} = \hat{\mathbf{n}}\hat{\mathbf{n}}, \tag{3.16}$$

and the triadic as:

$$\overline{\overline{\overline{\mathbf{n}}}} = \hat{\mathbf{n}}\hat{\mathbf{n}}\hat{\mathbf{n}}. \tag{3.17}$$

These are really just rank 2 and rank 3 tensors, and can be properly specified as $\overline{\overline{n}}_{ij} = \hat{n}_i\hat{n}_j$, and $\overline{\overline{\overline{n}}}_{ijk} = \hat{n}_i\hat{n}_j\hat{n}_k$, where the indices range from 1 to 3. Note that these are symmetric tensors. Making use of the identity:

$$\tilde{\mathbf{n}}\cdot\tilde{\mathbf{n}} = -\hat{\mathbf{n}}\cdot\hat{\mathbf{n}}\overline{\overline{\mathbf{U}}} + \hat{\mathbf{n}}\hat{\mathbf{n}} = -\overline{\overline{\mathbf{U}}} + \overline{\overline{\mathbf{n}}},$$

where $\overline{\overline{\mathbf{U}}}$ is the unit dyadic

$$\overline{\overline{\mathbf{U}}}_{ij} = \delta_{ij}, \tag{3.18}$$

and δ_{ij} is the Kronecker delta function defined as:

$$\delta_{ij} = \begin{cases} 1 & i = j \\ 0 & i \neq j \end{cases}, \tag{3.19}$$

the differential forces can be stated as

$$d\mathbf{F}_n = -P(r)a_1\hat{\mathbf{r}}\cdot\overline{\overline{\mathbf{n}}}dA\cdot\hat{\mathbf{r}} + P(r)a_2\hat{\mathbf{r}}\cdot\overline{\overline{\mathbf{n}}}dA, \tag{3.20}$$

and

$$d\mathbf{F}_t = P(r)a_3\hat{\mathbf{r}}\cdot\hat{\mathbf{n}}\overline{\overline{\mathbf{U}}}dA\cdot\hat{\mathbf{r}} - P(r)a_3\hat{\mathbf{r}}\cdot\overline{\overline{\overline{\mathbf{n}}}}dA\cdot\hat{\mathbf{r}}. \tag{3.21}$$

The products of these tensors and the sun's position unit vector can be stated in terms of the summation convention as:

$$\begin{aligned}\hat{\mathbf{r}}\cdot\overline{\overline{\overline{\mathbf{n}}}}\cdot\hat{\mathbf{r}} &= \hat{n}_i\hat{n}_j\hat{n}_k\hat{\mathbf{r}}_i\hat{\mathbf{r}}_k,\\ \hat{\mathbf{r}}\cdot\overline{\overline{\mathbf{n}}} &= \hat{n}_i\hat{n}_j\hat{\mathbf{r}}_i,\\ \hat{\mathbf{r}}\cdot\overline{\mathbf{n}} &= \hat{n}_i\hat{\mathbf{r}}_i,\end{aligned}$$

where equal indices imply summation, i.e., $a_ib_i = \sum_{i=1}^{3} a_ib_i$.

Adding Eqs. (3.20) and (3.21), the differential force due to a differential sail element is

$$d\mathbf{F} = P\Big[a_2\hat{\mathbf{n}}\hat{\mathbf{n}}dA\cdot\hat{\mathbf{r}} + \hat{\mathbf{r}}\cdot\Big(-2\rho s\hat{\mathbf{n}}\hat{\mathbf{n}}\hat{\mathbf{n}}dA - a_3\hat{\mathbf{n}}\overline{\overline{\mathbf{U}}}dA\Big)\cdot\hat{\mathbf{r}}\Big]. \tag{3.22}$$

The total force is obtained by integrating over the sail surface area:

$$\mathbf{F} = P\Big[\int a_2\hat{\mathbf{n}}\hat{\mathbf{n}}dA\cdot\hat{\mathbf{r}} + \hat{\mathbf{r}}\cdot\Big(-2\int\rho s\hat{\mathbf{n}}\hat{\mathbf{n}}\hat{\mathbf{n}}dA - \int a_3\hat{\mathbf{n}}\overline{\overline{\mathbf{U}}}dA\Big)\cdot\hat{\mathbf{r}}\Big]. \tag{3.23}$$

The integrands of all these expressions are independent of the solar radiation incidence, they can be computed off-line for a given sail shape, re-used over a range of sail attitudes, and ideally can accommodate non-uniformities in the sail optical properties.

Now we will introduce a more systematic notation for these integrals. Define the force surface normal distribution integrals as:

$$\mathbf{J}^1 = \frac{1}{A}\int_A a_3\hat{\mathbf{n}}dA, \tag{3.24}$$

$$\mathbf{J}^2 = \frac{1}{A}\int_A a_2\hat{\mathbf{n}}\hat{\mathbf{n}}dA, \tag{3.25}$$

$$\mathbf{J}^3 = \frac{1}{A}\int_A \rho s\hat{\mathbf{n}}\hat{\mathbf{n}}\hat{\mathbf{n}}dA, \tag{3.26}$$

where $\mathbf{J}^m$ is a rank-m tensor, computed by integrating the product of the normal vectors and local optical and thermal properties over the surface area of the sail. When the sail optical and thermal parameters are constant, the force tensors can be computed by:

$$\overline{\mathbf{J}}^1 = \frac{1}{A}\int_A \hat{\mathbf{n}} dA, \tag{3.27}$$

$$\overline{\mathbf{J}}^2 = \frac{1}{A}\int_A \hat{\mathbf{n}}\hat{\mathbf{n}} dA, \tag{3.28}$$

$$\overline{\mathbf{J}}^3 = \frac{1}{A}\int_A \hat{\mathbf{n}}\hat{\mathbf{n}}\hat{\mathbf{n}} dA. \tag{3.29}$$

The force for a sail of arbitrary parameters can now be rewritten as:

$$\mathbf{F} = PA\Big[\mathbf{J}^2 \cdot \hat{\mathbf{r}} - 2\hat{\mathbf{r}} \cdot \mathbf{J}^3 \cdot \hat{\mathbf{r}} - (\mathbf{J}^1 \cdot \hat{\mathbf{r}})\hat{\mathbf{r}}\Big], \tag{3.30}$$

which in tensor notation becomes

$$\mathbf{F}_j = PA\Big[\mathbf{J}^2_{jk} \cdot \hat{\mathbf{r}}_k - 2\hat{\mathbf{r}}_i \cdot \mathbf{J}^3_{ijk} \cdot \hat{\mathbf{r}}_k - (\mathbf{J}^1_i \cdot \hat{\mathbf{r}}_i)\hat{\mathbf{r}}_j\Big]. \tag{3.31}$$

The force for constant parameters is

$$\mathbf{F} = PA\Big[a_2\overline{\mathbf{J}}^2 \cdot \hat{\mathbf{r}} - 2\rho s\hat{\mathbf{r}} \cdot \overline{\mathbf{J}}^3 \cdot \hat{\mathbf{r}} - a_1(\overline{\mathbf{J}}^1 \cdot \hat{\mathbf{r}})\hat{\mathbf{r}}\Big]. \tag{3.32}$$

Thus, we have arrived at a completely analytic formula for the force acting on a solar sail, which is an extremely general and new result. It is important to note that the force tensor coefficients when specified in the sail-fixed frame are independent of the sail position and independent of the sail orientation. Due to the symmetry of these tensors, a total number of 19 independent coefficients are needed to model the force on an arbitrary sail.

Since these tensors are defined as integrations, it is always possible to add additional sail elements by adding the $\mathbf{J}^m$ term for that additional piece, so long as they are computed relative to the same coordinate frame.

It is also possible to transform a given $\mathbf{J}^m$ defined in one coordinate frame into a different coordinate frame. Suppose we have a $\mathbf{J}^m$ defined for a panel of our sail, computed in the panel-fixed frame. Also assume we have a transformation matrix T that takes a vector from the panel-fixed frame into the sail-fixed frame. Thus, to transform a normal vector $\hat{\mathbf{n}}$ from the panel-fixed frame to the sail-fixed frame we just need to perform a matrix multiply, $\hat{\mathbf{n}}' = T\hat{\mathbf{n}}$, where the $'$ signifies that the vector is specified in the new frame. Using tensor notation, this same transformation would be expressed as $\hat{n}'_j = T^i_j \hat{n}_i$, where the i index signifies the column number for the T matrix, and j signifies the row number, and the summation convention is assumed (equal indexes are summed over, i.e., $T^i_j \hat{n}_i = \sum_{i=1}^{3} T^i_j \hat{n}_i$). Then the following operations would transform the $\mathbf{J}^m$ tensor computed relative to the panel frame into the sail-fixed frame, where they could be directly added to obtain the sail's complete $\mathbf{J}^m$ tensors. As these transformation matrices are known in general, this would be a simple operation to define and extremely simple to carry out in an algorithm:

$$\mathbf{J}^{m'}_{j_1 j_2 \ldots j_m} = T^{i_1}_{j_1} T^{i_2}_{j_2} \ldots T^{i_m}_{j_m} \mathbf{J}^m_{i_1 i_2 \ldots i_m}. \tag{3.33}$$

3.3 Derivation of the Generalized Sail Moment Equation

The total moment acting on the sail can be found by integrating the expression:

$$d\mathbf{M} = \vec{\varrho} \times d\mathbf{F} = \tilde{\varrho} \cdot d\mathbf{F}, \tag{3.34}$$

where $\vec{\varrho}$ is the moment arm of the differential sail area to the point where the moment is being evaluated. Thus, the differential moment acting on the sail is just

$$\begin{aligned} d\mathbf{M} &= P\tilde{\varrho} \cdot \Big[a_2 \hat{\mathbf{n}}\hat{\mathbf{n}} dA \cdot \hat{\mathbf{r}} + \hat{\mathbf{r}} \cdot \Big(-2\rho s \hat{\mathbf{n}}\hat{\mathbf{n}}\hat{\mathbf{n}} dA - a_3 \hat{\mathbf{n}} \overline{\overline{\mathbf{U}}} dA \Big) \cdot \hat{\mathbf{r}} \Big] \\ &= P\Big[a_2 \tilde{\varrho} \cdot \hat{\mathbf{n}}\hat{\mathbf{n}} dA \cdot \hat{\mathbf{r}} + \hat{\mathbf{r}} \cdot \Big(-2\rho s \tilde{\varrho} \cdot \hat{\mathbf{n}}\hat{\mathbf{n}}\hat{\mathbf{n}} dA - a_3 \tilde{\varrho} \cdot \hat{\mathbf{n}} \overline{\overline{\mathbf{U}}} dA \Big) \cdot \hat{\mathbf{r}} \Big], \end{aligned} \tag{3.35}$$

where $d\mathbf{F}$ is given by Eq. 3.22. Define the moment integrals as:

$$\mathbf{K}^2 = \frac{1}{Al_r}\int_A a_2\tilde{\varrho}\cdot\hat{\mathbf{n}}\hat{\mathbf{n}}dA, \tag{3.36}$$

$$\mathbf{K}^3 = \frac{1}{Al_r}\int_A \Big[\rho s\Big(-2\tilde{\varrho}\cdot\hat{\mathbf{n}}\hat{\mathbf{n}}\hat{\mathbf{n}}+\tilde{\varrho}\cdot\hat{\mathbf{n}}\overline{\overline{\mathbf{U}}}\Big)-\tilde{\varrho}\cdot\hat{\mathbf{n}}\overline{\overline{\mathbf{U}}}\Big]\,dA, \tag{3.37}$$

where l_r is an arbitrary reference length. Thus, the total moment is

$$\mathbf{M} = PAl_r\Big[\mathbf{K}^2\cdot\hat{\mathbf{r}}+\hat{\mathbf{r}}\cdot\mathbf{K}^3\cdot\hat{\mathbf{r}}\Big], \tag{3.38}$$

which in tensor notation is

$$\mathbf{M}_j = PAl_r\Big[\mathbf{K}^2_{ij}\cdot\hat{\mathbf{r}}_i+\hat{\mathbf{r}}_i\cdot\mathbf{K}^3_{ijk}\cdot\hat{\mathbf{r}}_k]. \tag{3.39}$$

The tensor $\mathbf{K}^2$ requires 9 terms, however $\mathbf{K}^3$ is a rank-3 tensor symmetric in its last two indices, i.e. $\mathbf{K}^3_{ijk}=\mathbf{K}^3_{ikj}$, requiring 18 coefficients. This can be seen from the fact that $\overline{\overline{\mathbf{U}}}_{ij}=\overline{\overline{\mathbf{U}}}_{ji}$. Thus, only 27 parameters are needed to capture the moment being generated by an arbitrary sail. Note that this a more compact definition than defined previously in Reference [27], where the moment was defined by a set of three tensors, two rank-2 tensors and one rank-3 tensor requiring a total of 36 parameters to capture the moment generated by an arbitrary sail.

Transformations from different coordinate frames might be necessary in some cases. For these situations the use of Eq. (3.33) will be still appropriate, so long as the transformation is a pure rotation and does not involve translation. If the panel is to be translated as well, an additional term $\vec{\varrho}_t\times\mathbf{F}$ must be added, where $\vec{\varrho}_t$ is the translation vector, and $\mathbf{F}$ is the total force acting on that panel.

3.4 Center of Pressure

Of special interest is to find the center of pressure of the sail, $\mathbf{r}_p$. The center of pressure is the point where the total moment is zero, and need not lie in the sail. In

general this vector can be defined by the condition:

$$\mathbf{M} = \mathbf{r}_p \times \mathbf{F} \tag{3.40}$$

$$= \mathbf{r}_p \cdot \tilde{\mathbf{F}}, \tag{3.41}$$

where $\mathbf{F}$ is the total computed force, $\mathbf{M}$ is the total computed moment for a given point where the moments are being computed, and $\mathbf{r}_p$ is measured from that point. Let us dot both sides on the right with $-\tilde{\mathbf{F}}$ to obtain:

$$-\mathbf{r}_p \cdot \tilde{\mathbf{F}} \cdot \tilde{\mathbf{F}} = -\mathbf{M} \cdot \tilde{\mathbf{F}} = \tilde{\mathbf{F}} \cdot \mathbf{M}. \tag{3.42}$$

Dividing by the square of the total force magnitude, F^2, this equation becomes:

$$\mathbf{r}_p \cdot \left[\overline{\overline{\mathbf{U}}} - \hat{\mathbf{F}}\hat{\mathbf{F}}\right] = \frac{1}{F^2}\tilde{\mathbf{F}} \cdot \mathbf{M}. \tag{3.43}$$

The terms in the brackets is a dyad that projects the center of pressure vector into a vector perpendicular to the force line. Taking the pseudo-inverse of this operator yields the center of pressure vector and the associated line of action for the sail force:

$$\mathbf{r}_p = \frac{1}{F^2}\mathbf{F} \times \mathbf{M} + \sigma\hat{\mathbf{F}}, \tag{3.44}$$

where σ is an arbitrary distance.

Using this, if the center of mass of the sail is given, $\mathbf{r}_{CM}$, we can compute the center of pressure, $\mathbf{r}_p$, and the total moment acting on the sail about its center of mass:

$$\mathbf{M}_{CM} = (\mathbf{r}_p - \mathbf{r}_{CM}) \times \mathbf{F} \tag{3.45}$$

$$= \mathbf{M} - \mathbf{r}_{CM} \times \mathbf{F}. \tag{3.46}$$

3.5 Properties of the Tensor Coefficients and Symmetric Sails

For symmetric sails, some of the force and moment tensor coefficients go to zero or become equal to each other, thus the total number of coefficients necessary to characterize the force or moment is reduced.

Here, two types of symmetry are considered: discrete symmetry and rotational symmetry. Discrete symmetry refers to any sail shape that has a finite number of symmetry axes, such as a square sail, the sail recently deployed by the Japanese Aerospace Exploration Agency [24], and the Planetary Society's Cosmos I sail[9]. Rotational symmetry indicates that a sail has continuous axis of symmetry, such as a billowed circular sail. Several examples of these different types of symmetry are shown in Figure 3.1.

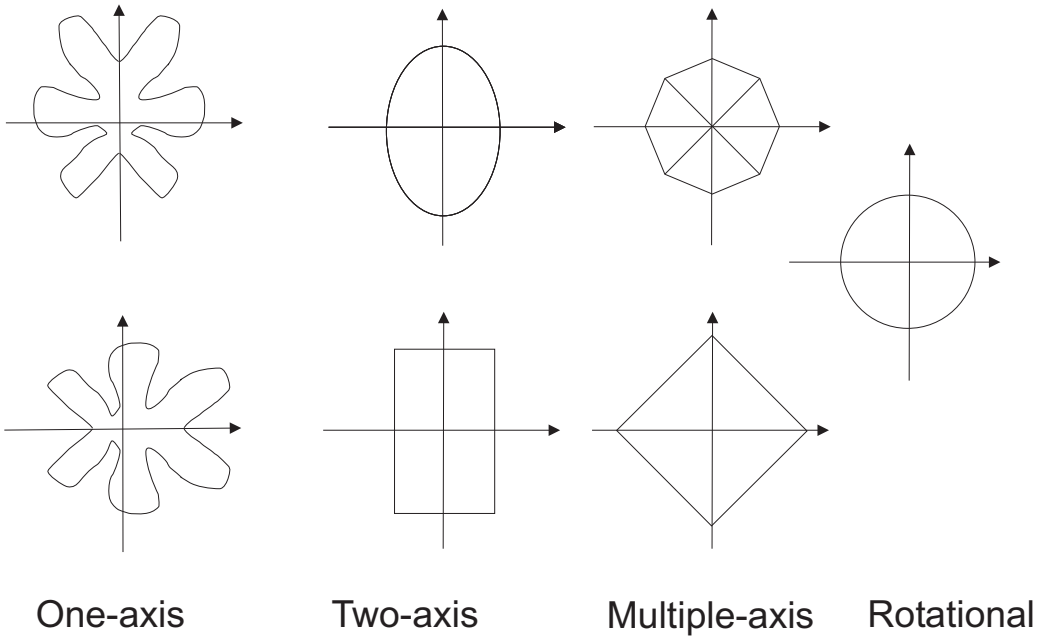

Figure 3.1: Symmetric sail planforms and axis of symmetry.

In this section, 1-axis and 2-axes discrete symmetry and rotational symmetry are treated. Let the sail surface shape be given by the function $S(x, y)$, which is dependent on the x and y body-fixed coordinates. A sail is symmetric about an axis if $S(x, y) = S(-x, y)$ or $S(x, y) = S(x, -y)$. Here, we assume that the coordinate axis coincides with with a symmetry axis. Furthermore, if $S(x, y) = S(-x, y) = S(x, -y) = S(-x, -y)$, then the sail has 2-axis discrete symmetry.

Recall from calculus that if a function has the property $S(x, y) = S(-x, y)$ then its Taylor series expansion in the x variable will contain only even powers of x about zero. Thus, the function $S(x, y)$ is called even in the x-variable. Similarly, if $S(x, y) = S(x, -y)$, then $S(x, y)$ is called even in the y-variable.

Without loss of generality, assume that $S(x, y)$ is even in x, then its first derivative (or integral) with respect to x will be odd, i.e. its Taylor series expansion with respect to x will have odd powers of x. With this in mind it can be shown that:

$$\int_{-a}^{a} S_x(x, y)dx = 0. \tag{3.47}$$

Eq. (3.47) shows that for a symmetric sail, several of the force and moment tensor coefficients will be zero. Thus, the number of parameters needed to model the force or moment generated by a symmetric sail is reduced. These are identified in the following sections.

3.5.1 Force Tensors

As mentioned earlier, the force tensor coefficients are completely symmetric in their indices, i.e., $J^m_{i_1 i_2 \ldots i_m} = J^m_{i_2 i_1 \ldots i_m}$, and so on for any two indices. Thus, for a symmetric rank-3 tensor, which could have up to 27 entries, we only need to compute 10 independent values. For a symmetric rank-2 tensor there are only 6 unique coefficients among its 9 entries. Thus, the three integrals in Eqs. (3.24)-

(3.26) are specified by $3 + 6 + 10 = 19$ numbers for the general case.

Some geometric properties are embedded in the force tensor coefficients. First consider the $\mathbf{J}^1$ tensor. Defining the nominal sail plane to be the $x - y$ plane, the third element of the $\mathbf{J}^1$ tensor, $\mathbf{J}^1_3$, represents the projection of the sail surface area into the sail x-y plane. The first element, $\mathbf{J}^1_1$, is the projection of the sail area onto the $y - z$ plane and the second element, $\mathbf{J}^1_2$, projects the area into the $x - z$ plane as shown in Figure 3.2.

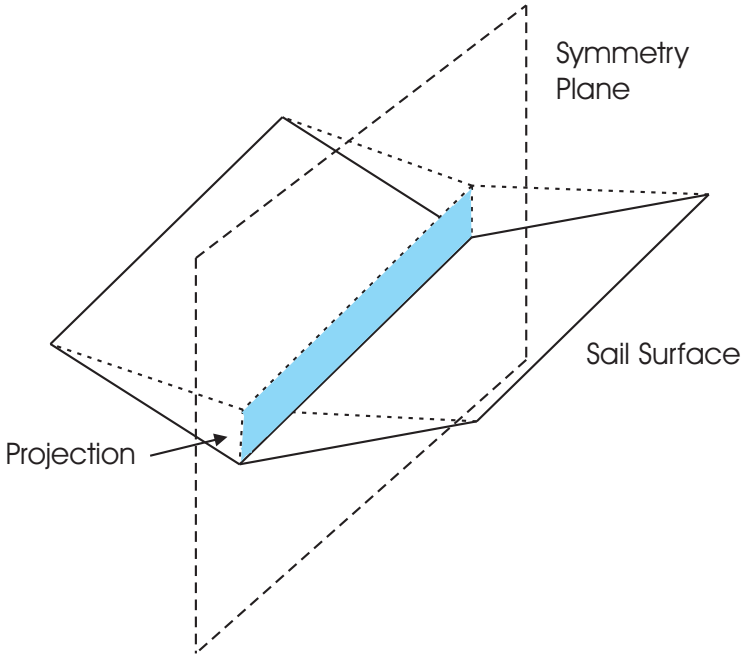

Figure 3.2: Projection of sail area into symmetry plane.

Using the arguments in the previous section it is now possible to find conditions for sails with symmetric shapes. In Reference [26], it was shown that a sail symmetric about the y-axis (1-axis symmetric) will have J^1_1, J^2_{13}, J^2_{12}, J^3_{111}, J^3_{221}, and J^3_{331}, equal to zero.

If the sail is symmetric about the $y - z$ plane, then $\mathbf{J}^1_1$ will be zero due to its even property as shown by Eq. (3.47). Similarly, if the sail is symmetric about the $x - z$ plane, $\mathbf{J}^1_2$ will be zero, since the projection onto their respective planes will be

cancelled from opposite sides of the sail as can be seen in Figure 3.2

Consider the $\mathbf{J}^2$ tensor. The $\mathbf{J}^2_{11}$, $\mathbf{J}^2_{22}$, and $\mathbf{J}^2_{33}$ elements are expected to be non-zero even for symmetric shapes, unless the sail is completely flat, then the only non-zero element will be $\mathbf{J}^2_{33}$. This can be seen from the fact that the product $\hat{\mathbf{n}}_i(x,y)\hat{\mathbf{n}}_i(x,y)$ is always an even function in both variables, hence

$$\mathbf{J}^2_{ii} = \int\int_A a_2 \hat{\mathbf{n}}_i \hat{\mathbf{n}}_i dA, \tag{3.48}$$

is not zero in general except when $\hat{\mathbf{n}}_i(x,y) \equiv 0$. For the case of a flat sail $\hat{\mathbf{n}}(x,y) = [0,0,1]^T$, thus $\mathbf{J}^2_{33}$ is the only non-zero element.

Now consider the case when

$$\mathbf{J}^2_{ij} = \int\int_A a_2 \hat{\mathbf{n}}_i \hat{\mathbf{n}}_j dA. \tag{3.49}$$

Then, $\mathbf{J}^2_{ij}$ is zero when either $\hat{\mathbf{n}}_i$ or $\hat{\mathbf{n}}_i$ is zero or both are zero. However this is true for a limited number of sail shapes. For an arbitrarily shaped sail $\mathbf{J}^2_{ij}$ is zero when $\hat{\mathbf{n}}_i(x,y)\hat{\mathbf{n}}_j(x,y)$ is odd in at least one of the x or y variables as given by Eq. (3.47).

A sail symmetric about the x-axis will have as zero elements J^2_{23} and J^2_{12}. If the symmetry is along the y-axis, then J^2_{13} and J^2_{12} are zero.

The coefficients of the $\mathbf{J}^3$ tensor are found from the expression:

$$\mathbf{J}^3_{ijk} = \int\int_A \rho s \hat{\mathbf{n}}_i \hat{\mathbf{n}}_j \hat{\mathbf{n}}_k dA. \tag{3.50}$$

When the product $\hat{\mathbf{n}}_i\hat{\mathbf{n}}_j\hat{\mathbf{n}}$ is an odd function in any of the variables of integration then J_{ijk} is zero. For a sail symmetric about the x-axis the coefficients J^3_{211}, J^3_{222}, and J^3_{332} are zero. Conversely, if a sail is symmetric about the y-axis, the the elements J^3_{111}, J^3_{221}, and J^3_{331} are zero.

Table 3.1: Simplification of Force Tensor Coefficients due to Symmetry.

Symmetry	Zero or Non-zero	Coefficients	Equal Coefficients	Independent Coefficients.
x-axis	Zero	$J^1_2, J^2_{23}, J^2_{12}, J^3_{211}, J^3_{222}, J^3_{332}$		13
y-axis	Zero	$J^1_1, J^2_{13}, J^2_{12}, J^3_{111}, J^3_{221}, J^3_{331}$		13
2-axis	Non-zero	$J^1_3, J^2_{11}, J^2_{22}, J^2_{33}, J^3_{131}, J^3_{232}, J^3_{333}$		7
Rotational	Non-zero	$J^2_{11}, J^3_{131}, J^3_{333}, J^2_{33}, J^1_3$	$J^2_{11} = J^2_{22}$ $J^3_{131} = J^3_{232}$	5

For a 2-axis symmetric sail the elements several of the force coefficients are zero. The non-zero elements are J^1_3, J^2_{11}, J^2_{22}, J^2_{33}, J^3_{131}, J^3_{232} J^3_{333} in general. The number of coefficients needed to model the force of a two-axis symmetric sail reduces to only 7 independent coefficients from a total of 19.

For a sail with rotational symmetry $J^2_{11} = J^2_{22}$, $J^3_{113} = J^3_{223}$, which are in general non-zero as well as J^3_{333}, J^2_{33}, and J^1_3. Thus, only five coefficients are needed to represent the force.

A summary of these simplifications is shown in Table 3.1. The rows show the axis of symmetry followed by the value of the coefficients (zero or non-zero), the equivalent coefficients if any, and the number of independent coefficients.

3.5.2 Moment Tensors

The moment tensor $\mathbf{K}^2$ does not have any symmetry at all. Thus, $\mathbf{K}^2$ requires 9 unique coefficients. $\mathbf{K}^3$, however, is symmetric in two of its indices, $\mathbf{K}^3_{ijk} = \mathbf{K}^3_{ikj}$, and only requires 18 entries instead of 27. Thus, a total of 27 unique coefficients are needed to model the moment generated by an arbitrary sail.

The moment arm of a differential element is given by:

$$\varrho = \begin{bmatrix} x \\ y \\ S(x,y) \end{bmatrix}, \tag{3.51}$$

thus, the first term of the $\mathbf{K}^2$ tensor is

$$\begin{aligned} K_{11}^2 &= \int\int a_2(\hat{n}_1\hat{n}_3 y - \hat{n}_1\hat{n}_2 z)dA \\ &= \int_{y_1}^{y_2}\int_{x_1}^{x_2} a_2\left(\frac{S_x y}{\sqrt{1+S_x^2+S_y^2}} - \frac{S_x S_y S(x,y)}{\sqrt{1+S_x^2+S_y^2}}\right)dxdy. \end{aligned} \tag{3.52}$$

Note that the vector $\varrho(x,y)$ is an even function of x if the sail is symmetric about the y-axis and an even function of y if the sail is symmetric about the x-axis. Then, for a sail symmetric about the y-axis, the first term is odd in x and since $x_1 = -x_2$ it integrates to zero. The second term is also odd in x and has no contribution. Hence, for a symmetric sail about the y-axis K_{11}^2 is zero. For symmetry about the x-axis, the first term as well as the second term are odd in y. Thus, for this type of sail K_{11}^2 is also zero.

With the same arguments, the zero terms for a sail symmetric about the x-axis the $\mathbf{K}^2$ zero terms are K_{11}^2, K_{13}^2, K_{22}^2, K_{31}^2, and K_{33}^2. For a symmetric sail about the y-axis are K_{11}^2, K_{22}^2, K_{23}^2, K_{32}^2, and K_{33}^2.

The elements of $\mathbf{K}^3$ are given by

$$K_{ijk}^3 = \frac{1}{Al_r}\int_A \Big[\rho s\Big(-2\tilde{\varrho}_{ij}\cdot\hat{n}_i\hat{n}_j\hat{n}_k + \tilde{\varrho}_{ij}\cdot\hat{n}_i\overline{\overline{U}}_{jk}\Big) - \tilde{\varrho}_{ij}\cdot\hat{n}_i\overline{\overline{U}}_{jk}\Big]\,dA. \tag{3.53}$$

The first term of $\mathbf{K}^3$ is:

$$K_{111}^3 = \int_{y_1}^{y_2}\int_{x_1}^{x_2} -\rho s\left(\frac{S_x^2 y}{1+S_x^2+S_y^2} - \frac{S_x^2 S_y S(x,y)}{1+S_x^2+S_y^2}\right)dxdy. \tag{3.54}$$

For a symmetric sail about the x-axis the first and second inside the integral are both odd functions in the y variable. Thus the integration is zero as predicted by

Table 3.2: Simplification of Moment Tensor Coefficients due to Symmetry.

Symmetry	Zero Non-zero	Coefficients	Equal Coefficients	Independent Coefficients
x-axis	Zero	$K^2_{11}, K^2_{13}, K^2_{22}, K^2_{31}, K^2_{33}$ $K^3_{111}, K^3_{131}, K^3_{221}, K^3_{311}$ $K^3_{331}, K^3_{122}, K^3_{232}, K^3_{322}, K^3_{133}, K^3_{333}$		12
y-axis	Zero	$K^2_{11}, K^2_{22}, K^2_{23}, K^2_{32}, K^2_{33}$ $K^3_{121}, K^3_{131}, K^3_{211}, K^3_{311}$ $K^3_{222}, K^3_{232}, K^3_{322}, K^3_{332}, K^3_{233}, K^3_{333}$		12
2-axis	Non-zero	$K^2_{12}, K^2_{21},$ $K^3_{213}, K^3_{321}, K^3_{312}$		5
Rotational	Non-zero	K^2_{12}, K^3_{231}	$K^2_{12} = -K^2_{21}$ $K^3_{231} = -K^3_{132}$	2

Eq. 3.47. Now, for a sail symmetric about the y-axis, both terms inside the integral are even functions in the x variable and the integration is not necessarily zero.

This analysis can be performed for all the coefficients of the $\mathbf{K}^3$ tensor. For a sail symmetric about the x-axis the zero terms are K^3_{111}, K^3_{131}, K^3_{221}, K^3_{311}, K^3_{331}, K^3_{122}, K^3_{232}, K^3_{322}, K^3_{133}, and K^3_{333}.

For a sail symmetric about the y-axis, the $\mathbf{K}^3$ tensor coefficients that are zero are K^3_{121}, K^3_{131}, K^3_{211}, K^3_{311}, K^3_{222}, K^3_{232}, K^3_{322}, K^3_{332}, K^3_{233}, and K^3_{333}.

For a 2-axis symmetric sail the terms K^2_{12}, K^2_{21}, K^3_{213}, K^3_{321}, and K^3_{132} are non-zero in general. For a sail with rotational symmetry $K^2_{12} = -K^2_{21}$, $K^3_{321} = 0$, $K^3_{231} = -K^3_{132}$. A summary of these results is shown in Table 3.2.

CHAPTER IV

Applications of the Generalized Sail Model

In this chapter the generalized sail model is applied to a number of practical case studies. First, various sail shapes are modeled and their force and moment tensors are computed. Next, partial derivatives of the force are developed, which are useful for studying optimization of orbits and trajectories. Then, classical problems in solar system escape guidance laws are developed for a non-flat sail model. Finally a description of the use of the GSM in the solar sail spaceflight simulation software (S5) is described.

4.1 Solar Sail Models

In this section we compute force and moment coefficients for sails of increasing complexity. These include a flat sail model, a symmetric circular sail with billow, a more complex four-panel sail with billow in each panel, and finally a sail of arbitrary sinusoid shape to elucidate the effects of sail shape performance. Then, their performance are compared as a function of the sun-sail angle.

4.1.1 Flat Sail

For the case of a flat sail, the normal vector is invariant with location on the sail in the sail body-fixed frame, thus, the unit normal is just $\hat{\mathbf{n}} = \begin{bmatrix} 0, 0, 1 \end{bmatrix}^T$. The $\mathbf{J}^m$

tensors reduce to:

$$\mathbf{J}^1 = \frac{a_3\hat{\mathbf{n}}}{A}\int_A dA = a_3\hat{\mathbf{n}}, \tag{4.1}$$

$$\mathbf{J}^2 = \frac{a_2\hat{\mathbf{n}}\hat{\mathbf{n}}}{A}\int_A dA = a_2\hat{\mathbf{n}}\hat{\mathbf{n}}, \tag{4.2}$$

$$\mathbf{J}^3 = \frac{\rho s\hat{\mathbf{n}}\hat{\mathbf{n}}\hat{\mathbf{n}}}{A}\int_A dA = \rho s\hat{\mathbf{n}}\hat{\mathbf{n}}\hat{\mathbf{n}}, \tag{4.3}$$

and the force equation becomes:

$$\mathbf{F} = PA\Big[a_2\hat{\mathbf{n}}^2\cdot\hat{\mathbf{r}} - 2\rho s(\hat{\mathbf{n}}^3\cdot\hat{\mathbf{r}})\cdot\hat{\mathbf{r}} + a_3(\hat{\mathbf{n}}\cdot\hat{\mathbf{r}})\cdot\hat{\mathbf{r}}\Big]. \tag{4.4}$$

Recall that for a flat sail $\hat{\mathbf{n}} = [0,0,1]^T$, thus the only non-zero force coefficients are $\mathbf{J}^1_3$, $\mathbf{J}^2_{33}$, and $\mathbf{J}^3_{333}$ with values equal to a_3, a_2, and ρs, respectively. A more familiar equation is obtained if Eq. (3.8) is substituted in the above expression to obtain:

$$\mathbf{F} = -PA\Big[a_2\cos\alpha\hat{\mathbf{n}} + 2\rho s\cos^2\alpha\hat{\mathbf{n}} + a_3\cos\alpha\hat{\mathbf{r}}\Big], \tag{4.5}$$

which is the force generated by a flat sail in the body fixed frame. For an ideal flat sail a_2 and a_3 are both zero and Eq. (2.20) is recovered which is the force of a flat ideal sail.

For a symmetric shape, the products $\tilde{\varrho}\cdot\hat{\mathbf{n}}^m$ and $\hat{\mathbf{n}}\vec{\varrho}$ tensor are odd functions, implying that the $\mathbf{K}^m$ tensors will be zero about the geometric center of the sail. Hence, the total moment is zero at the sail geometric center. This is expected for a symmetric flat sail since the geometric center is the same as the center of pressure and does not change with attitude.

4.1.2 Circular Sail with Billow

Next consider a circular sail. Let us assume that the surface is curved by design or by the solar radiation pressure and can be modeled by:

$$z_b = -\frac{\alpha_{max}}{2R_0}(x_b^2 + y_b^2) + \frac{\alpha_{max} R_0}{2}, \tag{4.6}$$

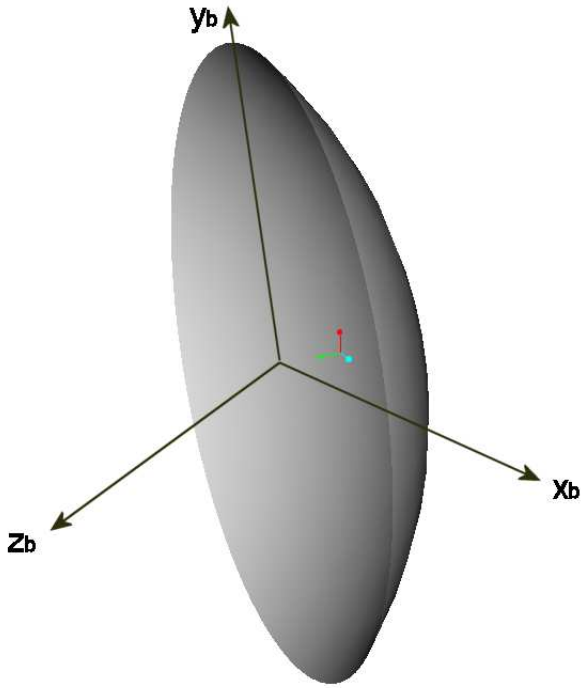

Figure 4.1: Circular Sail Geometry.

where R_0 is the sail radius, α_{max} the surface slope at the rim (and must be negative for this case), and x_b, y_b, z_b are the sail coordinates in the body-fixed frame as shown in Figure 4.1. If polar coordinates are used, it can be noted that the slope varies linearly with distance from center. The surface function $\phi(x_b, y_b, z_b) = 0$ is obtained by setting Eq. (4.7) to zero to obtain:

$$\phi = z_b + \frac{\alpha_{max}}{2R_0}(x_b^2 + y_b^2) - \frac{\alpha_{max} R_0}{2}, \tag{4.7}$$

and the surface normal is obtained by taking the gradient of $\phi(x_b, y_b, z_b)$:

$$\hat{\mathbf{n}} = \frac{1}{\sqrt{1 + (\frac{\alpha_{max}}{R_0})^2 x_b^2 + (\frac{\alpha_{max}}{R_0})^2 y_b^2}} \begin{bmatrix} \frac{\alpha_{max}}{R_0} x_b \\ \frac{\alpha_{max}}{R_0} y_b \\ 1 \end{bmatrix}. \tag{4.8}$$

Introducing polar coordinates by letting $x_b = r_b \cos\delta$ and $y_b = r_b \sin\delta$, the surface normal can also be stated as:

$$\hat{\mathbf{n}} = \frac{1}{\sqrt{1 + (\frac{\alpha_{max}}{R_0} r_b)^2}} \begin{bmatrix} \frac{\alpha_{max}}{R_0} r_b \cos\delta \\ \frac{\alpha_{max}}{R_0} r_b \sin\delta \\ 1 \end{bmatrix}, \tag{4.9}$$

and the differential area is given by:

$$dA = \sqrt{1 + (\frac{\alpha_{max}}{R_0} r_b)^2} r_b dr_b d\delta. \tag{4.10}$$

With these terms defined and using πR_0^2 as the reference area, the coefficient integrals can be computed analytically. Note that this shape is symmetric along the x_b and y_b axis. Hence, J_1^1 and J_2^1 are both zero. The $\mathbf{J}^1$ tensor for this sail is

$$\mathbf{J}^1 = a_3 \begin{bmatrix} 0 \\ 0 \\ 1 \end{bmatrix}. \tag{4.11}$$

Also due to this symmetry, the non-zero terms for the $\mathbf{J}^2$ tensor are J_{11}^2, J_{22}^2, and J_{333}^2. Furthermore due to the rotational symmetry $J_{11}^2 = J_{22}^2$. Therefore, $\mathbf{J}^2$ is

$$\mathbf{J}^2 = a_2 \begin{bmatrix} \frac{2+(-2+\alpha_{max})\sqrt{1+\alpha_{max}^2}}{3\alpha_{max}^2} & 0 & 0 \\ 0 & \frac{2+(-2+\alpha_{max})\sqrt{1+\alpha_{max}^2}}{3\alpha_{max}^2} & 0 \\ 0 & 0 & \frac{2\left(-1+\sqrt{1+\alpha_{max}^2}\right)}{\alpha_{max}^2} \end{bmatrix}, \quad (4.12)$$

and the non-zero elements of the $\mathbf{J}^3$ tensor are:

$$\mathbf{J}^3_{113} = \frac{\rho s}{2\alpha_{max}^2}(\alpha_{max}^2 - \log(1+\alpha_{max}^2)), \quad (4.13)$$

$$\mathbf{J}^3_{333} = \frac{\rho s}{\alpha_{max}^2}\log(1+\alpha_{max}^2), \quad (4.14)$$

Recall that due to symmetry

$$\mathbf{J}^3_{131} = \mathbf{J}^3_{311} = \mathbf{J}^3_{223} = \mathbf{J}^3_{232} = \mathbf{J}^3_{322} = \mathbf{J}^3_{113}. \quad (4.15)$$

The moment acting on the sail can also be computed analytically. Let the reference length be R_0, and let the position of a differential area on the sail be defined as $\tilde{\varrho} = [r_b\cos\delta, r_b\sin\delta, z]$.

Due to rotational symmetry the only nonzero element of the $\mathbf{K}^2$ tensor is K^2_{12} and $K_{21} = -K_{12}$. Thus, $\mathbf{K}^2$ is

$$\mathbf{K}^2 = \frac{a_2\left(6-5\alpha_{max}^2 - \sqrt{1+\alpha_{max}^2}(6-8\alpha_{max}^2+\alpha_{max}^4)\right)}{15\alpha_{max}^3} \begin{bmatrix} 0 & 1 & 0 \\ -1 & 0 & 0 \\ 0 & 0 & 0 \end{bmatrix}. \quad (4.16)$$

The $\mathbf{K}^3$ tensor non-zero element is K^3_{213} given by

$$K^3_{213} = -\frac{1}{8\alpha_{max}}\left(\alpha_{max}^2(-2+\alpha_{max}^2) - 2(-1+\alpha_{max}^2)\log(1+\alpha_{max}^2)\right). \quad (4.17)$$

Recall that due to rotational symmetry

$$K^3_{213} = K^3_{312}, \tag{4.18}$$

$$K^3_{123} = K^3_{132} = -K^3_{213}. \tag{4.19}$$

4.1.3 Four-Panel Sail with Billow

A square solar sail with beams along its main diagonals can be modeled by combining four panels as shown in Figure 4.2; each section being of triangular form. The billow of the sail membrane will be modeled by approximating each quadrant as a section of an oblique circular cone [37]. Several of the solar sails being built by different manufacturers can be approximated by this shape. L'Garde has proposed a square sail [6] for the Team Encounter mission and has performed several tests of sail deployment in vacuum chambers [18].

Due to the complexity of this shape, the coefficients will be found using numerical integration. The equation for an oblique cone with its base centered at the origin and vertex positioned at $(h_c, 0, z_{co})$, as shown in Figure 4.3, is given by:

$$(x_c - h_c)^2 = -\frac{h_c^2\Big((r_c\cos\theta - z_{co})^2 + (-r_c\sin\theta)^2\Big)}{(R_c\cos\theta - z_{co})^2 + (-R_c\sin\theta)^2}, \tag{4.20}$$

where the polar coordinates $z_c = r_c\cos\theta$, $y_c = -r_c\sin\theta$ have been substituted, R_c is the radius at the base of the cone, and h_c is the height of the cone. The cone-fixed coordinates are related to the body-fixed coordinates by $x_c = 2(x_b - y_b)/\sqrt{2}$ and $y_c = 2(y_b + x_b)/\sqrt{2}$. Each panel of the sail surface is modeled as a section of the cone as shown in Figure 4.3.

It is assumed that the sail beams are perpendicular with half-length l and the sail billow is described by h_b as shown in Figure 4.3. With this information the oblique

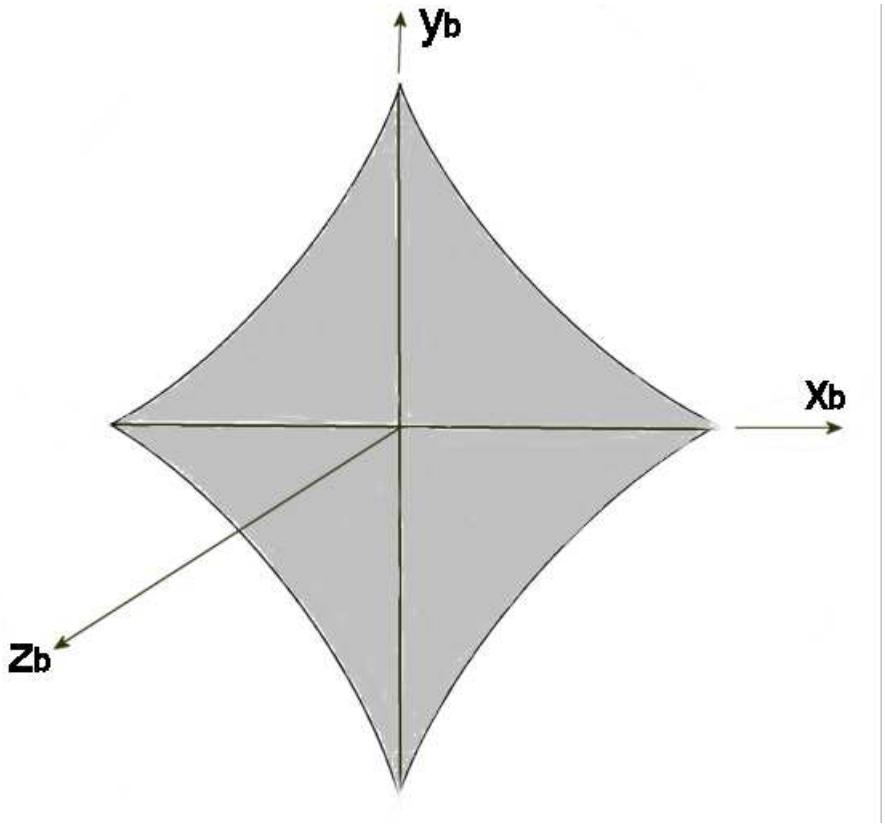

Figure 4.2: Square Sail Modeling.

cone can be fully described. Notice that the cone height and the distance between the tip of the beams are related to l by:

$$h_c = \frac{l}{\sqrt{2}}, \tag{4.21}$$

$$d_c = \sqrt{2}l. \tag{4.22}$$

Using a top view, the base centered at (0,0,0) can be described as shown in Figure 4.4, a view looking down the panel along the x_c axis. If three points are known to lie on the circumference of a circle, the circle radius and center can be found by finding the intersection of lines perpendicular to and passing through the center of the lines joining the three points as shown in Figure 4.4. In order to find the cone radius at the base for the sail, the three points chosen on the cone base are the points defined

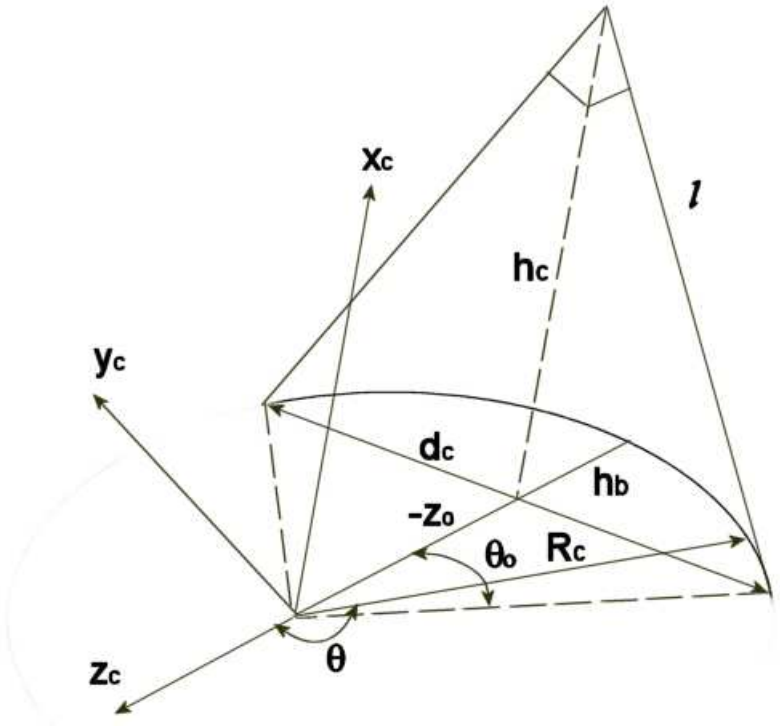

Figure 4.3: Sail Area Modeling.

by the tip of the beams and the third point is equidistant from the first two located on the sail rim. Let y_1 and y_2 be two lines that meet the restrictions mentioned, then they are described by:

$$y_1 = \frac{\sqrt{2}h_b}{l}z_c + \frac{3l}{2\sqrt{2}} - \frac{h_b^2}{l\sqrt{2}}, \tag{4.23}$$

$$y_2 = -\frac{\sqrt{2}h_b}{l}z_c + \Big(\frac{\sqrt{2}l}{2} + \frac{\sqrt{2}h_b^2}{l}\Big). \tag{4.24}$$

Since these two equations intersect at the center, the value of z_{co} can be obtained by equating the two lines, thus the radius is found from:

$$R_c = h_b - z_{co} = \frac{h_b}{2} + \frac{l^2}{4h_b}. \tag{4.25}$$

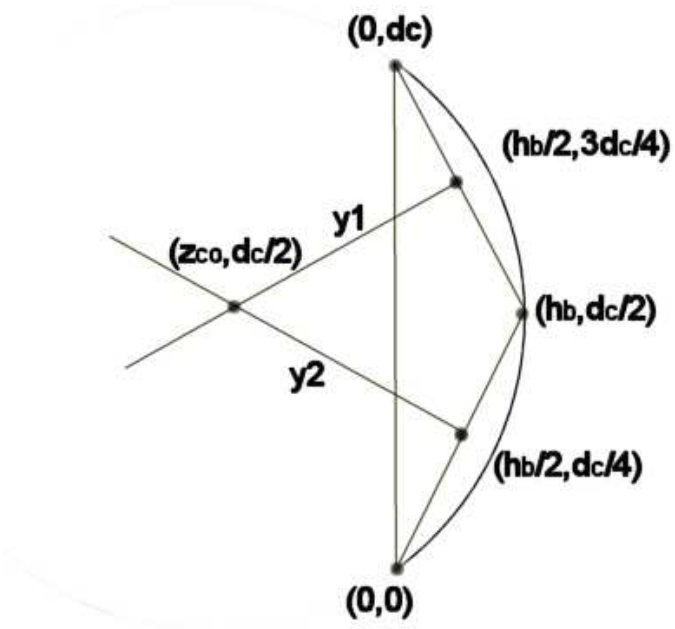

Figure 4.4: Cone Radius.

The angle θ_0 can be found from:

$$\cos\theta_0 = \frac{|d|}{R_c}. \tag{4.26}$$

The surface equation for a sail quadrant modeled by a section of an oblique cone in cartesian coordinates can be written as:

$$\phi = (x_c - h_c)^2 - \frac{h_c^2(y_c^2 + (z_c - z_0)^2)}{Y_c^2 + (Z_c - z_0)^2}, \tag{4.27}$$

where $Y_c = -R_0 \sin\theta$ $Z_c = R_0 \cos\theta$. The normal vector is found in the usual way, by taking the gradient of $\phi(x_c, y_c, z_c) = 0$ in cartesian coordinates and dividing by its magnitude. The gradient for the oblique cone equation in polar coordinates is given by:

$$\nabla\phi = \begin{bmatrix} -h_c\sqrt{\frac{(-z_{c0}+r\cos\theta)^2+(r\sin\theta)^2}{(-z_{c0}+R_c\cos\theta)^2+(R_0\sin\theta)^2}} \\ \frac{h_c^2 r_c\sin\theta}{(R_c\cos\theta-z_{c0})^2+(R_c\sin\theta)^2} \\ -\frac{h_c^2(r_c\cos\theta-z_{c0})}{(R_c\cos\theta-z_{c0})^2+(R_c\sin\theta)^2} \end{bmatrix}. \tag{4.28}$$

The next step is to find an equation for computing the surface area of an oblique cone. Let a differential area be given by a small triangle with one of its vertex at the cone apex, and the other two at the cone base separated by a distance $r_c d\theta$. The height of the triangle l_c, the distance form the cone apex to the point on the surface, is given by:

$$l_c = \sqrt{(R_c\cos\theta - z_{c0})^2 + (-R_c\sin\theta)^2 + h_c^2}, \tag{4.29}$$

the base of the triangle is given by $r_c d\theta \sin d$, where d is the angle between $\vec{l_c}$ and the tangent line at the circular base. Then, the differential area is given by:

$$dA = \frac{1}{2}\sqrt{(R_c - z_{co}\cos\theta)^2 + h_c^2}R_c d\theta. \tag{4.30}$$

When computing the $\mathbf{J}^m$ and $\mathbf{K}^m$ tensors, the limits of integration go from $\pi - \theta_0$ to $\pi + \theta_0$ if z_{c0} is negative. There is no known analytical solution for any of these integrals, so numerical integration is necessary for computing the tensors. The computation of the $\mathbf{K}^m$ tensors require the knowledge of the area element position with respect to a specific point. For a triangle, the position can be defined at its center of mass given by:

$$\vec{\varrho} = \frac{1}{3}(\vec{\varrho_1} + \vec{\varrho_2} + \vec{\varrho_3}), \tag{4.31}$$

where the vectors ($\vec{\varrho_1}$ $\vec{\varrho_2}$ $\vec{\varrho_3}$) define the position of the triangle vertices relative to a chosen reference point. If, for instance, the reference point is chosen to be the oblique cone apex, which represents the sail center, then the element triangle will have its vertices given by:

$$\vec{\varrho_1} = \mathbf{v}_3 - \mathbf{v}_1, \tag{4.32}$$

$$\vec{\varrho_2} = \mathbf{v}_3 - \mathbf{v}_2, \tag{4.33}$$

$$\vec{\varrho_3} = 0, \tag{4.34}$$

where

$$\mathbf{v}_1 = \begin{bmatrix} 0 \\ -R_c \sin\theta \\ R_c \cos\theta - z_{c0} \end{bmatrix}, \tag{4.35}$$

$$\mathbf{v}_2 = \begin{bmatrix} 0 \\ -R_c \sin(\theta + d\theta) \\ R_c \cos(\theta + d\theta) - z_{c0} \end{bmatrix}, \tag{4.36}$$

$$\mathbf{v}_3 = \begin{bmatrix} z_{c0} \\ 0 \\ h_c \end{bmatrix}. \tag{4.37}$$

Let us apply these results to a 100 m by 100 m sail. One triangular quadrant approximated by an oblique cone will have the following values: $h_c = 50m$, $l = 70.71m$. Furthermore, if h_b is assumed to be 10% of l, then $h_b = 7.071m$, $Rc = 180.3m$, $z_{c0} = -173.2m$, and $\theta_0 = 16.1^o$.

The results were obtained by integration of the equations numerically with a step size of $d\theta = 0.0001$ radians. Let the force tensors for one of the sail quadrants be denoted by $\tilde{\mathbf{J}}^m$ whose numerical value are

$$\tilde{\mathbf{J}}^1 = \begin{bmatrix} -4.0115e-003 \\ 5.4001e-018 \\ 2.5000e-002 \end{bmatrix}, \tag{4.38}$$

$$\tilde{\mathbf{J}}^2 = \begin{bmatrix} -2.6311e-004 & 1.9895e-019 & 1.5640e-003 \\ 1.9895e-019 & -1.8641e-004 & -2.5011e-018 \\ 1.5640e-003 & -2.5011e-018 & -9.7788e-003 \end{bmatrix}, \tag{4.39}$$

$$\tilde{\mathbf{J}}^3_{ij1} = \begin{bmatrix} -1.0143e-003 & 1.7586e-018 & 5.7520e-003 \\ 1.7586e-018 & -7.8083e-004 & 1.2790e-018 \\ 5.7520e-003 & 1.2790e-018 & -3.4308e-002 \end{bmatrix}, \tag{4.40}$$

$$\tilde{\mathbf{J}}^3_{ij2} = \begin{bmatrix} 1.7586e-018 & -7.8083e-004 & 1.2790e-018 \\ -7.8083e-004 & 1.4388e-018 & 4.0493e-003 \\ 1.2790e-018 & 4.0493e-003 & 3.5811e-017 \end{bmatrix}, \tag{4.41}$$

$$\tilde{\mathbf{J}}^3_{ij3} = \begin{bmatrix} 5.7520e-003 & 1.2790e-018 & -3.4308e-002 \\ 1.2790e-018 & 4.0493e-003 & 3.5811e-017 \\ -3.4308e-002 & 3.5811e-017 & 2.1520e-001 \end{bmatrix}. \tag{4.42}$$

Following the same procedure, the $\tilde{\mathbf{K}}^m$ and $\tilde{\mathbf{L}}$ tensors are:

$$\tilde{\mathbf{K}}^2 = \begin{bmatrix} -4.6519e-017 & 2.5517e-002 & 1.2705e-016 \\ 5.2697e-002 & -3.0070e-017 & -3.2975e-001 \\ -2.2325e-017 & 1.1197e-002 & 6.3324e-017 \end{bmatrix}, \tag{4.43}$$

$$\tilde{\mathbf{K}}^3_{ij1} = \begin{bmatrix} 2.0771e-016 & -1.0689e-001 & -4.8484e-011 \\ 9.6366e+002 & 1.6471e-016 & 8.3327e+004 \\ -1.2844e-011 & -4.7425e-002 & -3.0280e-016 \end{bmatrix}, \tag{4.44}$$

$$\tilde{\mathbf{K}}^3_{ij2} = \begin{bmatrix} -1.0689e-001 & 1.0183e-013 & 5.5430e-001 \\ 9.6385e+002 & -1.3610e-001 & 8.3326e+004 \\ -4.7425e-002 & -1.1868e-011 & 2.4299e-001 \end{bmatrix}, \tag{4.45}$$

$$\tilde{\mathbf{K}}^3_{ij3} = \begin{bmatrix} -9.5444e-016 & 5.5430e-001 & -4.8481e-011 \\ 9.6501e+002 & -8.0831e-016 & 8.3319e+004 \\ -1.2844e-011 & 2.4299e-001 & 1.3193e-015 \end{bmatrix}. \tag{4.46}$$

The results for the single quadrant must now be rotated to account for the complete sail geometry. The objective is achieved by performing the rotations about the z_b body-fixed axis, which is parallel to the z_c cone-fixed axis, and performing the transformation outlined in Eq. (3.33). The transformation T is given by:

$$T = \begin{bmatrix} \cos\psi & \sin\psi & 0 \\ -\sin\psi & \cos\psi & 0 \\ 0 & 0 & 1 \end{bmatrix}. \tag{4.47}$$

Since the x_c and y_c cone axes are not aligned to the x_b and y_b sail body-fixed axes, the initial rotation is through 45^0. The subsequent rotation angles are 135^0, 225^0 and 315^0. After performing these transformations to the **J**, **K**, and **L** integrals and adding the results, the complete sail integrals obtained are:

$$\mathbf{J}^1 = \begin{bmatrix} 2.8422e-014 \\ -2.8422e-014 \\ 1.0258e+004 \end{bmatrix}, \tag{4.48}$$

$$\mathbf{J}^2 = \begin{bmatrix} 5.6634e+001 & 8.8818e-016 & 2.8422e-014 \\ 8.8818e-016 & 5.6634e+001 & -2.8422e-014 \\ 2.8422e-014 & -2.8422e-014 & 1.0202e+004 \end{bmatrix}, \tag{4.49}$$

$$\mathbf{J}^3_{ij1} = \begin{bmatrix} 4.4409e-016 & -3.3307e-016 & 5.5988e+001 \\ -2.2204e-016 & 5.5511e-016 & 8.8818e-016 \\ 5.5988e+001 & 8.8818e-016 & 2.8422e-014 \end{bmatrix}, \tag{4.50}$$

$$\mathbf{J}^3_{ij2} = \begin{bmatrix} -3.3307e-016 & 4.4409e-016 & 8.8818e-016 \\ 5.5511e-016 & 0 & 5.5988e+001 \\ 8.8818e-016 & 5.5988e+001 & -2.8422e-014 \end{bmatrix}, \tag{4.51}$$

$$\mathbf{J}^3_{ij3} = \begin{bmatrix} 5.5988e+001 & 8.8818e-016 & 2.8422e-014 \\ 8.8818e-016 & 5.5988e+001 & -2.8422e-014 \\ 2.8422e-014 & -2.8422e-014 & 1.0146e+004 \end{bmatrix}, \tag{4.52}$$

$$\mathbf{K}^2 = \begin{bmatrix} -1.4849e+000 & 4.7676e-004 & -3.5527e-015 \\ -4.7676e-004 & -1.4849e+000 & 3.5527e-015 \\ 1.3878e-017 & -1.3878e-017 & 2.9697e+000 \end{bmatrix}, \tag{4.53}$$

$$\mathbf{K}^3_{ij1} = \begin{bmatrix} -6.9389e-018 & 0 & -1.4698e+000 \\ 2.0817e-017 & -5.2042e-018 & -4.6713e-004 \\ 3.0366e-002 & 0 & 1.3878e-017 \end{bmatrix}, \tag{4.54}$$

$$\mathbf{K}^3_{ij2} = \begin{bmatrix} 0 & -3.4694e-017 & 4.6713e-004 \\ -5.2042e-018 & 1.3878e-017 & -1.4698e+000 \\ 0 & 3.0366e-002 & -1.3878e-017 \end{bmatrix}, \tag{4.55}$$

$$\mathbf{K}^3_{ij3} = \begin{bmatrix} -1.4698e+000 & 4.6713e-004 & -3.5527e-015 \\ -4.6713e-004 & -1.4698e+000 & 3.5527e-015 \\ 1.3878e-017 & -1.3878e-017 & 2.9396e+000 \end{bmatrix}, \tag{4.56}$$

$$\mathbf{L} = \begin{bmatrix} -7.6362e-004 & -7.6334e-004 & 5.4210e-020 \\ 7.6334e-004 & -7.6362e-004 & 2.7105e-020 \\ -2.1684e-019 & -4.3368e-019 & 3.0544e-003 \end{bmatrix}. \tag{4.57}$$

4.1.4 Generic Sail Model

For a generic sail, or numerically defined sail, such as what might be defined by a Finite Element program, a simple approach can be outlined. Assume the sail is defined by a set of triangular facets denoted by an index a, each of which with an

area A_a, position (to its center of mass) $\vec{\varrho}_a$, and unit vector normal $\hat{\mathbf{n}}_a$. Then the coefficients for a sail are simply defined as summations over these quantities:

$$\mathbf{J}^m = \sum_i a_i^m \hat{\mathbf{n}}_i^m A_i, \tag{4.58}$$

$$\mathbf{K}^m = \sum_i a_i^m \tilde{\varrho}_i \cdot \hat{\mathbf{n}}_i^m A_i. \tag{4.59}$$

with these formulae it is simple to compute a sail's coefficients at any step of the modeling process.

Let's apply this approach to a general sail model that is square but non-symmetric. To generate the sail shape a surface of the form is used:

$$\begin{aligned} z &= 1 - \left(1 + \cos(\frac{\pi x}{l}) + a_x \cos(\frac{f_x \pi x}{l}) + b_x \sin(\frac{2\pi x}{l})\right)\left(1 + \cos(\frac{\pi y}{l})\right. \\ &+ \left. a_y \cos(\frac{f_y \pi y}{l}) + b_y \sin(\frac{2\pi y}{l})\right), \end{aligned} \tag{4.60}$$

where l is the sail length, a and b are the amplitude of deformations along the x and y axes, and f is the frequency. a, b, and f allows to change the sail shape easily. Choosing values of $l = 100$m, $a_x = a_y = 0.2$, $b_x = b_y = 0$, and $f_x = f_y = 5$. The sail shape for the values is shown in Figure 4.5. Note that this is an arbitrary , but generally non-symmetric shape, used for example purposes only.

This shape can be modified by assigning values to b_x and b_y. The force and moment tensor coefficients were computed by discretizing the surface and performing a numeric integration of all the panels. The resulting GSM tensor coefficients for this shape are given next:

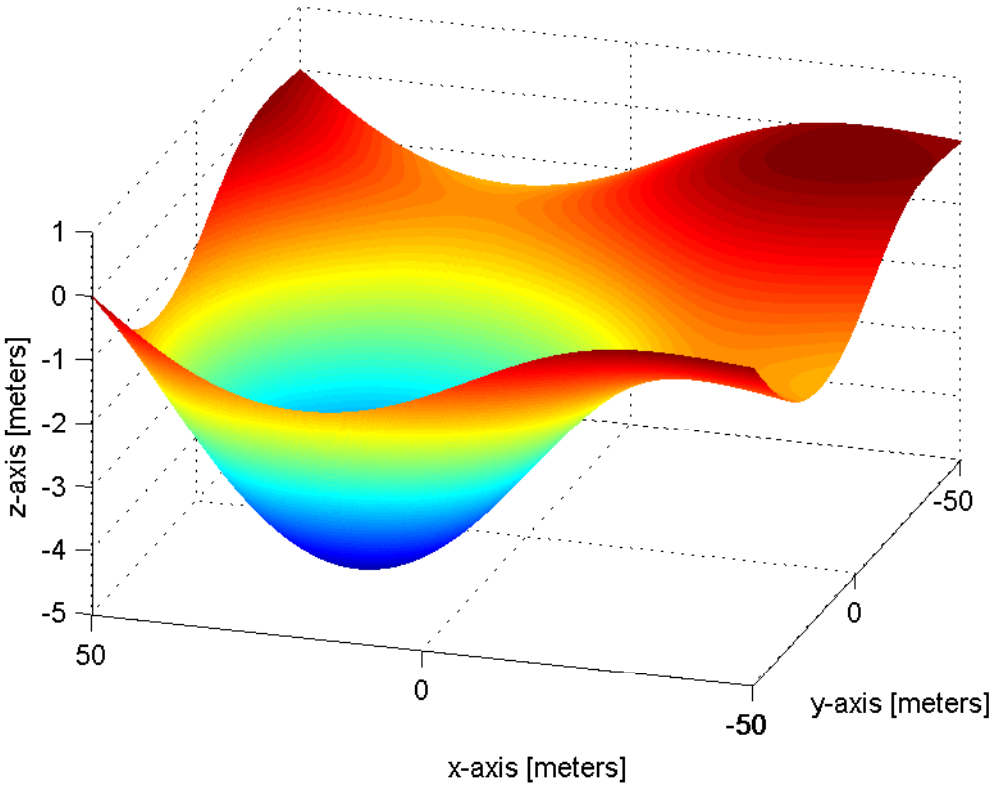

Figure 4.5: Sinusoid Sail Shape.

$$\mathbf{J}^1 = \begin{bmatrix} 0 \\ 0 \\ 1.0560E-001 \end{bmatrix}, \tag{4.61}$$

$$\mathbf{J}^2 = \begin{bmatrix} -1.7835E-004 & 5.6948E-010 & -3.9270E-006 \\ 5.6948E-010 & -1.7835E-004 & -3.9270E-006 \\ -3.9270E-006 & -3.9270E-006 & -4.2180E-002 \end{bmatrix}, \tag{4.62}$$

$$\mathbf{J}^3_{ij1} = \begin{bmatrix} -3.2865E-004 & -1.2754E-007 & 7.4675E-003 \\ -1.2754E-007 & -1.2754E-007 & -4.7843E-008 \\ 7.4675E-003 & -4.7843E-008 & 3.2878E-004 \end{bmatrix}, \tag{4.63}$$

$$\mathbf{J}^3_{ij2} = \begin{bmatrix} -1.2754E-007 & -1.2754E-007 & -4.7843E-008 \\ -1.2754E-007 & -3.2865E-004 & 7.4675E-003 \\ -4.7843E-008 & 7.4675E-003 & 3.2878E-004 \end{bmatrix}, \quad (4.64)$$

$$\mathbf{J}^3_{ij3} = \begin{bmatrix} 7.4675E-003 & -4.7843E-008 & 3.2878E-004 \\ -4.7843E-008 & 7.4675E-003 & 3.2878E-004 \\ 3.2878E-004 & 3.2878E-004 & 1.7739E+000 \end{bmatrix}, \quad (4.65)$$

$$\mathbf{K}^2 = \begin{bmatrix} -5.5317E-007 & 4.3586E-004 & 2.9039E-005 \\ -4.3586E-004 & 5.5317E-007 & -2.9039E-005 \\ 2.0073E-005 & -2.0073E-005 & 1.2131E-018 \end{bmatrix}, \quad (4.66)$$

$$\mathbf{K}^3_{ij1} = \begin{bmatrix} -5.2438E+000 & 1.0109E-006 & -4.6226E-005 \\ 5.2447E+000 & -1.0109E-006 & -1.8246E-002 \\ -4.6161E-005 & -9.0270E-019 & 8.3802E-004 \end{bmatrix}, \quad (4.67)$$

$$\mathbf{K}^3_{ij2} = \begin{bmatrix} 1.0109E-006 & -5.2446E+000 & 1.8246E-002 \\ -1.0109E-006 & 5.2439E+000 & 4.6226E-005 \\ -9.0615E-019 & 4.6161E-005 & -8.3802E-004 \end{bmatrix}, \quad (4.68)$$

$$\mathbf{K}^3_{ij3} = \begin{bmatrix} -4.6226E-005 & 1.8246E-002 & -5.2405E+000 \\ -1.8246E-002 & 4.6226E-005 & 5.2406E+000 \\ 8.3802E-004 & -8.3802E-004 & -1.8401E-017 \end{bmatrix}. \quad (4.69)$$

4.2 Comparison of Sail Geometries

Now that the coefficients for different sail models have been computed, let us compare the forces generated the flat sail, circular sail, and four-quadrant sail. This will be done by pitching the sail about the y_b body-fixed axis. The sail optical parameters were chosen as $\rho = 0.9$, $s = 1$, $B_f = 0.8$, $B_b = 0.55$, $\epsilon_f = 0.05$, $\epsilon_b = 0.3$. The flat sail area was chosen to be $10000m^2$. The circular sail is specified by $R_0 = 56.42m$ and $\alpha_{max} = 0.1$. All the sails have the same projected area (in the sail yx-plane)of $10000m^2$. The resultant normalized forces and normalized moments for all the geometries ate different sail attitudes are and shown in Figures 4.6 and 4.7, respectively.

Figure 4.6 shows that the force, normalized by the projected area, generated by all the sail geometries presented. The force along the z_b body-fixed axis is very similar their since their areas projected to the sun are very similar. The force along the x_b body-fixed axis presents differences for all the sail geometries. The flat sail produces the lowest magnitude force along this axis. The circular sail has the highest magnitude due to its concavity. The force from the sinusoid and four-panel sail are in between these two cases. The force along the y_b body-fixed axis is zero for all the sails for this specific maneuver and no plot is shown.

One effect that is present on flat solar sails is a moment that is dependent on the sail attitude as predicted in GSM. Figure 4.7 shows the moment, normalized by the sail area, solar radiation pressure, and characteristic length, for all the sail geometries except for the flat sail since its moment is zero. When the attitude is rotated about the x-axis, the moment along the x and z axes are zero for both the circular and four panel sail. Only the sinusoid sail generates a moment due to its

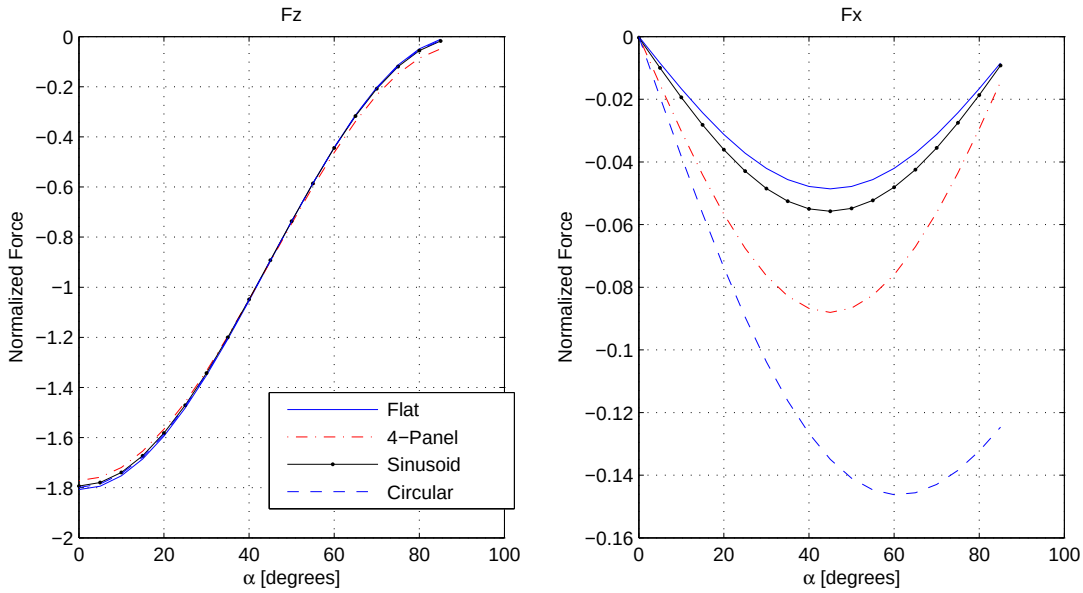

Figure 4.6: Normalized force comparison of different sail geometries.

asymmetries even when the sail is directly facing the sun . However, all the sails produce a moment along the y axis effected by their billow. The highest moment is produced by the sinusoid sail followed by the four panel sail and the circular sail.

4.3 GSM Partial Derivatives

In this section we derive the partial derivatives of the generalized sail model force equation. The partial derivatives are required when studying optimization of orbits and trajectories. We provide first and second order force partial derivatives as may be required by second-order gradient optimization algorithms. The first force partials are taken with respect to the position vector, and sail parameters and the second derivative of the force with respect to the position vector is also derived. The first and second force partials with respect to the control vector, consisting of the sun-sail angle and clock angle, are derived as well.

Several of the partial derivatives involve knowing the partial derivative of $\hat{\mathbf{r}}$ with

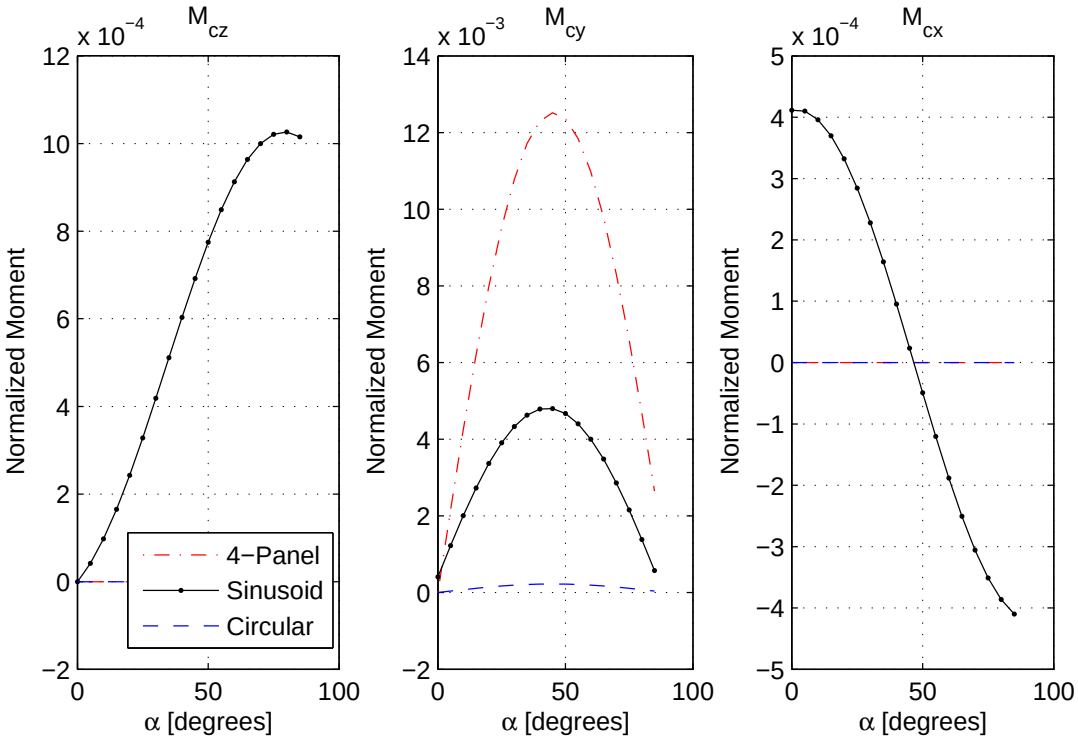

Figure 4.7: Normalized moment along the sail body-fixed axes.

respect to itself, which is given by:

$$\frac{\partial \hat{\mathbf{r}}}{\partial \hat{\mathbf{r}}} = \overline{\overline{\mathbf{U}}} - \hat{\mathbf{r}}\hat{\mathbf{r}} = \overline{\overline{\mathbf{U}}}_{\hat{\mathbf{r}}\hat{\mathbf{r}}}, \tag{4.70}$$

where $\overline{\overline{\mathbf{U}}}$ is the identity dyad. We note that any changes in $\hat{\mathbf{r}}$ will be perpendicular to its direction and cannot be along its direction, hence we see that $\overline{\overline{\mathbf{U}}}_{\hat{\mathbf{r}}\hat{\mathbf{r}}} \cdot \hat{\mathbf{r}} = 0$. Other derivatives that will be needed are:

$$\frac{\partial r}{\partial \mathbf{r}} = \frac{d(\mathbf{r}\cdot\mathbf{r})^{1/2}}{d\mathbf{r}} = (\mathbf{r}\cdot\mathbf{r})^{-1/2}\mathbf{r} = \hat{\mathbf{r}}, \tag{4.71}$$

$$\frac{\partial \hat{\mathbf{r}}}{\partial \mathbf{r}} = \frac{\partial}{\partial \mathbf{r}}\frac{\mathbf{r}}{(\mathbf{r}\cdot\mathbf{r})^{1/2}} = \frac{\overline{\overline{\mathbf{U}}}}{r} - \mathbf{r}\frac{\mathbf{r}}{r^3} = \frac{\overline{\overline{\mathbf{U}}}_{\hat{\mathbf{r}}\hat{\mathbf{r}}}}{r}. \tag{4.72}$$

4.3.1 First-Order Partial Derivatives of the Force Equation

Recall the force acting on a solar sail given by [27]:

$$\mathbf{F} \;=\; PA\Big[\mathbf{J}^2\cdot\hat{\mathbf{r}} - 2\hat{\mathbf{r}}\cdot\mathbf{J}^3\cdot\hat{\mathbf{r}} - (\mathbf{J}^1\cdot\hat{\mathbf{r}})\hat{\mathbf{r}}\Big]. \tag{4.73}$$

The $\mathbf{J}^m$ tensors are defined in Eqs. (3.24)-(3.26) [27]. The force can be thought as consisting of two functions. One being a function of r only, and the other a function of the unit position vector $\hat{\mathbf{r}}$. Thus, the force can be written as:

$$\mathbf{F} \;=\; P(r)\mathbf{P}(\hat{\mathbf{r}}). \tag{4.74}$$

The partial derivative of the force with respect to the position vector $\mathbf{r}$ can be expressed using the product rule as:

$$\frac{\partial\mathbf{F}(r,\hat{\mathbf{r}})}{\partial\mathbf{r}} \;=\; \frac{\partial P(r)}{\partial r}\frac{\partial r}{\partial\mathbf{r}}\mathbf{P}(\hat{\mathbf{r}}) + P(r)\frac{\partial\mathbf{P}(\hat{\mathbf{r}})}{\partial\hat{\mathbf{r}}}\cdot\frac{\partial\hat{\mathbf{r}}}{\partial\mathbf{r}}, \tag{4.75}$$

and in tensor notation:

$$\Big(\frac{\partial\mathbf{F}(r,\hat{\mathbf{r}})}{\partial\mathbf{r}}\Big)_{ij} \;=\; \frac{\partial P(r)}{\partial r}\hat{\mathbf{r}}_j\mathbf{P}_i(\hat{\mathbf{r}}) + \frac{P(r)}{r}\frac{\partial\mathbf{P}_i(\hat{\mathbf{r}})}{\partial\hat{\mathbf{r}}_k}\frac{\partial\hat{\mathbf{r}}_k}{\partial\mathbf{r}_j}. \tag{4.76}$$

The partial derivative of the force with respect to $\hat{\mathbf{r}}$ is given by:

$$\begin{aligned}\frac{\partial\mathbf{P}(\hat{\mathbf{r}})}{\partial\hat{\mathbf{r}}} \;&=\; \Big[a_2\mathbf{J}^2\cdot\overline{\overline{\mathbf{U}}}_{\hat{\mathbf{r}}\hat{\mathbf{r}}} - 2\rho s\hat{\mathbf{r}}\cdot(\mathbf{J}^3\cdot\overline{\overline{\mathbf{U}}}_{\hat{\mathbf{r}}\hat{\mathbf{r}}}) - 2\rho s(\mathbf{J}^3\cdot\hat{\mathbf{r}})\cdot\overline{\overline{\mathbf{U}}}_{\hat{\mathbf{r}}\hat{\mathbf{r}}} \\ &\quad -a_3\hat{\mathbf{r}}(\mathbf{J}^1\cdot\overline{\overline{\mathbf{U}}}_{\hat{\mathbf{r}}\hat{\mathbf{r}}}) - a_3(\mathbf{J}^1\cdot\hat{\mathbf{r}})\overline{\overline{\mathbf{U}}}_{\hat{\mathbf{r}}\hat{\mathbf{r}}}\Big] \\ &= \Big[a_2\mathbf{J}^2 - 4\rho s\hat{\mathbf{r}}\cdot\mathbf{J}^3 - a_3\hat{\mathbf{r}}\mathbf{J}^1 - a_3(\mathbf{J}^1\cdot\hat{\mathbf{r}})\overline{\overline{\mathbf{U}}}\Big]\cdot\overline{\overline{\mathbf{U}}}_{\hat{\mathbf{r}}\hat{\mathbf{r}}},\end{aligned} \tag{4.77}$$

or in tensor notation:

$$\Big(\frac{\partial \mathbf{P}(\hat{\mathbf{r}})}{\partial \hat{\mathbf{r}}}\Big)_{ik} = \Big[a_2\mathbf{J}^2_{ij} - 4\rho s\hat{\mathbf{r}}_m\mathbf{J}^3_{mij} - a_3\hat{\mathbf{r}}_i\mathbf{J}^1_j - a_3\mathbf{J}^1_m\hat{\mathbf{r}}_m\overline{\overline{\mathbf{U}}}_{ij}\Big]\overline{\overline{\mathbf{U}}}_{\hat{\mathbf{r}}\hat{\mathbf{r}}jk}, \quad (4.78)$$

note that:

$$\overline{\overline{\mathbf{U}}}_{\hat{\mathbf{r}}\hat{\mathbf{r}}} \cdot \overline{\overline{\mathbf{U}}}_{\hat{\mathbf{r}}\hat{\mathbf{r}}} = (\overline{\overline{\mathbf{U}}} - \hat{\mathbf{r}}\hat{\mathbf{r}}) \cdot (\overline{\overline{\mathbf{U}}} - \hat{\mathbf{r}}\hat{\mathbf{r}}) = \overline{\overline{\mathbf{U}}} - \hat{\mathbf{r}}\hat{\mathbf{r}} = \overline{\overline{\mathbf{U}}}_{\hat{\mathbf{r}}\hat{\mathbf{r}}}, \quad (4.79)$$

from which it follows that:

$$\Big(\frac{\partial \mathbf{P}(\hat{\mathbf{r}})}{\partial \hat{\mathbf{r}}}\Big)_{ik}\overline{\overline{\mathbf{U}}}_{\hat{\mathbf{r}}\hat{\mathbf{r}}kj} = \Big(\frac{\partial \mathbf{P}(\hat{\mathbf{r}})}{\partial \hat{\mathbf{r}}}\Big)_{ij}. \quad (4.80)$$

The partial derivative of the solar radiation pressure with respect to distance from the sun r is given by:

$$\frac{\partial P(r)}{\partial r} = -\frac{2\pi I_0 R_s^2}{cr^3}\sqrt{1 - \frac{R_s^2}{r^2}}. \quad (4.81)$$

With all the parameters defined, the force derivative with respect to the position vector $\mathbf{r}$ is given by:

$$\begin{aligned}\frac{\partial \mathbf{F}(r,\hat{\mathbf{r}})}{\partial \mathbf{r}} &= \frac{\partial P(r)}{\partial r}\hat{\mathbf{r}}\Big[a_2\mathbf{J}^2 \cdot \hat{\mathbf{r}} - 2\rho s\hat{\mathbf{r}} \cdot \mathbf{J}^3 \cdot \hat{\mathbf{r}} + a_3(\mathbf{J}^1 \cdot \hat{\mathbf{r}})\hat{\mathbf{r}}\Big] \\ &+ \frac{P(r)}{r}\Big[a_2\mathbf{J}^2 - 4\rho s\hat{\mathbf{r}} \cdot \mathbf{J}^3 - a_3\hat{\mathbf{r}}\mathbf{J}^1 - a_3(\mathbf{J}^1 \cdot \hat{\mathbf{r}})\overline{\overline{\mathbf{U}}}\Big] \cdot \overline{\overline{\mathbf{U}}}_{\hat{\mathbf{r}}\hat{\mathbf{r}}}, \quad (4.82)\end{aligned}$$

which in tensor notation is given by:

$$\begin{aligned}\mathbf{F}_{\mathbf{r}ij} &= \frac{\partial P(r)}{\partial r}\hat{\mathbf{r}}_j\Big[a_2\mathbf{J}^2_{il}\hat{\mathbf{r}}_l - 2\rho s\hat{\mathbf{r}}_l\mathbf{J}^3_{lik}\hat{\mathbf{r}}_k + a_3\mathbf{J}^1_l\hat{\mathbf{r}}_l\hat{\mathbf{r}}_i\Big] \\ &+ \frac{P(r)}{r}\Big[a_2\mathbf{J}^2_{il} - 4\rho s\hat{\mathbf{r}}_m\mathbf{J}^3_{mil} - a_3\hat{\mathbf{r}}_i\mathbf{J}^1_l - a_3\mathbf{J}^1_m\hat{\mathbf{r}}_m\delta_{il}\Big]\overline{\overline{\mathbf{U}}}_{\hat{\mathbf{r}}\hat{\mathbf{r}}lj}, \quad (4.83)\end{aligned}$$

where δ is the Kronecker delta function.

The force partial derivatives with respect to the optical parameters ρ and s are given by:

$$\frac{\partial \mathbf{F}}{\partial \rho} = P(r)\Big[\mathbf{J}^2 \cdot \hat{\mathbf{r}}\frac{\partial a_2}{\partial \rho} - 2s\hat{\mathbf{r}} \cdot \mathbf{J}^3 \cdot \hat{\mathbf{r}} - (\mathbf{J}^1 \cdot \hat{\mathbf{r}})\hat{\mathbf{r}}\frac{\partial a_3}{\partial \rho}\Big]$$
$$= P(r)\Big[\mathbf{J}^2 \cdot \hat{\mathbf{r}}(B_f(1-s) - \frac{\epsilon_f B_f - \epsilon_b B_b}{\epsilon_f + \epsilon_b}) - 2s\hat{\mathbf{r}} \cdot \mathbf{J}^3 \cdot \hat{\mathbf{r}} + (\mathbf{J}^1 \cdot \hat{\mathbf{r}})\hat{\mathbf{r}}s\Big], \tag{4.84}$$

$$\frac{\partial \mathbf{F}}{\partial s} = P(r)\Big[\mathbf{J}^2 \cdot \hat{\mathbf{r}}\frac{\partial a_2}{\partial s} - 2\rho\hat{\mathbf{r}} \cdot \mathbf{J}^3 \cdot \hat{\mathbf{r}} - (\mathbf{J}^1 \cdot \hat{\mathbf{r}})\hat{\mathbf{r}}\frac{\partial a_3}{\partial s}\Big]$$
$$= P(r)\Big[- \mathbf{J}^2 \cdot \hat{\mathbf{r}}B_f\rho - 2\rho\hat{\mathbf{r}} \cdot \mathbf{J}^3 \cdot \hat{\mathbf{r}} + (\mathbf{J}^1 \cdot \hat{\mathbf{r}})\hat{\mathbf{r}}\rho\Big], \tag{4.85}$$

$$\begin{aligned}\frac{\partial \mathbf{F}}{\partial B_f} &= P(r)\Big[\mathbf{J}^2 \cdot \hat{\mathbf{r}}\frac{\partial a_2}{\partial B_f}\Big] \\ &= P(r)\Big[\mathbf{J}^2 \cdot \hat{\mathbf{r}}\Big((1-s)\rho + (1-\rho)\frac{\epsilon_f}{\epsilon_f + \epsilon_b}\Big)\Big].\end{aligned} \tag{4.86}$$

The force partial derivative with respect to B_b, ϵ_f, and ϵ_b are given by:

$$\begin{aligned}\frac{\partial \mathbf{F}}{\partial B_b} &= P(r)\mathbf{J}^2 \cdot \hat{\mathbf{r}}\frac{\partial a_2}{\partial B_b} \\ &= -P(r)\mathbf{J}^2 \cdot \hat{\mathbf{r}}(1-\rho)\frac{\epsilon_b}{\epsilon_f + \epsilon_b},\end{aligned} \tag{4.87}$$

$$\begin{aligned}\frac{\partial \mathbf{F}}{\partial \epsilon_f} &= P(r)\Big[\mathbf{J}^2 \cdot \hat{\mathbf{r}}\frac{\partial a_2}{\partial \epsilon_f}\Big] \\ &= P(r)\Big[\mathbf{J}^2 \cdot \hat{\mathbf{r}}(1-\rho)\frac{B_f}{\epsilon_f + \epsilon_b} - \mathbf{J}^2 \cdot \hat{\mathbf{r}}(1-\rho)\frac{\epsilon_f B_f - \epsilon_b B_b}{(\epsilon_f + \epsilon_b)^2}\Big],\end{aligned} \tag{4.88}$$

$$\begin{aligned}\frac{\partial \mathbf{F}}{\partial \epsilon_b} &= P(r)\Big[\mathbf{J}^2 \cdot \hat{\mathbf{r}}\frac{\partial a_2}{\partial \epsilon_b}\Big] \\ &= P(r)\Big[- \mathbf{J}^2 \cdot \hat{\mathbf{r}}(1-\rho)\frac{B_b}{\epsilon_f + \epsilon_b} - \mathbf{J}^2 \cdot \hat{\mathbf{r}}(1-\rho)\frac{\epsilon_f B_f - \epsilon_b B_b}{(\epsilon_f + \epsilon_b)^2}\Big].\end{aligned} \tag{4.89}$$

Note that the last four equations are linearly dependent and can be expressed in terms of a known partial derivative. For instance, taking the partial of the force with respect to B_f as our basis, the other partial derivatives can be expressed as:

$$\frac{\partial \mathbf{F}}{\partial B_f} = c_1 \frac{\partial \mathbf{F}}{\partial B_b}, \tag{4.90}$$

$$\frac{\partial \mathbf{F}}{\partial B_f} = c_2 \frac{\partial \mathbf{F}}{\partial B_b}, \tag{4.91}$$

$$\frac{\partial \mathbf{F}}{\partial \epsilon_f} = c_3 \frac{\partial \mathbf{F}}{\partial B_b}, \tag{4.92}$$

where

$$c_1 = -\frac{1-\rho}{(1-s)\rho + \frac{\epsilon_f}{\epsilon_b}(1-s\rho)}, \tag{4.93}$$

$$c_2 = -\frac{B_b + B_f}{\epsilon_f + \epsilon_b} \frac{1-\rho}{(1-s)\rho + \frac{\epsilon_f}{\epsilon_b}(1-s\rho)}, \tag{4.94}$$

$$c_3 = \frac{B_b + B_f}{\epsilon_f + \epsilon_b} \frac{1-\rho}{\frac{\epsilon_f}{\epsilon_b}(1-s)\rho + (1-s\rho)}. \tag{4.95}$$

4.4 Second-Order Force Partial Derivatives

The second force partial wrt to the position vector $\mathbf{r}$ follows from Eq. 4.76:

$$\begin{aligned}\frac{\partial^2 \mathbf{F}(\mathbf{r})}{\partial \mathbf{r}^2} &= \frac{\partial^2 P(r)}{\partial r^2}\frac{\partial r}{\partial \mathbf{r}}\hat{\mathbf{r}}\mathbf{P}(\hat{\mathbf{r}}) + \frac{\partial P(r)}{\partial r}\frac{\partial \hat{\mathbf{r}}}{\partial \mathbf{r}}\mathbf{P}(\hat{\mathbf{r}}) + \frac{\partial P(r)}{\partial r}\hat{\mathbf{r}}\frac{\partial \mathbf{P}(\hat{\mathbf{r}})}{\partial \hat{\mathbf{r}}} \cdot \frac{\partial \hat{\mathbf{r}}}{\partial \mathbf{r}} \\ &+ \frac{\partial}{\partial r}\Big(\frac{P(r)}{r}\Big)\frac{\partial r}{\partial \mathbf{r}}\Big(\frac{\partial \mathbf{P}(\hat{\mathbf{r}})}{\partial \hat{\mathbf{r}}} \cdot \overline{\overline{\mathbf{U}}}_{\hat{\mathbf{r}}\hat{\mathbf{r}}}\Big) + \frac{P(r)}{r}\Big(\frac{\partial}{\partial \hat{\mathbf{r}}}\Big)\Big(\frac{\partial \mathbf{P}(\hat{\mathbf{r}})}{\partial \hat{\mathbf{r}}} \cdot \overline{\overline{\mathbf{U}}}_{\hat{\mathbf{r}}\hat{\mathbf{r}}}\Big) \cdot \frac{\partial \hat{\mathbf{r}}}{\partial \mathbf{r}},\end{aligned} \tag{4.96}$$

or in tensor form:

$$\mathbf{F}_{\mathbf{rr}ijk} = \frac{\partial^2 P(r)}{\partial r^2}\hat{\mathbf{r}}_k \mathbf{P}_i(\hat{\mathbf{r}})\hat{\mathbf{r}}_j + \frac{\partial P(r)}{\partial r}\mathbf{P}_i(\hat{\mathbf{r}})\frac{\overline{\overline{\mathbf{U}}}_{\hat{\mathbf{r}}\hat{\mathbf{r}}jk}}{r} + \frac{\partial P(r)}{\partial r}\hat{\mathbf{r}}_j\Big(\frac{\partial \mathbf{P}(\hat{\mathbf{r}})}{\partial \hat{\mathbf{r}}}\Big)_{im}\frac{\overline{\overline{\mathbf{U}}}_{\hat{\mathbf{r}}\hat{\mathbf{r}}mk}}{r}$$
$$+\frac{\partial}{\partial r}\Big(\frac{P(r)}{r}\Big)\frac{\partial \mathbf{P}_i(\hat{\mathbf{r}})}{\partial \hat{\mathbf{r}}_j}\hat{\mathbf{r}}_k + \frac{P(r)}{r}\Big(\frac{\partial}{\partial \hat{\mathbf{r}}_m}\frac{\partial \mathbf{P}_i(\hat{\mathbf{r}})}{\partial \hat{\mathbf{r}}_j}\Big)\frac{\overline{\overline{\mathbf{U}}}_{\hat{\mathbf{r}}\hat{\mathbf{r}}mk}}{r}. \quad (4.97)$$

Some of these terms have already been defined. The rest are derived next. The second partial with respect to $\hat{\mathbf{r}}$ is:

$$\Big(\frac{\partial}{\partial \hat{\mathbf{r}}}\Big(\frac{\partial \mathbf{P}(\hat{\mathbf{r}})}{\partial \hat{\mathbf{r}}}\cdot\overline{\overline{\mathbf{U}}}_{\hat{\mathbf{r}}\hat{\mathbf{r}}}\Big)\Big)_{ikn} = \Big[-4\rho s\overline{\overline{\mathbf{U}}}_{\hat{\mathbf{r}}\hat{\mathbf{r}}nm}\mathbf{J}^3_{mij} - a_3\mathbf{J}^1_j\overline{\overline{\mathbf{U}}}_{\hat{\mathbf{r}}\hat{\mathbf{r}}in} - a_3\mathbf{J}^1_m\overline{\overline{\mathbf{U}}}_{\hat{\mathbf{r}}\hat{\mathbf{r}}mn}\delta_{ij}\Big]\overline{\overline{\mathbf{U}}}_{\hat{\mathbf{r}}\hat{\mathbf{r}}jk}$$
$$+\Big[a_2\mathbf{J}^2_{il} - 4\rho s\hat{\mathbf{r}}_m\mathbf{J}^3_{mil} - a_3\hat{\mathbf{r}}_i\mathbf{J}^1_l - a_3\mathbf{J}^1_m\hat{\mathbf{r}}_m\overline{\overline{\mathbf{U}}}_{il}\Big]\Big(\frac{\partial\overline{\overline{\mathbf{U}}}_{\hat{\mathbf{r}}\hat{\mathbf{r}}}}{\partial\hat{\mathbf{r}}}\Big)_{lkn} \quad (4.98)$$

We also need the second Partial with respect to the distance from the sun r:

$$\frac{\partial^2 P(r)}{\partial r^2} = \frac{2\pi I_0 R_s^2}{cr^6}(3r^2 - 4Rs^2)\Big(1 - \frac{R_s^2}{r^2}\Big)^{-1/2}, \quad (4.99)$$

and

$$\frac{\partial}{\partial r}\Big(\frac{P(r)}{r}\Big) = \frac{2\pi I_0}{3cr^4}\Big[-r^2 + r^2\Big(1 - \frac{R_s^2}{r^2}\Big)^{1/2} - 4Rs^2\Big(1 - \frac{R_s^2}{r^2}\Big)^{1/2}\Big]. \quad (4.100)$$

The last term needed is:

$$\frac{\partial\overline{\overline{\mathbf{U}}}_{\hat{\mathbf{r}}\hat{\mathbf{r}}}}{\partial\hat{\mathbf{r}}} = -\overline{\overline{\mathbf{U}}}_{\hat{\mathbf{r}}\hat{\mathbf{r}}}\hat{\mathbf{r}} - \hat{\mathbf{r}}\overline{\overline{\mathbf{U}}}_{\hat{\mathbf{r}}\hat{\mathbf{r}}}, \quad (4.101)$$

which can be expressed in tensor notation:

$$\Big(\frac{\partial\overline{\overline{\mathbf{U}}}_{\hat{\mathbf{r}}\hat{\mathbf{r}}}}{\partial\hat{\mathbf{r}}}\Big)_{ijk} = -\overline{\overline{\mathbf{U}}}_{\hat{\mathbf{r}}\hat{\mathbf{r}}ki}\hat{\mathbf{r}}_j - \hat{\mathbf{r}}_i\overline{\overline{\mathbf{U}}}_{\hat{\mathbf{r}}\hat{\mathbf{r}}jk}. \quad (4.102)$$

4.5 Force Partial Derivatives with respect to Control Angles

The force partial with respect to the control sun-sail-line angle α and the clock angle δ can be expressed using the product rule:

$$\frac{\partial \mathbf{F}}{\partial \alpha} = \mathbf{F}_{\hat{\mathbf{r}}} \cdot \hat{\mathbf{r}}_{\alpha}, \tag{4.103}$$

$$\frac{\partial \mathbf{F}}{\partial \delta} = \mathbf{F}_{\hat{\mathbf{r}}} \cdot \hat{\mathbf{r}}_{\delta}, \tag{4.104}$$

where $\mathbf{F}_{\hat{\mathbf{r}}}$, $\hat{\mathbf{r}}_{\alpha}$, and $\hat{\mathbf{r}}_{\delta}$ are defined as:

$$\mathbf{F}_{\hat{\mathbf{r}}} = \frac{\partial \mathbf{F}}{\partial \hat{\mathbf{r}}}, \tag{4.105}$$

$$\hat{\mathbf{r}}_{\alpha} = \frac{\partial \hat{\mathbf{r}}}{\partial \alpha}, \tag{4.106}$$

$$\hat{\mathbf{r}}_{\delta} = \frac{\partial \hat{\mathbf{r}}}{\partial \delta}. \tag{4.107}$$

In tensor form $\mathbf{F}_{\hat{\mathbf{r}}}$ is:

$$\mathbf{F}_{\hat{\mathbf{r}}ik} = \frac{P(r)}{r}\Big[a_2\mathbf{J}^2_{il} - 4\rho s\hat{\mathbf{r}}_m\mathbf{J}^3_{mil} - a_3\mathbf{J}^1_i\hat{\mathbf{r}}_l - a_3\mathbf{J}^1_m\hat{\mathbf{r}}_m\delta_{il}\Big]\overline{\overline{\mathbf{U}}}_{\hat{\mathbf{r}}\hat{\mathbf{r}}lk}. \tag{4.108}$$

The unit position vector can be written in terms of the sun-line angle α and the cone angle δ_n in the sail-fixed frame as:

$$\hat{\mathbf{r}} = \begin{bmatrix} -\cos\delta\sin\alpha \\ -\sin\delta\sin\alpha \\ -\cos\alpha \end{bmatrix}, \tag{4.109}$$

where δ_n is taken in the positive sense from the x-body-fixed axis.

Now the partial derivatives with respect to the sun-line angle can be evaluated:

$$\hat{\mathbf{r}}_{\alpha} = \begin{bmatrix} -\cos\delta\cos\alpha \\ -\sin\delta\cos\alpha \\ \sin\alpha \end{bmatrix}, \tag{4.110}$$

and for the cone angle:

$$\hat{\mathbf{r}}_\delta = \begin{bmatrix} \sin\delta\sin\alpha \\ -\cos\delta\sin\alpha \\ 0 \end{bmatrix}. \tag{4.111}$$

The force partial with respect to the control vector $\mathbf{u} = [\alpha, \delta]^T$ is:

$$\mathbf{F}_u = \begin{bmatrix} \mathbf{F}_\alpha^T \\ \mathbf{F}_\delta^T \end{bmatrix}. \tag{4.112}$$

4.6 Second Order Force Partial with respect to Control Angles

The second force partial derivatives with respect to the control angles are again obtained using the product rule:

$$\frac{\partial^2\mathbf{F}}{\partial\alpha^2} = \frac{\partial\mathbf{F}_{\hat{\mathbf{r}}}}{\partial\alpha}\cdot\hat{\mathbf{r}}_\alpha + \mathbf{F}_{\hat{\mathbf{r}}}\cdot\hat{\mathbf{r}}_{\alpha\alpha} \tag{4.113}$$

$$\frac{\partial^2\mathbf{F}}{\partial\delta^2} = \frac{\partial\mathbf{F}_{\hat{\mathbf{r}}}}{\partial\delta}\cdot\hat{\mathbf{r}}_\delta + \mathbf{F}_{\hat{\mathbf{r}}}\cdot\hat{\mathbf{r}}_{\delta\delta} \tag{4.114}$$

$$\frac{\partial^2\mathbf{F}}{\partial\delta\alpha} = \frac{\partial\mathbf{F}_{\hat{\mathbf{r}}}}{\partial\delta}\cdot\hat{\mathbf{r}}_\alpha + \mathbf{F}_{\hat{\mathbf{r}}}\cdot\hat{\mathbf{r}}_{\alpha\delta}, \tag{4.115}$$

where $\hat{\mathbf{r}}_{\alpha\alpha} = \partial^2\hat{\mathbf{r}}/\partial\alpha^2$, and similarly for $\hat{\mathbf{r}}_{\delta\delta}$, and $\hat{\mathbf{r}}_{\alpha\delta}$. Now:

$$\frac{\partial\mathbf{F}_{\hat{\mathbf{r}}}}{\partial\alpha} = \frac{\partial\mathbf{F}_{\hat{\mathbf{r}}}}{\partial\hat{\mathbf{r}}}\cdot\frac{\partial\hat{\mathbf{r}}}{\partial\alpha} = \mathbf{F}_{\hat{\mathbf{r}}\hat{\mathbf{r}}}\cdot\hat{\mathbf{r}}_\alpha. \tag{4.116}$$

Computing each of the terms we obtain: Second Partial with respect to $\hat{\mathbf{r}}$:

$$\mathbf{F}_{\hat{\mathbf{r}}\hat{\mathbf{r}}ikn} = \frac{P(r)}{r}[-4\rho s\overline{\overline{\mathbf{U}}}_{\hat{\mathbf{r}}\hat{\mathbf{r}}nm}\mathbf{J}^3_{mil} - a_3\mathbf{J}^1_i\overline{\overline{\mathbf{U}}}_{\hat{\mathbf{r}}\hat{\mathbf{r}}ln} - a_3\mathbf{J}^1_m\overline{\overline{\mathbf{U}}}_{\hat{\mathbf{r}}\hat{\mathbf{r}}mn}\delta_{il}\Big]\overline{\overline{\mathbf{U}}}_{\hat{\mathbf{r}}\hat{\mathbf{r}}lk} \tag{4.117}$$

$$+\frac{P(r)}{r}\Big[a_2\mathbf{J}^2_{il} - 4\rho s\hat{\mathbf{r}}_m\mathbf{J}^3_{mil} - a_3\mathbf{J}^1_i\hat{\mathbf{r}}_l - a_3\mathbf{J}^1_m\hat{\mathbf{r}}_m\overline{\overline{\mathbf{U}}}_{il}\Big]\Big(\frac{\partial\overline{\overline{\mathbf{U}}}_{\hat{\mathbf{r}}\hat{\mathbf{r}}}}{\partial\hat{\mathbf{r}}}\Big)_{lkn}, \tag{4.118}$$

and similarly for δ. The second partial derivatives of $\hat{\mathbf{r}}$ with respect to the control angles are:

$$\hat{\mathbf{r}}_{\alpha\alpha} = \begin{bmatrix} \cos\delta\sin\alpha \\ \sin\delta\sin\alpha \\ \cos\alpha \end{bmatrix}, \tag{4.119}$$

for the cone angle:

$$\hat{\mathbf{r}}_{\delta\delta} = \begin{bmatrix} \cos\delta\sin\alpha \\ \sin\delta\sin\alpha \\ 0 \end{bmatrix}, \tag{4.120}$$

and:

$$\hat{\mathbf{r}}_{\alpha\delta} = \begin{bmatrix} \sin\delta\cos\alpha \\ -\cos\delta\cos\alpha \\ 0 \end{bmatrix}. \tag{4.121}$$

The second partial of the force with respect to the control angles are:

$$\mathbf{F}_{\alpha\alpha i} = \mathbf{F}_{\hat{\mathbf{r}}\hat{\mathbf{r}}ikn}\hat{\mathbf{r}}_{\alpha k}\hat{\mathbf{r}}_{\alpha n} + \mathbf{F}_{\hat{\mathbf{r}}ik}\hat{\mathbf{r}}_{\alpha\alpha k}, \tag{4.122}$$

$$\mathbf{F}_{\delta\delta i} = \mathbf{F}_{\hat{\mathbf{r}}\hat{\mathbf{r}}ikn}\hat{\mathbf{r}}_{\delta k}\hat{\mathbf{r}}_{\delta n} + \mathbf{F}_{\hat{\mathbf{r}}ik}\hat{\mathbf{r}}_{\delta\delta k}, \tag{4.123}$$

$$\mathbf{F}_{\alpha\delta i} = \mathbf{F}_{\hat{\mathbf{r}}\hat{\mathbf{r}}ikn}\hat{\mathbf{r}}_{\alpha k}\hat{\mathbf{r}}_{\delta n} + \mathbf{F}_{\hat{\mathbf{r}}ik}\hat{\mathbf{r}}_{\alpha\delta k}. \tag{4.124}$$

Then the second partial with respect to the control vector $\mathbf{u}$ is:

$$\mathbf{F}_{uuij1} = \begin{bmatrix} \mathbf{F}_{\alpha\alpha}^T \\ \mathbf{F}_{\alpha\delta}^T \end{bmatrix}, \tag{4.125}$$

$$\mathbf{F}_{uuij2} = \begin{bmatrix} \mathbf{F}_{\delta\alpha}^T \\ \mathbf{F}_{\delta\delta}^T \end{bmatrix}. \tag{4.126}$$

4.7 Locally Optimal Control Laws

One advantage to having closed-form equations for the force acting on a solar sail is that we are able to easily define explicit control and guidance laws. In the following examples we take the advantage of this to implement simple guidance and orientation laws for a non-ideal sail. This examples are just meant to showcase how the GSM can be used analytically, and not meant to provide new results or optimal sail guidance laws.

4.7.1 Maximum Energy Increase

In Reference [32], a guidance law, using the sun-sail angle as the controller, was developed to find optimum escape trajectories from the sun using flat, ideal sails. In this section we extend the locally optimal control law developed in [32] to a four-quadrant non-ideal billowed solar sail. To accomplish this, the Gauss variational equation relating the semi-major axis change with respect to the true anomaly can be written as:

$$\frac{da}{df} = \frac{2pr^2}{\mu(1-e^2)^2} \begin{bmatrix} e\sin f \\ 0 \\ 1+e\cos f \end{bmatrix} \cdot \mathbf{F}_p, \tag{4.127}$$

where μ is the sun's gravitational parameter, e is the orbit eccentricity, f is the true anomaly, and $\mathbf{F}_p$ is the force expressed in local polar coordinates, p is the semi-latus rectum, r is the distance form the sun, and a is the orbit semi-major axis. A

coordinate transformation T is needed to obtain $\mathbf{F}_p$, as $\mathbf{F}_p = T \cdot \mathbf{F}$, where $\mathbf{F}$ is the sail force in the body-fixed frame. The relationship between these two coordinate frames is shown in Figure 4.8.

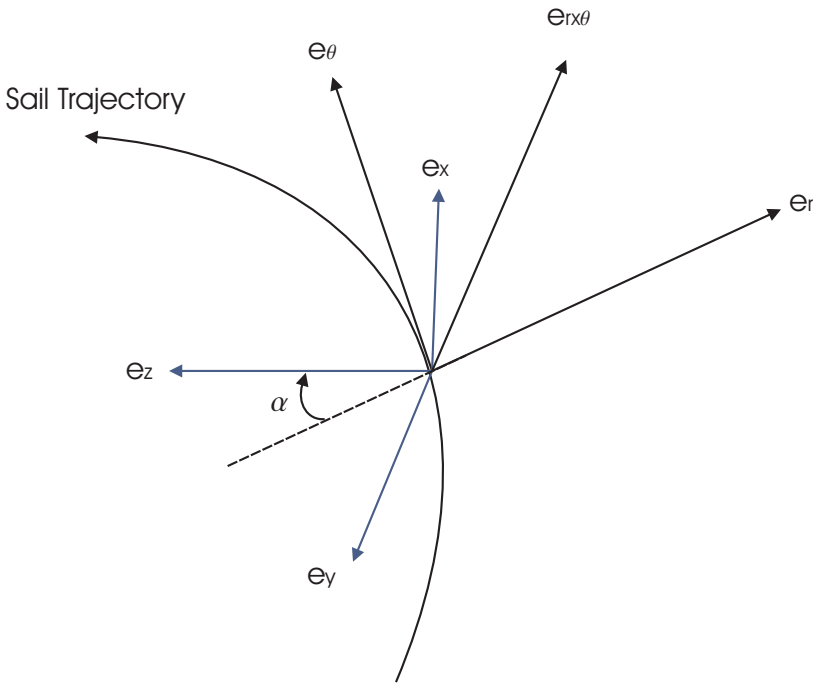

Figure 4.8: Local polar coordinate frame and sail body-fixed frame.

We only consider changes in the sail position and attitude in the orbit plane (i.e., set $\delta_f \equiv 0$). Then T is given by:

$$T = \begin{bmatrix} -\sin\alpha & 0 & -\cos\alpha \\ 0 & -1 & 0 \\ \cos\alpha & 0 & -\sin\alpha \end{bmatrix}, \tag{4.128}$$

where $\mathbf{F}_p$ has radial F_r, out of plane $F_{r\times\theta}$, and transverse F_θ force components. Finding the maximum energy increase at any point on the sail trajectory is equivalent to finding the maximum rate of change of da/df with respect to the sun-sail angle. Taking the partial derivative of Eq. (4.129) yields:

$$\frac{\partial}{\partial\alpha}\Big(\frac{\partial\mathbf{a}}{\partial f}\Big) = \frac{2pr^2}{\mu(1-e^2)^2}\begin{bmatrix} e\sin f \\ 0 \\ 1+e\cos f \end{bmatrix}\cdot\Big(\frac{\partial T}{\partial\alpha}\cdot\mathbf{F} + T\cdot\frac{\partial\mathbf{F}}{\partial\alpha}\Big). \tag{4.129}$$

The partial of T with respect to α is readily obtained from Eq. (4.128) and the partial of $\mathbf{F}$ with respect to α is given by Eq. (4.103). Setting the above equation equal to zero for the square-billowed sail model (coefficients found in Section 4.1.3), the optimal angle satisfies the relation:

$$\begin{aligned} 0 \;=\; & 1.9201(1+e\cos f) - 5.7604e\sin f\tan\alpha - 3.7804(1+e\cos f)\tan^2\alpha \\ & -0.0599e\sin f\tan^3\alpha. \end{aligned} \tag{4.130}$$

The solution of Eq. (4.130) is chosen so that Eq. (4.127) is maximized. The control law equation is close to the solution for an ideal flat solar sail. The force acting on an ideal flat sail in the local polar frame is given by:

$$\mathbf{F}_p = 2P(r)A\begin{bmatrix} \cos^3\alpha \\ 0 \\ \sin\alpha\cos^2\alpha \end{bmatrix}. \tag{4.131}$$

With this information the equation for the optimum angle is obtained from:

$$0 = 2(1+e\cos f) - 6e\sin f\tan\alpha - 4(1+e\cos f)\tan^2\alpha. \tag{4.132}$$

The solution of the above equation is obtained by solving the quadratic equation for $\tan\alpha$ and is presented in [32]. Both the ideal and the optimum control laws can be compared now on the squared-billowed sail model. Figure 6.2 is polar plot of the

orbit change using both guidance laws starting at 1 AU during a time of one year. The optimum control law has a faster energy increase, as expected. The orbital energy increase for both guidance laws is shown in Figure 4.10, which clearly shows that the non-ideal guidance law is optimum. The values for the optical parameters used in the simulation were $\rho = 0.9$, $s = 1$, $B_f = 0.8$, $B_b = 0.5$, $\epsilon_f = 0.05$, $\epsilon_b = 0.3$ and the mass chosen was $80kg$.

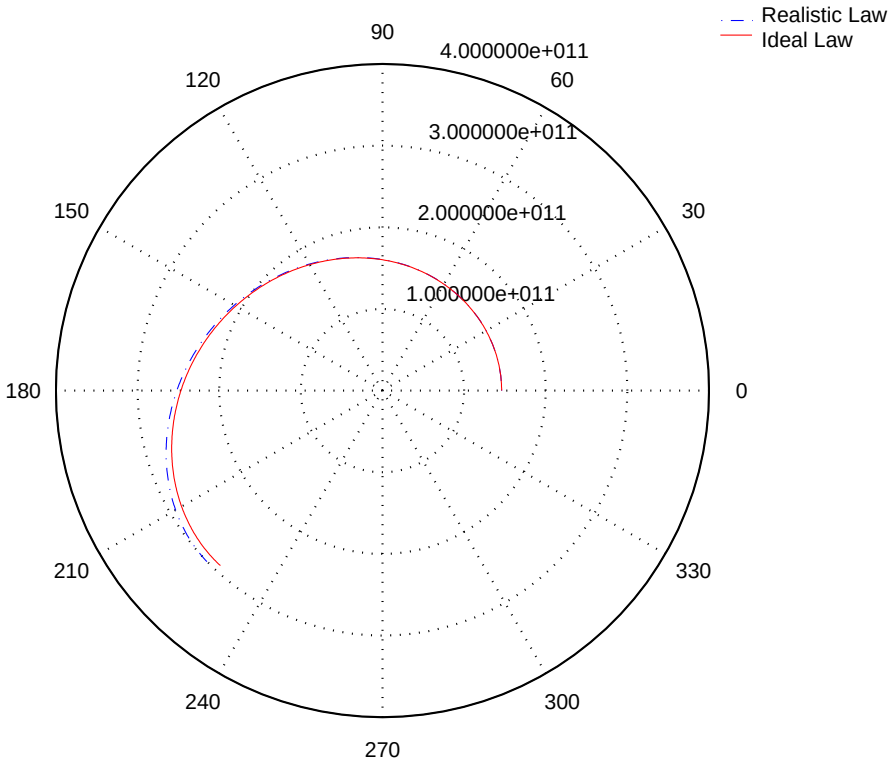

Figure 4.9: Trajectories for realistic and ideal guidance laws.

Thus, it was shown that the generalized sail model can be applied to more complex sail geometries resulting in more realistic guidance laws development.

4.7.2 Maximum Propulsive Force

As another example, we can compute the planar orientation that gives the maximum propulsive force on the sail. This can be found by differentiating the square

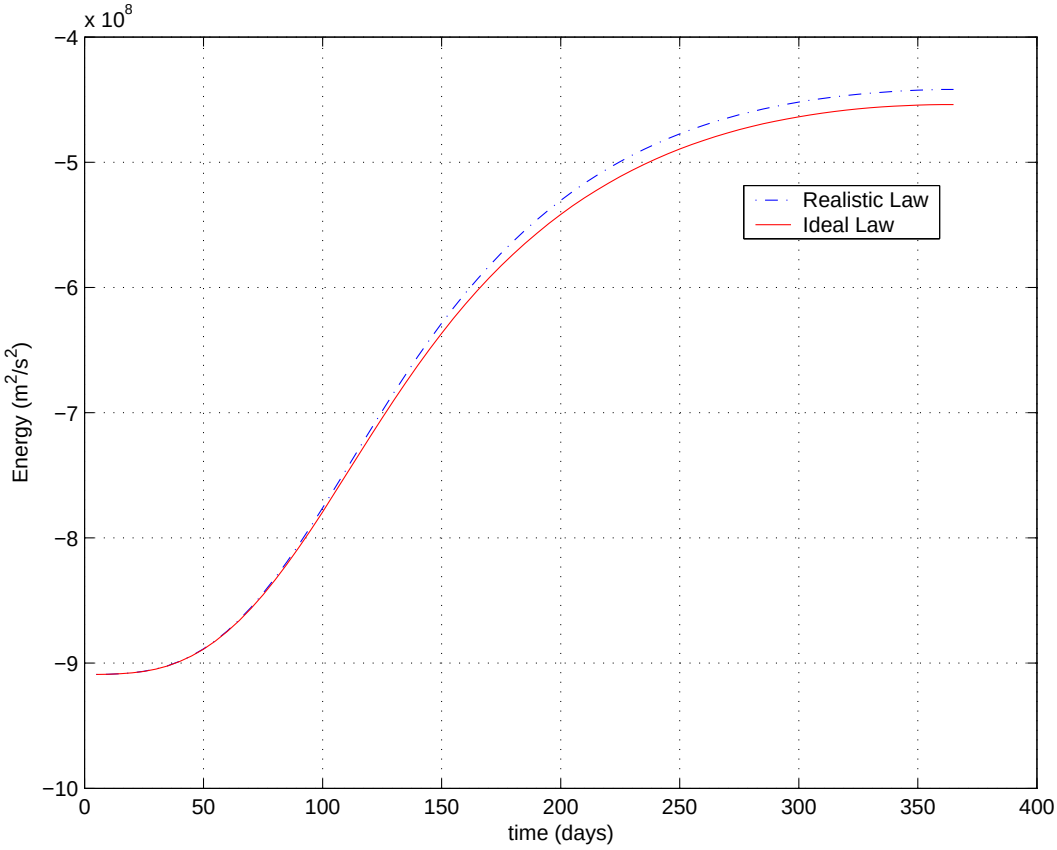

Figure 4.10: Energy increase for realistic and ideal guidance laws.

of the force magnitude with respect to the sun-sail angle and setting the resulting expression equal to zero:

$$\frac{\partial(\mathbf{F}\cdot\mathbf{F})}{\partial\alpha} = 2\mathbf{F}\cdot\frac{\partial\mathbf{F}}{\partial\alpha} = 0. \tag{4.133}$$

The corresponding equation for the four-quadrant sail example is:

$$\Big(-3.3735 - 3.3040\cos 2\alpha\Big)\cos\alpha\sin\alpha = 0, \tag{4.134}$$

which has its extrema when α equals 0, $\pi/2$, π, and $3\pi/2$. The term in the parenthesis is zero for α complex. These solutions are the same as that of an ideal solar sail. When $\alpha = 0$, the maximum force is achieved, and with α equal to $\pi/2$ or $3\pi/2$, the

force is zero. Finally, the solution $\alpha = \pi$ implies that the sail is facing away from the sun, an orientation we do not consider. This simple result occurs due to the overall symmetry of the four quadrant sail.

Now we consider a more general situation. Let us find the sun-sail angle that provides the maximum force for only one quadrant of the square-billowed sail whose force tensors coefficients are given in Section 4.1.3. Following the same procedure as for the complete sail, the equation that needs to be satisfied is now:

$$-83.806 - 759.262 \tan\alpha + 248.428 \tan^2\alpha - 27.134 \tan^3\alpha + \tan^4\alpha = 0. \quad (4.135)$$

This equation has only two real solutions, -6.096^0 and 83.913^0. The first solution maximizes the force on the sail; the sign is negative due to the quadrant position with respect to the overall sail (the opposite quadrant would have the reverse sign on the solutions). The second solution minimizes the force on the sail. These examples showcase the ease with which we can work with complex sail shapes using the generalized sail model.

4.8 Applications of GSM to NASA's S5 Project

The study of mission design for solar sails possesses some unique problems that cannot be fully studied with tools existing for other type of spacecraft. Some of these issues are the sail controllability and the fact that the thrust vector is dependent on the sail attitude [12]. The Solar Sail Spaceflight Simulation Software (S5) is an integrated set of high fidelity software modules that enables the analysis of the optimal design of solar sail trajectories and of the guidance, navigation and control of these missions. Prior to S5 there was no single integrated tool that allowed this analysis [7].

S5 is a modular tool composed of several subroutines that can used in conjunction to study all the aspects of a solar sail mission or individually to study a specific part of the mission.

The Mission Design Module (OPT) determines the optimal trajectory and sail optimal control with respect to a given performance criteria subject to control and/or state constraints. A second order-gradient optimization algorithm is used to converge to the optimal trajectory, which uses the force partial derivatives of the GSM developed in Section 4.3.

The Solar Radiation Pressure Module (SRP) models the force and moment acting on the sail due to the solar radiation pressure, which are used by the OPT, ADC, and DET modules. The inputs for the SRP are the sail physical characteristics and optical properties, sailcraft state and attitude, and attitude control vanes (if available) position relative to the sail to compute the thrust and the total torque due to solar radiation pressure.

The Attitude Dynamics and Control Module (ADC) simulates the rotational dynamics of the solar sail, including torque induced by solar radiation pressure, environmental disturbances such as gravity gradient, aerodynamic, and magnetic moment, and conventional spacecraft actuators such as reaction wheel assembly and thrusters. Some of the attitude control methods used are articulated control vanes located at the sail tips and mass displacement. The ADC module takes into account structural dynamical effects.

The Trajectory Control Module (TCN) updates the thrust control profile based on the current estimate of the spacecraft state, provided by the Orbit Determination Module, and the nominal sail state trough a feedback control law. TCN uses the gain matrix from OPT and feedback control laws to update the control and predict the

updated target conditions. The commanded controls are fed into the ADC module.

The Orbit Determination Module (DET) simulates the navigation of the solar sail. DET propagates the equations of motion, simulates ground based and on board observations and processes the observables with a Kalman type filter to estimate the current state and statistics. DTE allows for covariance analysis or Monte Carlo studies.

The integrated version of S5 illustrating all the interaction and data flow between modules is shown in Figure 4.11.

Some of the outputs to evaluate the performance consists of optimal trajectories, control profiles and measures of performance, sailcraft attitude, angular velocity and angular acceleration, sailcraft control surface deflection angles for vanes systems, estimates and uncertainties of spacecraft position and and other dynamic parameters [7].

The organizations involved in the development of S5 were the Jet Propulsion Laboratory in charge of the OPT and DTE modules as well as integrating of all the modules into a complete software package. The University of Michigan which contributed in the development of SRP module, force and moment parameter estimation, and force partial derivatives. Ball Aerospace was in charge of the ADC module. The University of Colorado developed the TCN module. LGarde Inc. provided nominal sail design shape and measured force and moment characterization. NASA Marshall supervised the development of S5 to fulfill requirements, to stay on schedule, and to evaluate the progress on each of the three phases of development.

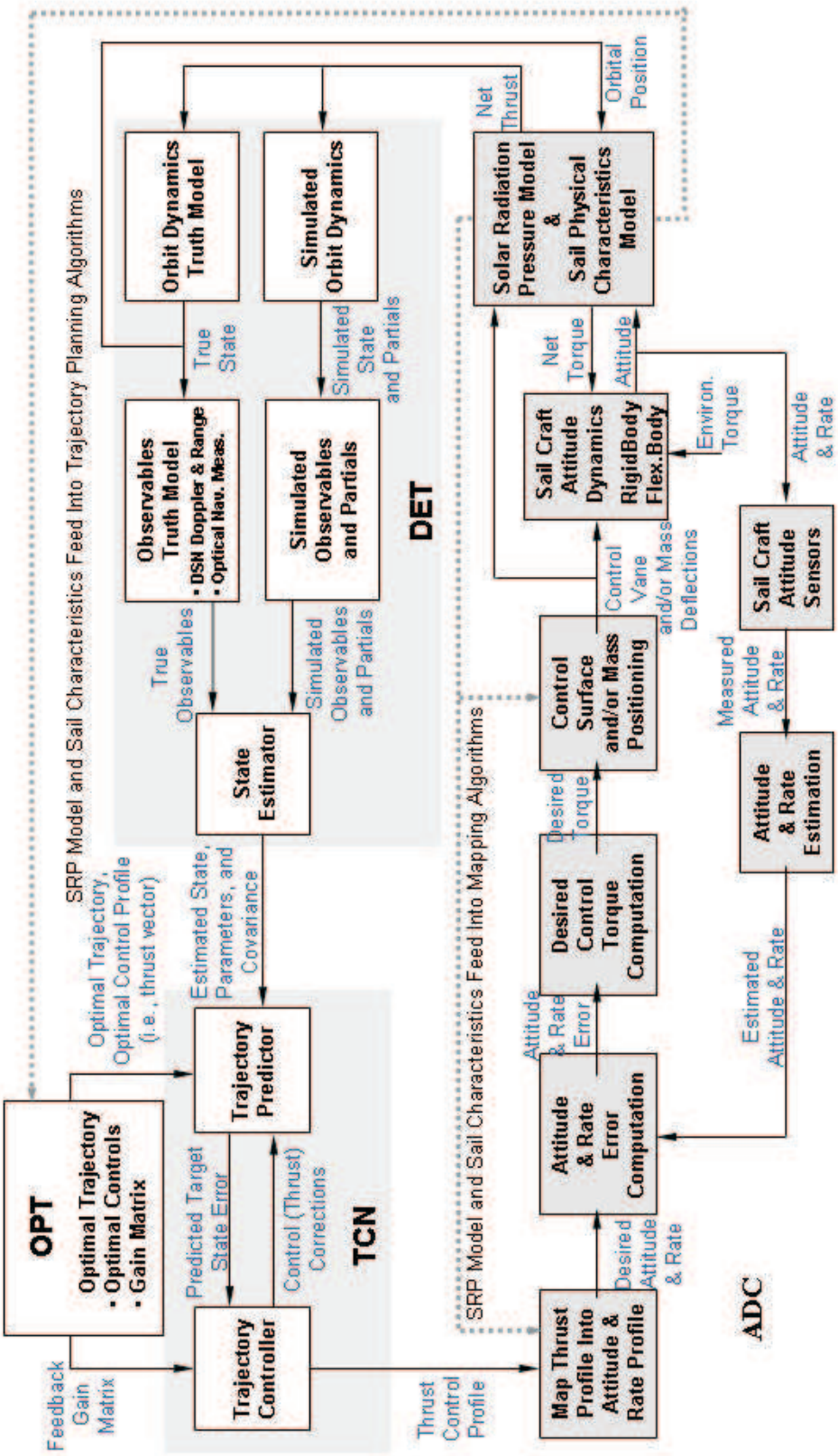

Figure 4.11: Integration of S5.

CHAPTER V

Estimation: Force, Moment, and Optical Parameters

As with all space missions, success depends on having a precise spacecraft model. Initial mission planning can be performed based on data from ground measurements. However, due to the complexity of sail shapes a refinement of the sail propulsion model will be necessary after launch for navigating the sail to its target. Sail wrinkles after in-space deployment, deformation from ideal shapes, and surface degradation due to the space environment[20] are some of the effects that make pre-launch sail propulsion determination inaccurate.

The generalized sail model [27] allows for the analytic computation of forces and moments acting on a solar sail of arbitrary fixed shape. The generalized equations for the sail force and moment are linear in the GSM coefficients. This fact and its analytic nature allows us to develop linear estimation methods for these coefficients using measured accelerations and moments as input data. The force and moment tensor coefficients are estimated using a least-squares algorithm from simulated navigation data and predictions from finite element models of solar sails. The estimation results are highly dependent on the attitudes at which the sail navigation data is taken. It is not only important to take measurements at several different sun-relative attitudes,

but also to find those attitudes that capture the geometry of the sail. The accuracy of the estimates will vary for different data sampling strategies. Here, we present several data sampling examples and comment on their impact to the accuracy of the estimation results.

5.1 Linear Estimation of GSM Tensor Coefficients

In the following the sail force and moments are reported in a normalized form by dividing the force values by the solar radiation pressure and total sail area and the moments by an additional reference length l_r [5]. Thus, the force and moment vectors can be written as:

$$\mathbf{F} = PA\mathbf{C}_F, \tag{5.1}$$

$$\mathbf{M} = PAl_r\mathbf{C}_M, \tag{5.2}$$

where $\mathbf{C}$ is a vector containing the normalized values with the subscripts denoting force or moment.

In the following we assume that the navigation data is reported as normalized force and moment vectors. The normalized version of the GSM equations are:

$$\mathbf{F}_c = \mathbf{J}^2 \cdot \hat{\mathbf{r}} - 2\hat{\mathbf{r}} \cdot \mathbf{J}^3 \cdot \hat{\mathbf{r}} - (\mathbf{J}^1 \cdot \hat{\mathbf{r}})\hat{\mathbf{r}}, \tag{5.3}$$

$$\mathbf{M}_c = \mathbf{K}^2 \cdot \hat{\mathbf{r}} + \hat{\mathbf{r}} \cdot \mathbf{K}^3 \cdot \hat{\mathbf{r}}. \tag{5.4}$$

Force and moment can be obtained from measurements taken through on-board instruments such as inertial measurement units, gyroscopes, and with ground tracking. Note that the measured on-board rotational accelerations must be related, via

the moment of inertia, to the total moment acting on the sailcraft. We do not consider the estimation of the inertia tensor or sailcraft mass in our current work.

5.2 Force and Moment in Linear Form

The normalized force and moment are linear in all the coefficients of the $\mathbf{J}^m$ and $\mathbf{K}^m$ tensors, thus a least-squares estimation can be easily employed for finding the best values of the tensor coefficients. But before this step is done, it is necessary to manipulate the equations and write them in a more useful way as the product of a matrix and a vector. The matrix contains information on the sail attitude while the vector contains the tensor coefficients that need to be estimated. Thus, the normalized force can be written as:

$$\mathbf{F}_c = \quad \mathbf{A}_F(\hat{\mathbf{r}})\mathbf{J}, \tag{5.5}$$

where the matrix $\mathbf{A}_F$ is 3×19 and a function of the sail attitude alone, and $\mathbf{J}$ is a 19×1 vector containing the independent force tensor coefficients.

The force matrix is defined as follows:

$$\mathbf{A}_F = \begin{bmatrix} -\mathbf{A}_{F1} & \mathbf{A}_{F2} & -2\mathbf{A}_{F3} \end{bmatrix}, \tag{5.6}$$

where

$$\mathbf{A}_{F1} = \begin{bmatrix} \hat{r}_1^2 & \hat{r}_1\hat{r}_2 & \hat{r}_1\hat{r}_3 \\ \hat{r}_1\hat{r}_2 & \hat{r}_2^2 & \hat{r}_2\hat{r}_3 \\ \hat{r}_1\hat{r}_3 & \hat{r}_2\hat{r}_3 & \hat{r}_3^2 \end{bmatrix}, \tag{5.7}$$

$$\mathbf{A}_{F2} = \begin{bmatrix} \hat{r}_1 & \hat{r}_2 & \hat{r}_3 & 0 & 0 & 0 \\ 0 & \hat{r}_1 & 0 & \hat{r}_2 & \hat{r}_3 & 0 \\ 0 & 0 & \hat{r}_1 & 0 & \hat{r}_2 & \hat{r}_3 \end{bmatrix}, \tag{5.8}$$

$$\mathbf{A}_{F3} = \begin{bmatrix} \hat{r}_1^2 & 2\hat{r}_1\hat{r}_2 & \hat{r}_2^2 & 2\hat{r}_2\hat{r}_3 & 2\hat{r}_1\hat{r}_3 & \hat{r}_3^2 & 0 & 0 & 0 & 0 \\ 0 & \hat{r}_1^2 & 2\hat{r}_1\hat{r}_2 & 2\hat{r}_1\hat{r}_3 & 0 & 0 & \hat{r}_2^2 & 2\hat{r}_2\hat{r}_3 & \hat{r}_3^2 & 0 \\ 0 & 0 & 0 & 2\hat{r}_1\hat{r}_2 & \hat{r}_1^2 & 2\hat{r}_1\hat{r}_3 & 0 & \hat{r}_2^2 & 2\hat{r}_2\hat{r}_3 & \hat{r}_3^2 \end{bmatrix}. \tag{5.9}$$

For one measurement the rank of $\mathbf{A}_f$ is 3. Thus, more than one measurement is needed to estimate a uniquely a full set of force coefficients. This is accomplished by taking at least 7 measurements at different sun-sail attitudes. The force coefficient vector is

$$\mathbf{J} = \begin{bmatrix} J_1^1 & J_2^1 & J_3^1 & J_{11}^2 & J_{12}^2 & J_{13}^2 & J_{22}^2 & J_{23}^2 & J_{33}^2 & J_{111}^3 & \cdots \\ \cdots & J_{121}^3 & J_{221}^3 & J_{231}^3 & J_{131}^3 & J_{331}^3 & J_{222}^3 & J_{232}^3 & J_{332}^3 & J_{333}^3 \end{bmatrix}^T. \tag{5.10}$$

Similarly, the moment equation also can be written as the product of a matrix, which contains information on the sail attitude at which the measurements are taken, and a vector, which includes the information of the moment tensor coefficients:

$$\mathbf{M}_c = \mathbf{A}_M \mathbf{K}, \tag{5.11}$$

where

$$\mathbf{A}_M = \begin{bmatrix} \mathbf{A}_{M2} & \mathbf{A}_{M3} \end{bmatrix}, \tag{5.12}$$

$$\mathbf{A}_{M2} = \begin{bmatrix} \hat{r}_1 & \hat{r}_2 & \hat{r}_3 & 0 & 0 & 0 & 0 & 0 & 0 \\ 0 & 0 & 0 & \hat{r}_1 & \hat{r}_2 & \hat{r}_3 & 0 & 0 & 0 \\ 0 & 0 & 0 & 0 & 0 & 0 & \hat{r}_1 & \hat{r}_2 & \hat{r}_3 \end{bmatrix}, \tag{5.13}$$

$$\mathbf{A}_{M3} = \begin{bmatrix} \hat{r}_1^2 & \hat{r}_1\hat{r}_2 & \hat{r}_1\hat{r}_3 & \hat{r}_1\hat{r}_2 & \hat{r}_2^2 & \hat{r}_2\hat{r}_3 & \hat{r}_1\hat{r}_3 & \hat{r}_2\hat{r}_3 & \hat{r}_3^2 & \cdots \\ 0 & \hat{r}_1^2 & 0 & 0 & \hat{r}_1\hat{r}_2 & 0 & 0 & \hat{r}_1\hat{r}_3 & 0 & \cdots \\ 0 & 0 & \hat{r}_1^2 & 0 & 0 & \hat{r}_1\hat{r}_2 & 0 & 0 & \hat{r}_1\hat{r}_3 & \cdots \end{bmatrix}$$

$$\begin{bmatrix} 0 & 0 & 0 & 0 & 0 & 0 & 0 & 0 & 0 \\ \hat{r}_1\hat{r}_2 & \hat{r}_1\hat{r}_3 & \hat{r}_2^2 & \hat{r}_2\hat{r}_3 & \hat{r}_2\hat{r}_3 & \hat{r}_3^2 & 0 & 0 & 0 \\ 0 & \hat{r}_1\hat{r}_2 & 0 & \hat{r}_2^2 & 0 & \hat{r}_2\hat{r}_3 & \hat{r}_1\hat{r}_3 & \hat{r}_2\hat{r}_3 & \hat{r}_3^2 \end{bmatrix}. \tag{5.14}$$

$\mathbf{A}_M$ is rank-3 in general. Since the moment requires 27 coefficients at least 9 measurements are necessary. There are, however, certain attitudes that must be avoided to have a full rank matrix. With 9 measurements a matrix of rank-27 can be achieved under the conditions that no measurements are taken when either $\hat{r}_1$ or $\hat{r}_2$ are equal to zero or equal to $\hat{r}_3$, or when $\hat{r}_1 = \hat{r}_2$. Thus, if the above requirements hold for the moment measurements, then the coefficients of $\mathbf{K}^2$ and $\mathbf{K}^3$ can be determined uniquely. The vector with the moment coefficients is:

$$\mathbf{K} = \begin{bmatrix} K_{11}^2 & K_{12}^2 & K_{13}^2 & K_{21}^2 & K_{22}^2 & K_{23}^2 & K_{31}^2 & K_{32}^2 & K_{33}^2 & K_{111}^3 & K_{121}^3 & K_{131}^3 & \cdots \end{bmatrix}$$

$$\cdots \quad K^3_{211} \quad K^3_{221} \quad K^3_{231} \quad K^3_{311} \quad K^3_{321} \quad K^3_{331} \quad K^3_{122} \quad K^3_{132} \quad K^3_{222} \quad K^3_{232} \quad \cdots$$

$$\cdots \quad K^3_{322} \quad K^3_{332} \quad K^3_{133} \quad K^3_{233} \quad K^3_{333} \Big]^T . \tag{5.15}$$

5.3 Least-Squares Estimation

For estimating the GSM tensor coefficients, a least-squares cost function is employed with the assumption of N measurements taken at different sun-relative attitudes. A covariance matrix P_{cc}, associated with the measurements $\mathbf{y}$, is given by:

$$P_{cc} = \mathbb{E}\left[(\mathbf{y}_j - \overline{\mathbf{y}}_j)(\mathbf{y}_j - \overline{\mathbf{y}}_j)^T\right], \tag{5.16}$$

where $\mathbb{E}[\ ]$ is the expected value operator. Ideally

$$P_{cc} = \begin{bmatrix} \sigma_\omega^2 & 0 & 0 \\ 0 & \sigma_\omega^2 & 0 \\ 0 & 0 & \sigma_\omega^2 \end{bmatrix}, \tag{5.17}$$

which is the covariance matrix for uncorrelated measurements with variance σ_ω^2. Note that the $\mathbf{y}_j$ vectors are either normalized force or moment measurements, depending on the application.

The least-squares cost function is defined as the square of the error between the measurements and the values due to estimated coefficients. Hence it is given by

$$V = \frac{1}{2}\sum_{j=1}^{N} \left(\mathbf{y}_j - \mathbf{A}_j\mathbf{x}\right)^T P_{cc}^{-1} \left(\mathbf{y}_j - \mathbf{A}_j\mathbf{x}\right), \tag{5.18}$$

where $\mathbf{y}_j$ are the normalized vector measurements obtained at an attitude corresponding to $\hat{\mathbf{r}}_j$, $\mathbf{A}_j$ is the corresponding matrix to $\mathbf{A}_F(\hat{\mathbf{r}}_j)$ or $\mathbf{A}_M(\hat{\mathbf{r}}_j)$, and $\mathbf{x}$ is $\mathbf{J}$ or $\mathbf{K}$. To minimize the error we take the partial derivative with respect to the GSM tensor coefficients and set it equal to zero:

$$\begin{aligned} \frac{\partial V}{\partial \mathbf{x}} &= \frac{1}{2}\sum_{j=1}^{N}\left[-\mathbf{A}_j^T P_{cc}^{-1}\left(\mathbf{y}_j - \mathbf{A}_j\mathbf{x}\right) - \left(\mathbf{y}_j - \mathbf{A}_j\mathbf{x}\right)^T \mathbf{A}_j^T P_{cc}^{-1}\right] \\ &= \sum_{j=1}^{N}\left[-\mathbf{A}_j^T P_{cc}^{-1}\left(\mathbf{y}_j - \mathbf{A}_j\mathbf{x}\right)\right] = 0, \end{aligned} \tag{5.19}$$

multiplying out:

$$\sum_{j=1}^{N}\left[-\mathbf{A}_j^T P_{cc}^{-1}\mathbf{y}_j + \mathbf{A}_j^T P_{cc}^{-1}\mathbf{A}_j\mathbf{x}\right] = 0. \tag{5.20}$$

Define the information matrix as:

$$\Lambda_{xx} = \sum_{j=1}^{N}\mathbf{A}_j^T P_{cc}^{-1}\mathbf{A}_j. \tag{5.21}$$

If the information matrix is non-singular, then a unique estimate can be found. For the force tensor coefficients $\mathbf{A}_j \in \mathbb{R}^{3\times 19}$, thus $\mathbf{A}_j^T\mathbf{A}_j$ has at best rank 3 for an individual measurement. Hence, at least 7 measurements are necessary for a unique solution to be feasible. For the moment tensor coefficients $\mathbf{A}_j \in \mathbb{R}^{3\times 27}$, meaning that at least 9 measurements are needed for a unique solution. Note that $\hat{\mathbf{r}}_j$ must span a rich enough set of values for Λ_{xx} to be non-singular. A trivial example is if the attitude never changes or only switches between a limited set of attitudes. Thus, to ensure a robust solution requires that a full set of attitudes be sampled by taking measurements at different sail attitudes and avoiding the attitudes that introduce singularities as mentioned earlier.

The covariance matrix of the estimates is $P_{xx} = \Lambda_{xx}^{-1}$. Then, the solution of the estimation problem can be written as [13]:

$$\mathbf{x} = P_{xx} \sum_{j=1}^{N} \mathbf{A}_j^T P_{cc}^{-1} \mathbf{y}_j. \tag{5.22}$$

Defining the data vector $\mathbf{Z}$ as:

$$\mathbf{Z} = \sum_{j=1}^{N} \mathbf{A}_j^T P_{cc}^{-1} \mathbf{y}_j, \tag{5.23}$$

the solution of $\mathbf{x}$ can be expressed in a compact more form as:

$$\mathbf{x} = P_{xx} \mathbf{Z}. \tag{5.24}$$

5.3.1 Predicted Force and Moment Uncertainty

Note that the predicted normalized force and moment at an attitude $\hat{\mathbf{r}}$ can then be written in the form

$$\mathbf{y} = \mathbf{A}(\hat{\mathbf{r}}) P_{xx} \mathbf{Z}, \tag{5.25}$$

where the matrix $\mathbf{A}(\hat{\mathbf{r}})$ is a function of the attitude and $\mathbf{y}$ is the predicted force or moment.

Uncertainties in the tensor coefficients translate into force or moment uncertainties. The mapping from tensor coefficients uncertainties into normalized vector uncertainties is given by:

$$\delta \mathbf{y} = \mathbf{A}(\hat{\mathbf{r}}) \delta \mathbf{x}. \tag{5.26}$$

The covariance of the estimates is obtained by

$$P_{yy} = \mathbb{E}[\delta\mathbf{y}\delta\mathbf{y}^T] = \mathbf{A}(\hat{\mathbf{r}})\mathbb{E}[\delta\mathbf{x}\delta\mathbf{x}^T]\mathbf{A}^T(\hat{\mathbf{r}}), \tag{5.27}$$

which is just

$$P_{yy} = \mathbf{A}(\hat{\mathbf{r}})P_{xx}\mathbf{A}^T(\hat{\mathbf{r}}), \tag{5.28}$$

where P_{xx} is the covariance of the estimated GSM tensor coefficients, and equals Λ_{xx}^{-1}. P_{xx} allows us to place bounds on the errors of the force and moment estimation. Thus, the force and moment covariance at a given attitude are

$$P_{FF} = \mathbf{A}_F(\hat{\mathbf{r}})P_{JJ}\mathbf{A}_F^T(\hat{\mathbf{r}}), \tag{5.29}$$

$$P_{MM} = \mathbf{A}_M(\hat{\mathbf{r}})P_{KK}\mathbf{A}_M^T(\hat{\mathbf{r}}), \tag{5.30}$$

respectively.

5.4 Numerical Linear Estimation

Due to the lack of actual navigation data, the square sinusoid sail, developed in Chapter IV, was used to generate simulated forces and moments at different sail attitudes. These force and moments were used to recover the force and moment tensors using the estimation algorithm developed and the results are shown next.

5.4.1 Force Estimation

The results from the estimation are dependent on how the sampling of the measurements is performed as is shown in the following test cases and can be seen from Eqs. (5.24) and (5.21) as $\mathbf{A}$ is dependent on the sail attitude when data is collected. In these figures, the covariance of each force tensor coefficient is shown as well as the correlation between them. Four cases with 70 measurements each, but with

different measurement sampling attitudes, were used for estimating the tensor coefficients. Comparison between their respective covariance and correlations are shown in Figures 5.5-5.12.

The case studies are defined as follows: Case I has measurements running along the two diagonals 45^0 from the x and y body-fixed axes as shown in Figure 5.1.

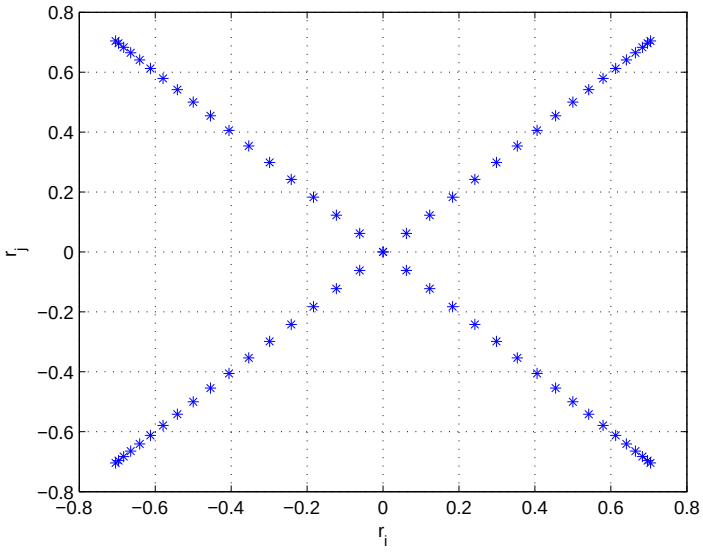

Figure 5.1: Case I. Projected attitude measurements

Case II has measurements taken along the x and y body-fixed axes as shown in Figure 5.2.

Case III forms a 4-loop curve in the xy-plane, while Case IV forms a spiral as shown in Figures 5.3 and 5.4.

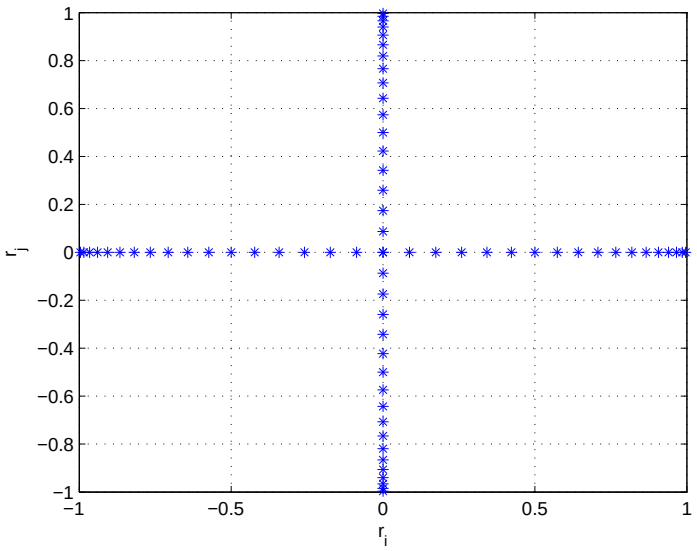

Figure 5.2: Case II. Projected attitude measurements

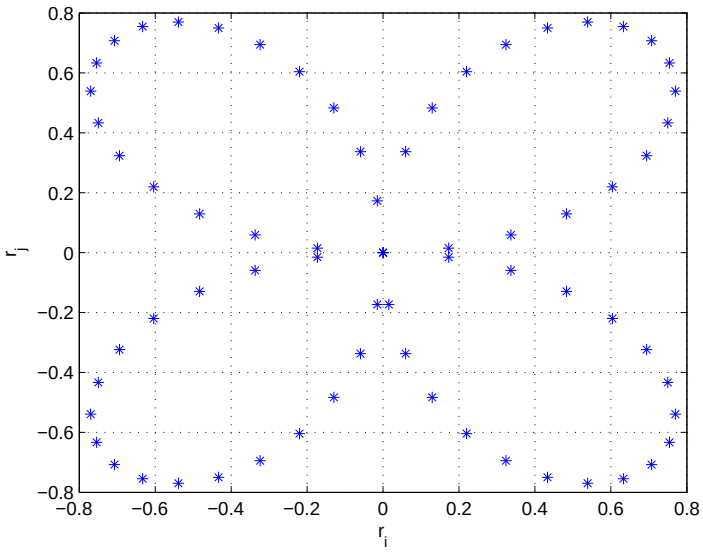

Figure 5.3: Case III. Projected attitude measurements

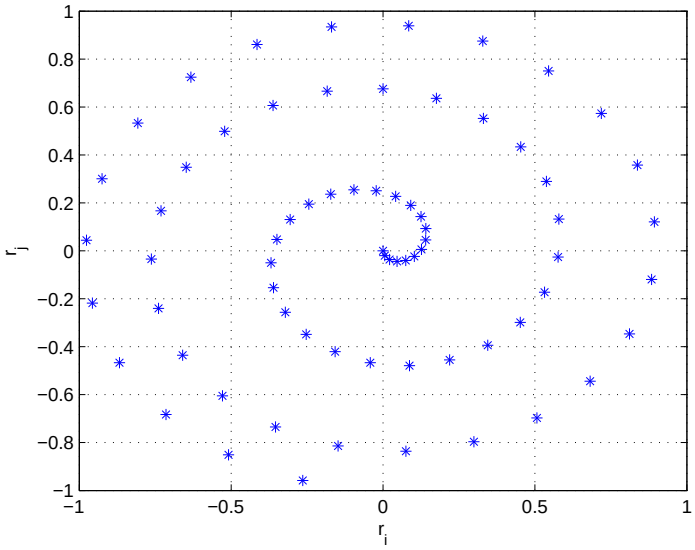

Figure 5.4: Case IV. Projected attitude measurements

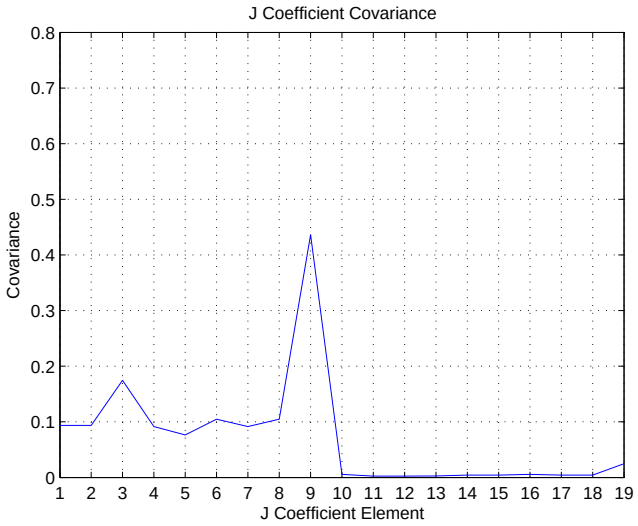

Figure 5.5: Case I. Covariance of GSM force coefficients

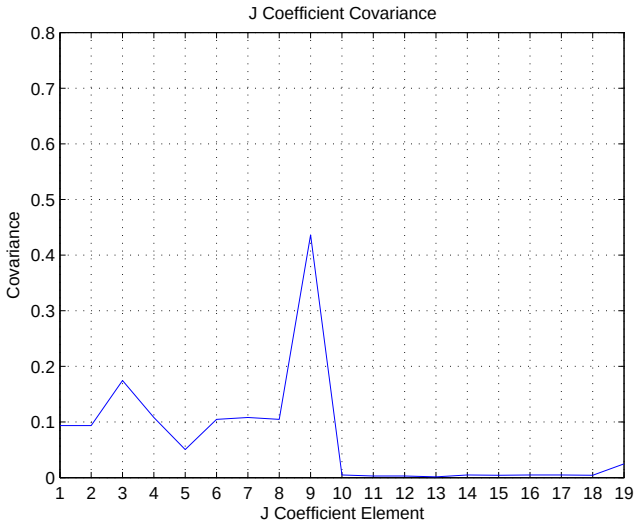

Figure 5.6: Case II. Covariance of GSM force coefficients

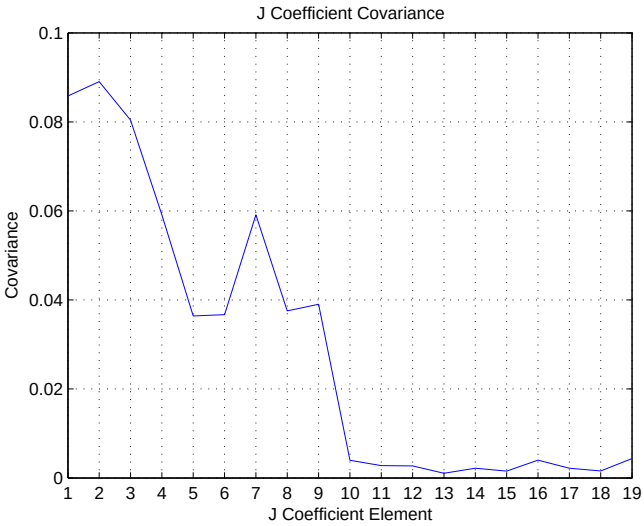

Figure 5.7: Case III. Covariance of GSM force coefficients

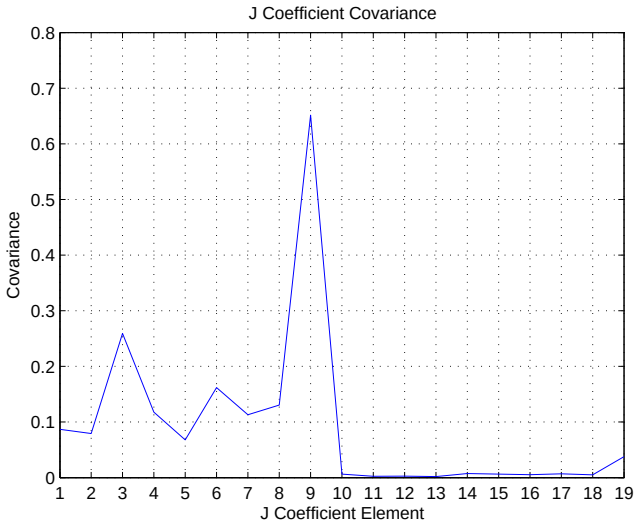

Figure 5.8: Case IV. Covariance of GSM force coefficients

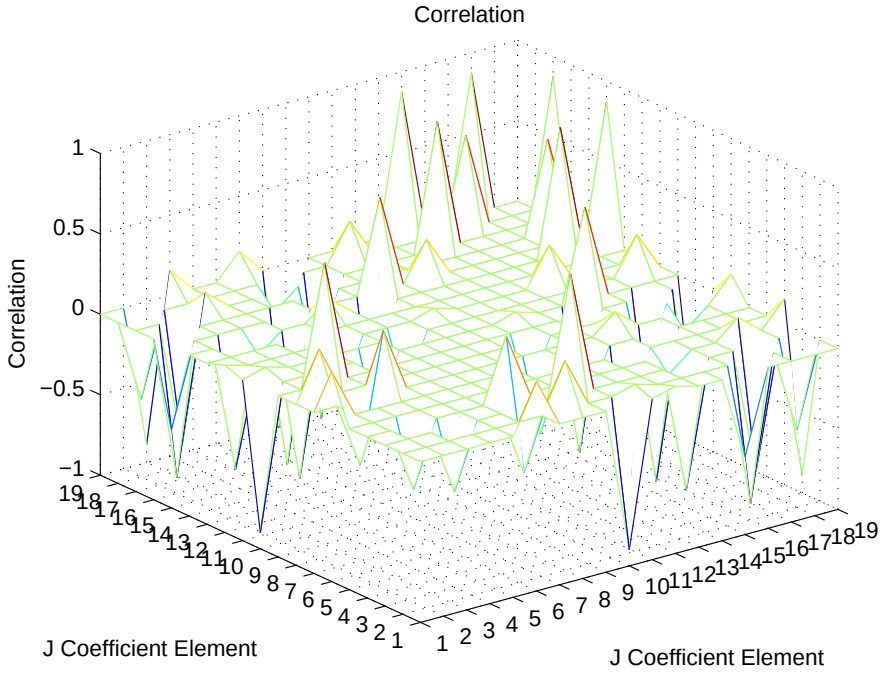

Figure 5.9: Case I. Correlation of GSM force coefficients

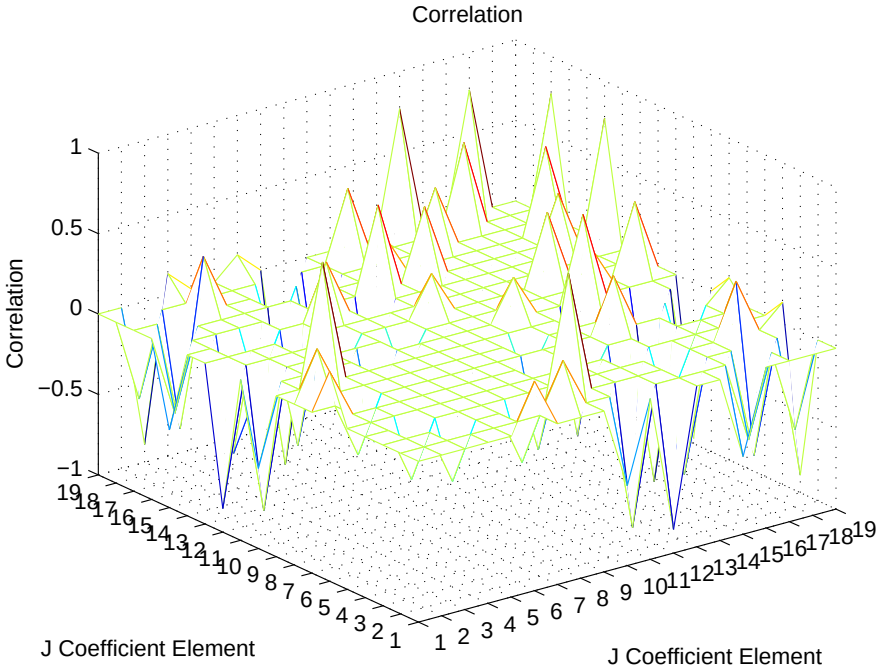

Figure 5.10: Case II. Correlation of GSM force coefficients

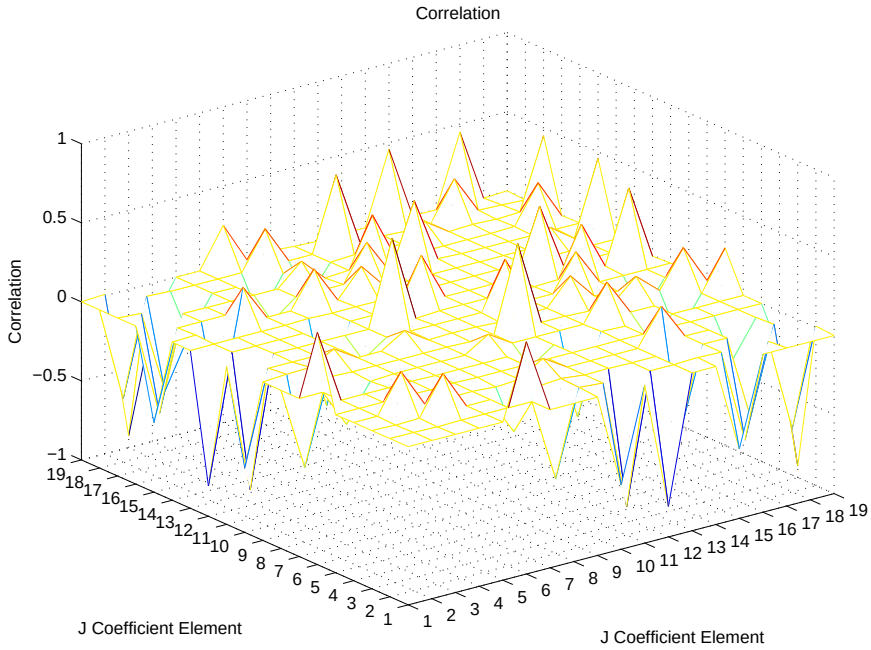

Figure 5.11: Case III. Correlation of GSM force coefficients

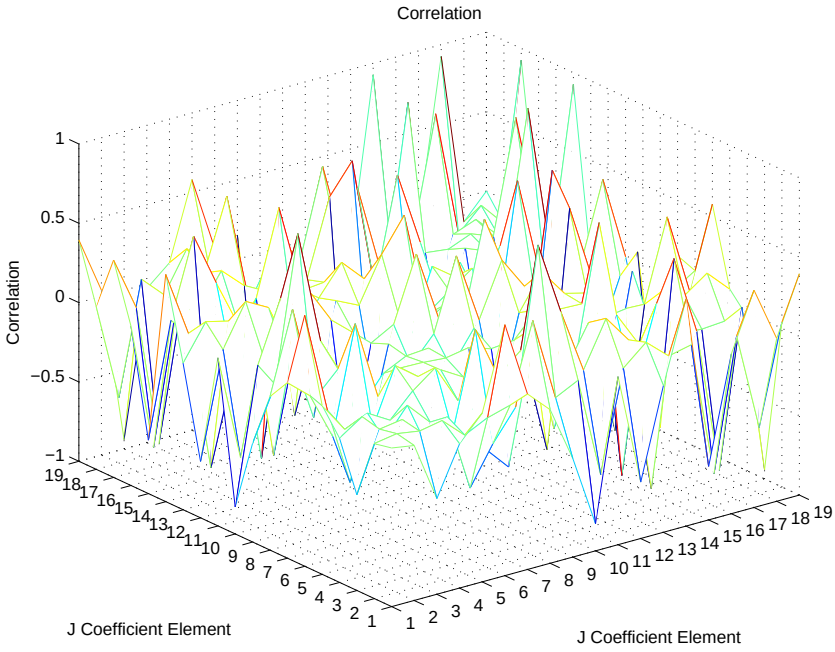

Figure 5.12: Case IV. Correlation of GSM force coefficients

In practice, the sail would be re-oriented to these different attitudes during a characterization phase and the accelerations and moments measured using on-board inertial measuring units (IMUs). The projected sail attitude is a plot of the y component versus the x component of $\hat{\mathbf{r}}$ on the sail xy-plane. Figures 5.5-5.8 show the covariance for each of four cases described. Case III is the data sampling with the lowest covariance. Figures 5.9-5.12 shoe the correlation of for the force tensor coefficients. The correlations of a given tensor coefficient with itself are suppressed from the plots since by definition it is unity. From these figures it can be seen that case III has the lowest covariance and correlation.

Figure 5.13 show the force covariance for each of the four cases as obtained from Eq. (5.28). Cases I and II have similar force covariance along all axes. Cases I, II, and IV perform similarly along the x-axis. Along the z-axis case III performs better at high sun-sail angles α.

All the cases have very similar results for the estimated force and comparable errors, showing that the estimation process converges upon the correct values. Figure 5.14 shows representative results of the actual normalized force of the sinusoid sail and the estimated normalized force as well as their respective error.

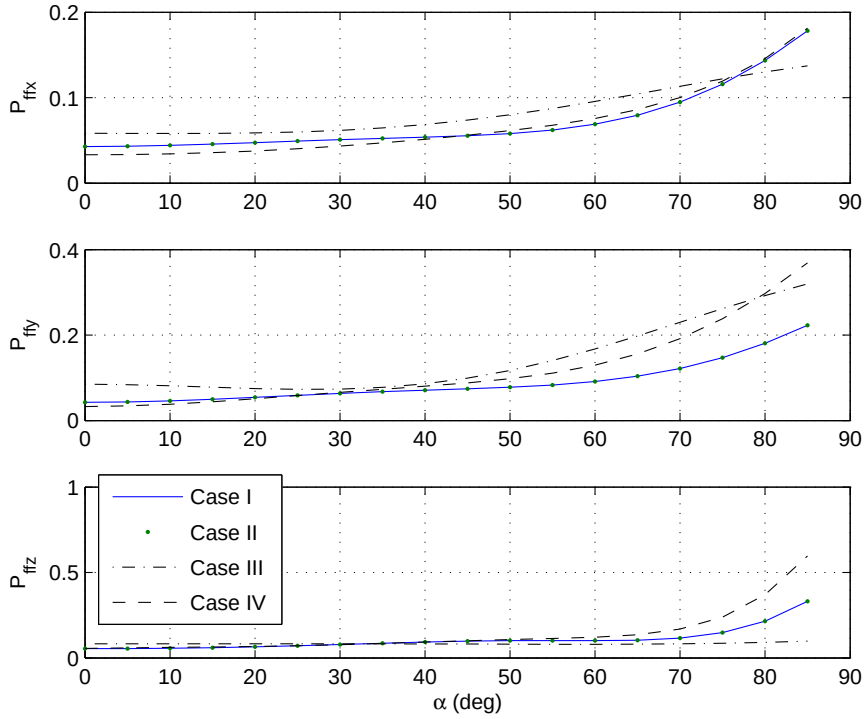

Figure 5.13: Force Covariance.

5.4.2 Moment Estimation

The moment covariance and correlation were computed for measurements as in Cases III and IV and are shown in Figures 5.15-5.18. Case I has measurements when $\hat{r}_1$ or $\hat{r}_2$ are zero and Case II has measurements when $\hat{r}_1 = \hat{r}_2$. Both situations make $\mathbf{A}_M$ rank deficient and Λ_{MM} singular and were not used in the estimation.

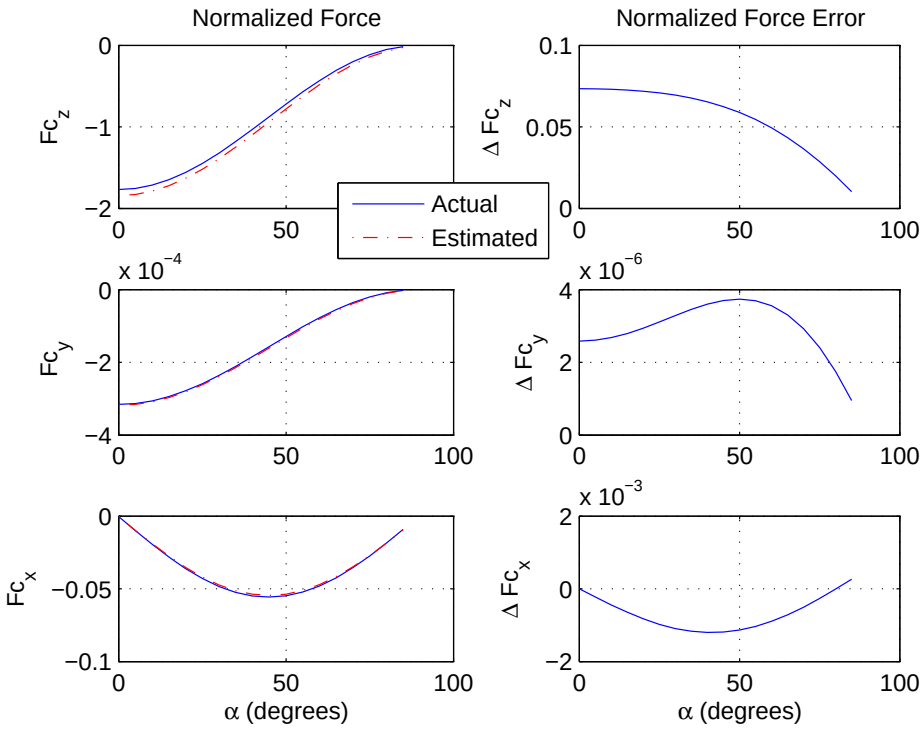

Figure 5.14: Representative Force Estimation Results.

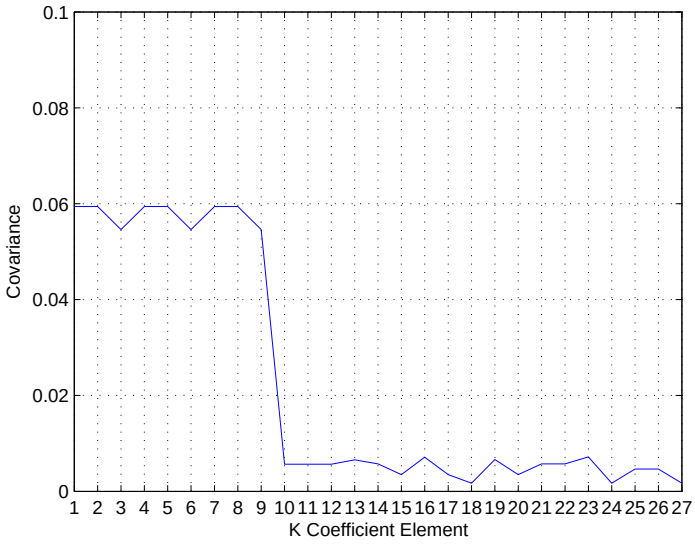

Figure 5.15: Case III. Covariance of GSM moment coefficients.

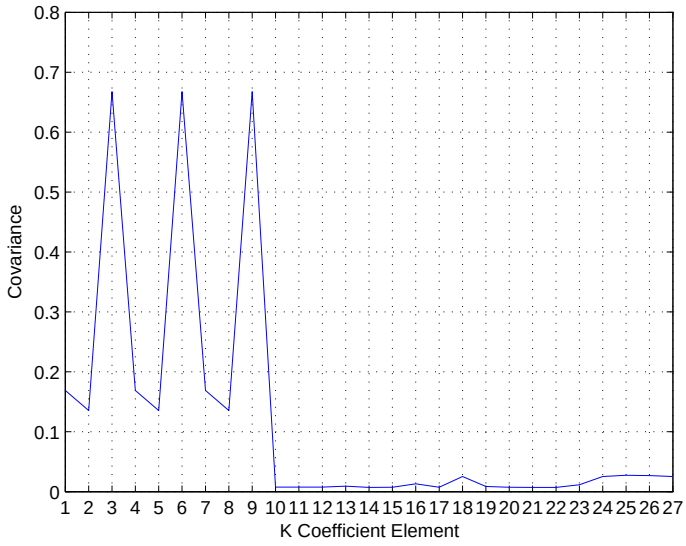

Figure 5.16: Case IV. Covariance of GSM moment coefficients.

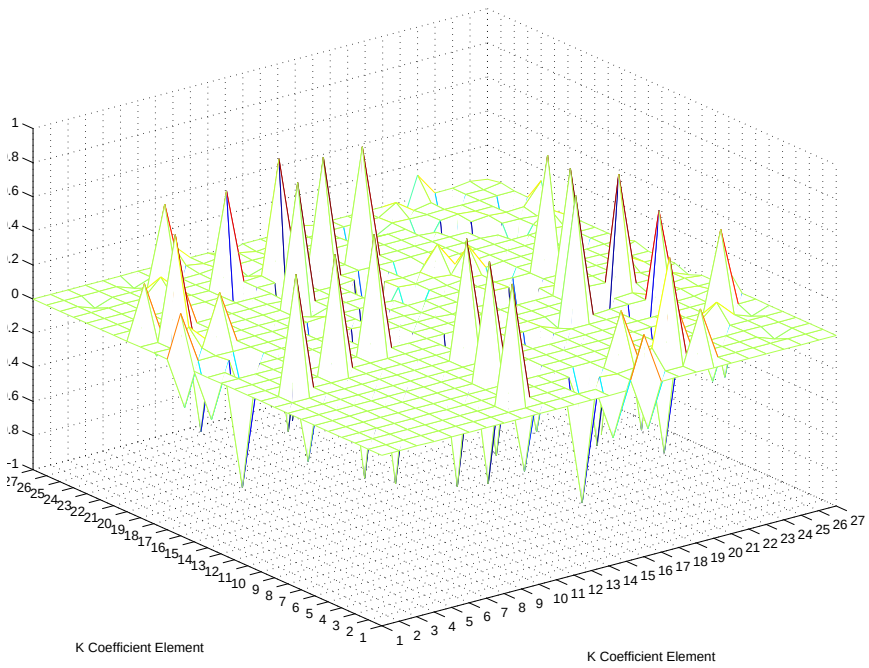

Figure 5.17: Case III. Correlation of GSM moment coefficients.

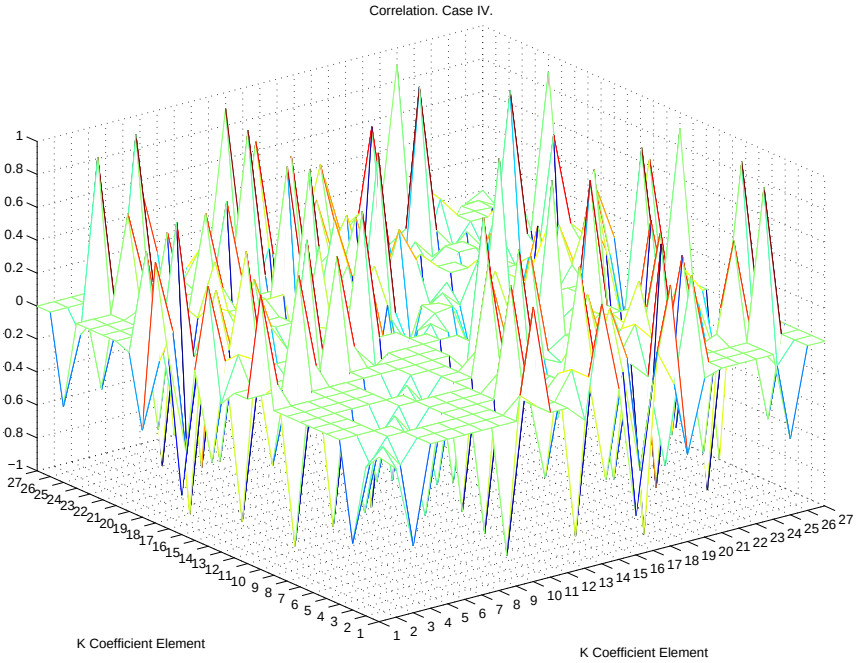

Figure 5.18: Case IV. Correlation of GSM moment coefficients.

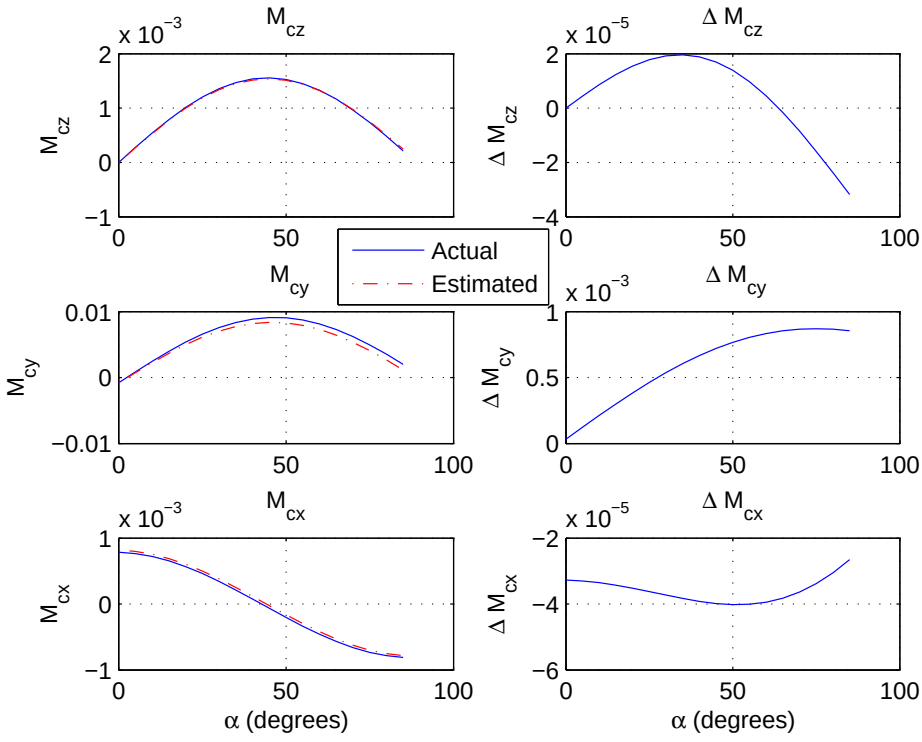

Figure 5.19: Representative Moment Estimation Results.

The moment coefficients were estimated and the moment results for each of the two cases were compared with the actual moment generated by the sinusoid sail. Both Cases III and IV replicate the sail moment although with comparable errors as shown representatively in Figure 5.19. This estimation was performed with 70 data measurements. Note the poor performance of Case IV covariance when compared to Case III.

One last case was carried out by performing a uniform data sampling across all the sail possible attitudes. The sampling was done with 8100 data measurements. The moment covariance shrinks to zero. The estimation was successful in recovering the moment generated by the sail with small deviations from the actual values and slight improvements over the previous two cases.

5.5 Symmetric Sail Shapes

In Chapter III it was shown earlier that for symmetric sails the number of coefficients needed to model their generated force and moment are greatly reduced. Thus, the amount of measurements needed for their estimation is reduced. In the rest of this chapter, the force and moment equations for the GSM parameter estimation are developed for a two-axis symmetric sail.

5.5.1 Force Tensor Coefficients

With these simplifications, the normalized force for a two-axis symmetric sail becomes

$$\mathbf{F} = PA \begin{bmatrix} \hat{r}_1 & 0 & 0 & -4\hat{r}_1\hat{r}_3 & 0 & 0 & -\hat{r}_1\hat{r}_3 \\ 0 & \hat{r}_2 & 0 & 0 & -4\hat{r}_2\hat{r}_3 & 0 & -\hat{r}_2\hat{r}_3 \\ 0 & 0 & \hat{r}_3 & -2\hat{r}_1^2 & -2\hat{r}_2^2 & -2\hat{r}_3^2 & -\hat{r}_3^2 \end{bmatrix} \begin{bmatrix} J_{11}^2 \\ J_{22}^2 \\ J_{33}^2 \\ J_{131}^3 \\ J_{232}^3 \\ J_{333}^3 \\ J_3^1 \end{bmatrix}. \quad (5.31)$$

5.5.2 Moment Tensor Coefficients

For a 2-axis symmetric sail the terms K_{12}^2, K_{21}^2, K_{213}^3, K_{321}^3, and K_{132}^3 are non-zero in general. Thus, for a 2-axis symmetrical sail the matrices given by Eqs. (5.13)-(5.14) reduce to

$$\mathbf{A}_M^2 = \begin{bmatrix} \hat{r}_1 & 0 \\ 0 & \hat{r}_2 \\ 0 & 0 \end{bmatrix}, \quad (5.32)$$

$$\mathbf{A}_M^L = \begin{bmatrix} \hat{r}_2\hat{r}_3 & \hat{r}_2\hat{r}_3 & 0 \\ 0 & \hat{r}_1\hat{r}_3 & \hat{r}_1\hat{r}_3 \\ \hat{r}_1\hat{r}_2 & 0 & \hat{r}_1\hat{r}_2 \end{bmatrix}, \quad (5.33)$$

and the vector with the independent moment tensor coefficients is

$$\mathbf{K} = \begin{bmatrix} K_{12}^2 & K_{21}^2 & K_{213}^3 & K_{321}^3 & K_{132}^3 \end{bmatrix}. \quad (5.34)$$

5.6 Discussion

In this chapter a methodology for estimating the forces and moments acting on a sail of arbitrary shape is presented based on the generalized sail model. The estimation is based on a least-squares algorithm. The accuracy of the estimation was dependent on the sail attitude relative to the sun when the measurement sampling was taken. The moment estimation is more sensitive to the data sampling; cases when $\hat{r}_1$ or $\hat{r}_2$ are zero or equal to $\hat{r}_3$ and $\hat{r}_1 = \hat{r}_2$ should be avoided for the moment estimation.

A non-symmetric sinusoid sail shape was used to simulate force and moment data. Forces and moments were estimated based on these data. Four different cases of data samplings were used to estimate the forces. All four cases recovered the force from the sinusoid sail with small errors. The moment tensor coefficients were also estimated using a least squares algorithm.

The estimation of both the force and moment included the optical parameters in the definition of the tensor coefficients, which made possible to estimate their combination. Since the tensor coefficients and optical parameters appear as a product there is no need to estimate them separately.

Finally, it was shown that symmetric sails required fewer tensor coefficients to capture the force and moment acting upon them. A 2-axis discretely symmetrical sail requires 7 coefficients for the force and 5 coefficients for the moment. A Sail with rotational symmetry requires only 5 coefficients for the force and 2 for the moment.

CHAPTER VI

Solar Sail Trajectory Control

Solar sail missions must be designed for a specific sail propulsion model [2, 19]. However, due to the complexity of solar sails and difficulties in providing precise predictions of their performance, our ability to precisely predict the sail acceleration performance is inherently limited. To account for this, trajectory design of a sail mission must be performed with a conservative propulsion model that provides adequate margin for uncertainties in the sail performance. Specifically, it is important that the sail provide a guaranteed minimum amount of thrust to ensure that the chosen mission can be flown. Due to this, however, the actual sail will most likely always have more thrust than the original mission planned for. Due to the nature of solar sails, this excess thrust cannot be easily modulated and will fundamentally change the trajectory of the sail and may make it difficult to achieve mission targets. While it is possible to estimate the actual sail propulsion after deployment and redesign the sail trajectory [30], this constitutes an open and continual design process that may not always be feasible to implement and which may not converge on the proper target. Similarly, as the sail surface suffers from degradation [20] throughout the mission, the thrust will change continuously and, if the maximum thrust of the sail is being used, constant re-optimization and redesign of the trajectory would be

necessary.

Previously, trajectory control laws have been developed for the same sail performance as the trajectory was designed for. In Reference [16], a trajectory control methodology is developed for stationing a solar sail at a sub-L_1 point and is noted the difficulties of achieving the mission objectives. In Reference [15] is suggested to use a sail with varying area in order to increase the control authority of the sail on a transfer trajectory. However, a sail with varying area may not be feasible to implement.

In this chapter we consider the case for controlling a sail with excess performance about a nominal trajectory. A sail with excess performance does not require a continually redesigned trajectory, as the sail properties change over time, it also does not require a varying area and still provides enough control authority to follow the mission. Our approach will allow a sail to follow a nominal mission design so long as the sail provides an excess of thrust, which will be the nominal design situation for any sail mission. Ideally, our approach can be applied to any trajectory, and will allow the sail to follow a nominal mission profile. In this chapter we consider the problems of maintaining a sail at a specific sub-L_1 equilibrium point location as well as tracking a moving point in a halo orbit about a sub-L_1 point. This work can be generalized to tracking an arbitrary trajectory as they can be considered as a sequence of moving points. The flat, ideal sail model is used throughout this chapter. The results can be generalized to real sail models using the GSM.

Consider the example of maintaining a specific sub-L_1 equilibrium point location. In general, if the sail generates less thrust than the design performance, it will not be possible for it to maintain this position and the mission cannot be achieved. If it has precisely the design performance, then it is possible to maintain the equilibrium

point and even perform control maneuvers to maintain itself close to this location, accounting for errors in initial condition and other factors [19]. If the sail has more thrust than its design performance, however, it becomes difficult to maintain the target location without actively modulating the total surface area of the sail. Such modulation would be a difficult and complex procedure to carry out with the sail structure.

The main problem in this situation is that the sail has excess thrust. A simple solution is to orient the sail so that it provides the appropriate thrust level along the line connecting the two primaries (the line of syzygies), and "dump" the excess thrust along the direction perpendicular to this line. In a short time, of course, the sail would veer off course and leave the equilibrium. A simple fix would be to switch, or dither, the sail back and forth – maintaining the proper thrust along the line of syzygy and producing a net zero thrust perpendicular to this line. Such an approach may work conceptually, but may be difficult to implement. Problems with this idea arise in changing the sail sense of rotation to average the perpendicular force to zero. Also, the dithering approach would be insufficient for tracking a non-planar trajectory in three-dimensions. Following this line of thought, however, we find a simple approach that can essentially achieve this goal of maintaining the appropriate thrust vector and forcing the excess thrust to average out to zero.

To accomplish this task we force the sail to "orbit" the equilibrium point (or a nominally moving point along a trajectory) in a small orbit centered on this nominal solution. Instead of forcing the sail to dither back and forth, however, we have the sail follow a near circular path about the nominal solution that has a centripetal acceleration equal to the amount of excess thrust generated after the sail is oriented to provide the nominal thrust. Thus, the sail will follow the nominal trajectory while

performing a controlled "orbit" about the trajectory. For a given value of excess thrust there is some freedom in designing this orbit, as the centripetal acceleration depends on both the radius of this orbit and the angular rate.

This control approach can be implemented by inducing the sail to rotate at the same rate as it "orbits" the nominal solution. Thus the attitude of the sail is fixed such that the excess thrust is always pointed towards the nominal solution. However, there may be instances where the excess force is modulated away from the center of rotation for control.

6.1 Circular Restricted Three Body Problem in Cylindrical Coordinates

If the sail produces a higher force than originally expected, then it cannot be stationed at the sub-L_1 point. One solution is to recompute a new sub-L_1 point $x'_{L_1} < x_{L_1}$, however, this approach may force the sail to fly in a regime that it was not designed for. Another possibility is to used the extra force to orbit the sub-L_1 point. The second option provides a better approach since it allows the sail to maintain the required x_{L_1} location.

For orbiting the sub-L_1 point it is helpful to write the circular, restricted, three-body problem equations of motion in a cylindrical coordinate frame rotating about the nominal equilibrium as shown in Figure 6.1. This describes a cylindrical coordinate frame with its axis of symmetry along the x-axis. Let $y = r\cos\theta$ and $z = r\sin\theta$.

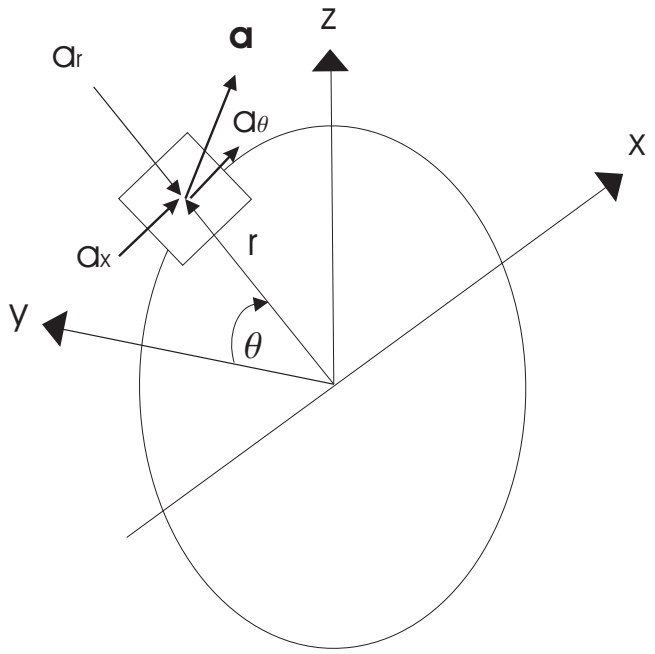

Figure 6.1: Sail in Orbit about Sub-L_1 Point.

The kinematics of the y and z coordinates in the new variables is:

$$\dot{y} = \dot{r}\cos\theta - r\dot{\theta}\sin\theta, \tag{6.1}$$

$$\dot{z} = \dot{r}\sin\theta + r\dot{\theta}\cos\theta, \tag{6.2}$$

$$\ddot{y} = \ddot{r}\cos\theta - 2\dot{r}\dot{\theta}\sin\theta - r\dot{\theta}^2\cos\theta - r\ddot{\theta}\sin\theta, \tag{6.3}$$

$$\ddot{z} = \ddot{r}\sin\theta + 2\dot{r}\dot{\theta}\cos\theta - r\dot{\theta}^2\sin\theta + r\ddot{\theta}\cos\theta. \tag{6.4}$$

Eqs. (2.9) - (2.10) become

$$\ddot{y} = -2\dot{x} + \Big(1 - \frac{1-\mu}{|\mathbf{r}_1|^3} - \frac{\mu}{|\mathbf{r}_2|^3}\Big) r\cos\theta + a_y, \tag{6.5}$$

$$\ddot{z} = -\Big(\frac{1-\mu}{|\mathbf{r}_1|^3} + \frac{\mu}{|\mathbf{r}_2|^3}\Big) r\sin\theta + a_z. \tag{6.6}$$

Substituting Eqs. (6.3) and (6.4) into the above equations:

$$\begin{bmatrix} \cos\theta & -r\sin\theta \\ \sin\theta & r\cos\theta \end{bmatrix} \begin{bmatrix} \ddot{r} \\ \ddot{\theta} \end{bmatrix} = \begin{bmatrix} -2\dot{x} + \left(1 - \frac{1-\mu}{|\mathbf{r}_1|^3} - \frac{\mu}{|\mathbf{r}_2|^3}\right) r\cos\theta + 2\dot{r}\dot{\theta}\sin\theta + r\dot{\theta}^2\cos\theta \\ -\left(\frac{(1-\mu)}{|\mathbf{r}_1|^3} + \frac{\mu}{|\mathbf{r}_2|^3}\right) r\sin\theta - 2\dot{r}\dot{\theta}\cos\theta + r\dot{\theta}^2\sin\theta \end{bmatrix} \quad (6.7)$$

solving for $\ddot{r}$ and $\ddot{\theta}$, the equations of motion in the new coordinate frame are:

$$\ddot{x} = 2\dot{r}\cos\theta - 2r\dot{\theta}\sin\theta + x - \frac{(1-\mu)(x+\mu)}{|\mathbf{r}_1|^3} - \frac{\mu}{|\mathbf{r}_2|^3}(x+\mu-1) + a_x, \quad (6.8)$$

$$\ddot{r} = -2\dot{x}\cos\theta + r\cos^2\theta - \left(\frac{1-\mu}{|\mathbf{r}_1|^3} + \frac{\mu}{|\mathbf{r}_2|^3}\right) r + r\dot{\theta}^2 + a_r, \quad (6.9)$$

$$\ddot{\theta} = 2\dot{x}\frac{\sin\theta}{r} - \sin\theta\cos\theta - 2\frac{\dot{r}\dot{\theta}}{r} + \frac{a_\theta}{r}. \quad (6.10)$$

6.2 Sail Propulsive Model

Our initial studies for this problem are done using an ideal flat sail, although the approach can be generalized to realistic sail models [27]. The sail acceleration can be defined in terms of the restricted three-body problem parameters. Thus, Eq. (2.22), which models the acceleration due to the propulsion of an ideal sail, can be written as:

$$\mathbf{a} = -\frac{\beta(1-\mu)}{|\mathbf{r}_1|^4}(\mathbf{r}_1 \cdot \hat{\mathbf{n}})^2\hat{\mathbf{n}}. \quad (6.11)$$

The acceleration given in terms of the controls angles by Eq. (2.26) is given in coordinates of a local vertical/local horizontal, LVLH, frame and must be transformed into the rotating frame through a rotation matrix in order to be employed in Eqs. (2.8)-(2.10). The transformation matrix from the LVLH frame into the rotating frame given by

$$T_{lr} = \begin{bmatrix} \frac{x^2}{|\mathbf{r}_1|^2} & -\frac{ry}{|\mathbf{r}_1|} & -\frac{xz}{|\mathbf{r}_1|^2} \\ \frac{xy}{|\mathbf{r}_1|^2} & \frac{x}{|\mathbf{r}_1|} & -\frac{yz}{|\mathbf{r}_1|^2} \\ \frac{z}{|\mathbf{r}_1|} & 0 & \frac{x}{|\mathbf{r}_1|} \end{bmatrix}. \tag{6.12}$$

The acceleration in the rotating frame is obtained from:

$$\mathbf{a} = T_{lr}\mathbf{a}_e, \tag{6.13}$$

where a_e is the sail acceleration in the LVLH frame. Making the change of variables into cylindrical variables, the acceleration due to the solar radiation pressure is:

$$\begin{aligned} a_x &= \frac{\beta(1-\mu)}{|\mathbf{r}_1|^2}\cos^2\alpha\left(\frac{x^2}{|\mathbf{r}_1|^2}\cos\alpha + \frac{r}{|\mathbf{r}_1|}\cos\delta\cos\theta\sin\alpha\right. \\ &+ \left.\frac{rx}{|\mathbf{r}_1|^2}\sin\alpha\sin\delta\sin\theta\right), \end{aligned} \tag{6.14}$$

$$\begin{aligned} a_r &= \frac{\beta(1-\mu)}{|\mathbf{r}_1|^2}\cos^2\alpha\left(-\frac{x}{|\mathbf{r}_1|}\cos\delta\cos\theta\sin\alpha - \sin\alpha\sin\delta\sin\theta(\frac{x}{|\mathbf{r}_1|} - \frac{r^2}{|\mathbf{r}_1|^2}\cos^2\theta)\right. \\ &+ \left.\frac{r}{|\mathbf{r}_1|}\cos\alpha(\frac{x}{|\mathbf{r}_1|}\cos^2\theta + \sin^2\theta)\right), \end{aligned} \tag{6.15}$$

$$\begin{aligned} a_\theta &= \frac{\beta(1-\mu)}{|\mathbf{r}_1|^2}\cos^2\alpha\left(\frac{x}{|\mathbf{r}_1|}\frac{\cos\delta\sin\alpha\sin\theta}{r} + \cos\alpha\cos\theta\sin\theta(\frac{1}{|\mathbf{r}_1|} - \frac{x}{|\mathbf{r}_1|^2})\right. \\ &- \left.\sin\alpha\sin\delta\cos\theta(\frac{x}{|\mathbf{r}_1|r} + \frac{r}{|\mathbf{r}_1|^2}\sin^2\theta\right). \end{aligned} \tag{6.16}$$

An approximation to this expression can be obtained if the terms $(r/|\mathbf{r}_1|)$ are ignored as $|\mathbf{r}_1| >> r$. Then, the approximate acceleration is just:

$$\begin{bmatrix} a_x \\ a_r \\ a_\theta \end{bmatrix} = \frac{\beta(1-\mu)}{|\mathbf{r}_1|^2}\cos^2\alpha\begin{bmatrix} \cos\alpha \\ -\sin\alpha\cos(\delta-\theta) \\ -\sin\alpha\sin(\delta-\theta) \end{bmatrix}, \tag{6.17}$$

where the control angles α and δ are shown in Figure 2.3.

6.3 Special Orbits in the Solar Sail CR3BP

The force generated by solar sails modify the dynamics of the circular restricted three body problem. New families of equilibrium points, called sub-L points, arise parameterized by the sail lightness number [1]. Associated with these equilibria are halo orbits, which have been considered for mission application purposes [19, 1].

6.3.1 Sub-L_1 Points

Solar sails allow a sailcraft to create artificial Lagrange points [21] so called sub-L_1 points [19]. These new locations have a number of applications since they are closer to the sun than the L_1 point. The location of a new sub-L_1 point is dependent on the sail lightness number β. In order to find a sub-L_1 point with the sail plane perpendicular to the solar flux, we need to write the equations of motion along the line of the primary bodies:

$$\ddot{x} = x - \frac{\mu(x-1+\mu)}{|x-1+\mu|^3} - \frac{(1-\mu)(x+\mu)}{|x+\mu|^3} + a_x, \tag{6.18}$$

where a_x is the force along the x direction, which for a sail facing the sun with $\alpha = 0$ is given by:

$$a_x = \beta\frac{(1-\mu)(x+\mu)}{|x+\mu|^3}. \tag{6.19}$$

Setting Eq. (6.18) equal to zero, we can solve for the lightness number that would yield an equilibrium point in terms of μ and for a specific $x = x_{L_1}$:

$$\beta = \frac{|(x_{L_1}+\mu)|^2}{1-\mu}\Big[-x_{L_1} + \frac{\mu(x_{L_1}-1+\mu)}{|x_{L_1}-1+\mu|^3} + \frac{(1-\mu)(x_{L_1}+\mu)}{|x_{L_1}+\mu|^3}\Big]. \tag{6.20}$$

It can be shown that the sub-L_1 are unstable by following the procedure outlined in Reference [4] and modifying it to account for the solar radiation pressure. Define the quantity γ as

$$\gamma = \frac{(1-\mu)(1-\beta)}{|x+\mu|^3} + \frac{\mu}{|x+\mu-1|^3}. \tag{6.21}$$

Then, through stability analysis it can be shown that the equilibria are stable if [4]

$$1-\gamma \;>\; 0, \tag{6.22}$$

setting Eq. (6.18) to zero, it can be manipulated into [4]

$$1-\gamma \;=\; \frac{\mu(1-\mu)}{x}\left(\frac{1}{|x+\mu|^3} - \frac{1}{|x+\mu-1|^3}\right). \tag{6.23}$$

For a sub-L_1 point the quantity in parenthesis is negative and hence the criteria for stability fails.

6.3.2 Halo Orbits about Sub-L_1 Points

As the force generated by the sail is taken into account in the equation of motion, new families of halo orbits arise around the sub-L_1 points. Two types of orbits about the sub-L_1 point are identified by McInnes [1]. Case I originates when the force is directed along the sun-line. Case II is when the force is directed along the x-axis of the rotating frame. We consider Case I halo orbits as a reference orbit for a sail, whose equations of motion are:

$$\ddot{x} = 2\dot{y} + x - \frac{(1-\mu)(x+\mu)}{|\mathbf{r}_1|^3} - \frac{\mu}{|\mathbf{r}_2|^3}(x+\mu-1) + \beta(1-\mu)\frac{x+\mu}{|\mathbf{r}_1|^3}, \quad (6.24)$$

$$\ddot{y} = -2\dot{x} + y - \frac{(1-\mu)y}{|\mathbf{r}_1|^3} - \frac{\mu y}{|\mathbf{r}_2|^3} + \beta(1-\mu)\frac{y}{|\mathbf{r}_1|^3}, \quad (6.25)$$

$$\ddot{z} = -\frac{(1-\mu)z}{|\mathbf{r}_1|^3} - \frac{\mu z}{|\mathbf{r}_2|^3} + \beta(1-\mu)\frac{z}{|\mathbf{r}_1|^3}. \quad (6.26)$$

The Case I halo orbits are found by using a third order approximation method described by McInnes [1]. Thus, the solution is expressed as

$$\tilde{x} = \tilde{x}_1 + \tilde{x}_2 + \tilde{x}_3, \quad (6.27)$$

$$\tilde{y} = \tilde{y}_1 + \tilde{y}_2 + \tilde{y}_3, \quad (6.28)$$

$$\tilde{z} = \tilde{z}_1 + \tilde{z}_2 + \tilde{z}_3, \quad (6.29)$$

where the origin of the $\tilde{x}, \tilde{y}$, and $\tilde{z}$ coordinates is the corresponding sub-L_1 point for a given β. For details of how to find the halo orbits the reader is directed to Reference [1].

6.4 Excess Performance in the Sail Propulsion Unit

The derivation of the above equilibrium point and its corresponding halo orbits was performed assuming exact knowledge of the propulsion force of the sail. Uncertainties present in the force sail model will change the location of this equilibrium point due to either insufficient or excess force available. If the sail resultant force is less that the required force, then it would be impossible to stay at the required equilibrium (or halo orbit) and a recalculation would be necessary. If the force is more than expected, then through some maneuvering it is still possible to stay at the required equilibrium or halo orbit. In the following we assume that it is desired

to stay at the original, designed equilibrium point. Later this result is generalized to a halo orbit.

Assume that the actual force created by the sail is larger than the force expected. To maintain the sail at the same fixed sub-L_1 point, one would have to orient the sail continuously in order to shed the excess force. There are several ways of doing this, for example, the orientation of the sail can be dithered by oscillating the sail in order to keep the average acceleration equal to the required acceleration:

$$\overline{\mathbf{a}} = \frac{1}{T}\int_0^T \mathbf{a}(t)dt = \begin{bmatrix} a_{x_{L_1}} \\ 0 \\ 0 \end{bmatrix}, \tag{6.30}$$

where $a_{x_{L_1}}$ is the nominal acceleration to station the sail at the equilibrium. Note that dithering of the sail changes the force magnitude through modulation of α, which may be feasible for a planar orbit but hard to implement to a general trajectory as δ would have to be modulated as well.

Another option is to use the excess force to orbit the equilibrium in a small orbit centered at the equilibrium. This can be achieved by continuously steering the sail in order to cancel the centrifugal forces with the excess force. The sun-sail angle, not necessarily constant, must be such that the average force along the r-direction is equal to the original nominal force. Assume that the actual acceleration exceeds the nominal acceleration by a constant k, so that the actual force along the x-direction is:

$$a_x = k\beta\frac{(1-\mu)(x+\mu)}{|x+\mu|^3} = \beta'\frac{(1-\mu)(x+\mu)}{|x+\mu|^3}, \tag{6.31}$$

where β' is the actual sail lightness number.

Since this acceleration is larger than required, the sail must be oriented with a non-zero α with the constraint that the force along the x-direction must be equal to the nominal acceleration. With this in mind, the following relation needs to be satisfied:

$$\beta \frac{(1-\mu)(x+\mu)}{|x+\mu|^3} = \beta' \frac{(1-\mu)(x+\mu)}{|x+\mu|^3} \cos^3 \alpha, \tag{6.32}$$

which provides the required sun-sail angle:

$$\alpha_0 = \cos^{-1}\left(\frac{1}{k^{1/3}}\right). \tag{6.33}$$

Certainly, if the sail is maintained at this constant attitude there will be a force generated orthogonal to the x-axis which will drive the sail away from the equilibrium. However, if the sail is to orbit the equilibrium in a quasi-circular orbit, then the excess force can be used to cancel the centrifugal acceleration by directing it toward the equilibrium. To generate a radial acceleration, $\delta - \theta$ must be set equal to zero in Eq. (6.17). Then, the acceleration due to the solar radiation pressure along the radial direction is:

$$a_r = -\frac{\beta'(1-\mu)}{r_1^2} \cos^2 \alpha_0 \sin \alpha_0. \tag{6.34}$$

The radial acceleration must balance the centrifugal acceleration in the orbit, thus $a_r = -a_c$. Given this available acceleration, it is now possible to design the relative orbit the sail has to follow. Assume that a radius r_d is desired, then the

velocity v_d and angular velocity $\dot{\theta}_d$ needed to stay in a circular orbit are:

$$v_d = \sqrt{a_c r_d}, \tag{6.35}$$

$$\dot{\theta}_d = \sqrt{\frac{a_c}{r_d}}. \tag{6.36}$$

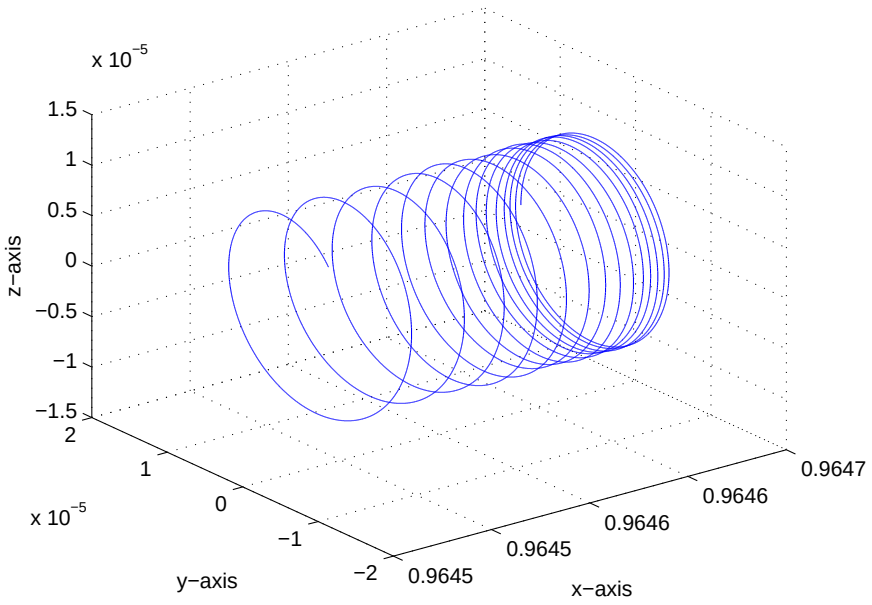

Figure 6.2: Long term orbit about sub-L_1 point for uncontrolled dynamics.

Choosing values of $r_d = 1 \times 10^{-5}$, in the normalized system, which corresponds to a value of 1.49×10^6 m, $k = 1.1$, and α and v_c determined from Eqs. (6.33) and (6.35), respectively, we can apply this concept in a simulation. The chosen initial conditions are $\mathbf{r}_0 = [x_{L_1}, r_d, 0]$, where x_{L_1} is the location of the sub-L_1 point, and $\dot{\mathbf{r}}_0 = [0, 0, v_c]$. The simulated free dynamics are shown in Figure 6.2. This orbit is unstable and slides away from the equilibrium point. This is expected as the equilibrium point is itself unstable.

6.5 Control of Sail Orbit about a Sub-L_1 Point

From the equations of motion, the sail control angles α and δ allow for the control of the sail about the equilibrium point. The sail position about the x-axis is affected by α and the r and θ directions by both α and δ.

The x-position is maintained at x_{L_1} by adjusting α in such a way that it will cancel disturbances that drive the sail away form x_{L_1}. This α can be chosen from a linearized controller or a proportional-derivative controller developed later in this section.

Once α is chosen, δ is left to control the r and θ directions. The objective is to keep the sail in a circular or quasi-circular orbit by driving $\dot{r}$ and $\ddot{r}$ to zero (or close to zero). The approach taken here is to design an orbit with a fixed radius and use energy as a reference for feedback in the control law.

6.5.1 Control of Sail x-Position

A linear-feedback controller is developed by linearizing the x-dynamics about x_{L_1} and α_0. This controller is then applied to the non-linear system. From Eq. (2.8), the linearized equations about the equilibrium are:

$$\begin{bmatrix} \delta\dot{x} \\ \\ \delta\ddot{x} \end{bmatrix} = \begin{bmatrix} 0 & 1 \\ \\ b & 0 \end{bmatrix} \begin{bmatrix} \delta x \\ \\ \delta\dot{x} \end{bmatrix} + \begin{bmatrix} 0 \\ \\ c \end{bmatrix} \delta\alpha, \tag{6.37}$$

where

$$
\begin{aligned}
b &= \frac{\partial a_x}{\partial x}\Big|_{L_1} + \frac{\partial f(\mathbf{x})}{\partial x}\Big|_{L_1}, && (6.38)\\
\frac{\partial a_x}{\partial x}\Big|_{L_1} &= -2\beta\frac{1-\mu}{|x_{L_1}+\mu|^3}\cos^3\alpha_0, && (6.39)\\
\frac{\partial f(\mathbf{x})}{\partial x}\Big|_{L_1} &= 1+2\frac{1-\mu}{|x_{L_1}+\mu|^3}+2\frac{\mu}{|x_{L_1}+\mu-1|^3}, && (6.40)\\
c &= \frac{\partial a_x}{\partial \alpha}\Big|_{L_1} = -3\beta\frac{1-\mu}{|x_{L_1}+\mu|^2}\cos^2\alpha_0\sin\alpha_0. && (6.41)
\end{aligned}
$$

Using simple controllability tests we see that the system is controllable along this direction. Now it is possible to design the linear feedback controller by letting:

$$
\delta\alpha = \begin{bmatrix} k_1 & k_2 \end{bmatrix} \begin{bmatrix} \delta x \\ \delta\dot{x} \end{bmatrix}. \tag{6.42}
$$

The closed-loop system becomes:

$$
\begin{bmatrix} \delta\dot{x} \\ \delta\ddot{x} \end{bmatrix} = \begin{bmatrix} 0 & 1 \\ b+k_1c & k_2c \end{bmatrix} \begin{bmatrix} \delta x \\ \delta\dot{x} \end{bmatrix}, \tag{6.43}
$$

with characteristic polynomial:

$$
p(\lambda) = \lambda^2 - \lambda(k_2c) - ck_1 - b. \tag{6.44}
$$

For stability we want the coefficients to be positive. Note that $b > 0$, and $c < 0$. Then the gains have to satisfy:

$$
\begin{aligned}
k_2 &> 0, && (6.45)\\
k_1 &> -\frac{b}{c}. && (6.46)
\end{aligned}
$$

A simulation using the linear feedback controller was performed using gains $k_1 = 7000$ and $k_2 = 200$. Figure 6.3 shows the simulation results. The sail was initially located sunward of the sub-L_1 point at a distance of 2×10^{-5} in normalized units. The controller stabilizes the sail around the equilibrium, but is not asymptotically stable since the control corrections are done on an average value of α and the linearized dynamics do not take into account the coupling with the r and θ variables, however the sail is kept within some ϵ of the equilibrium.

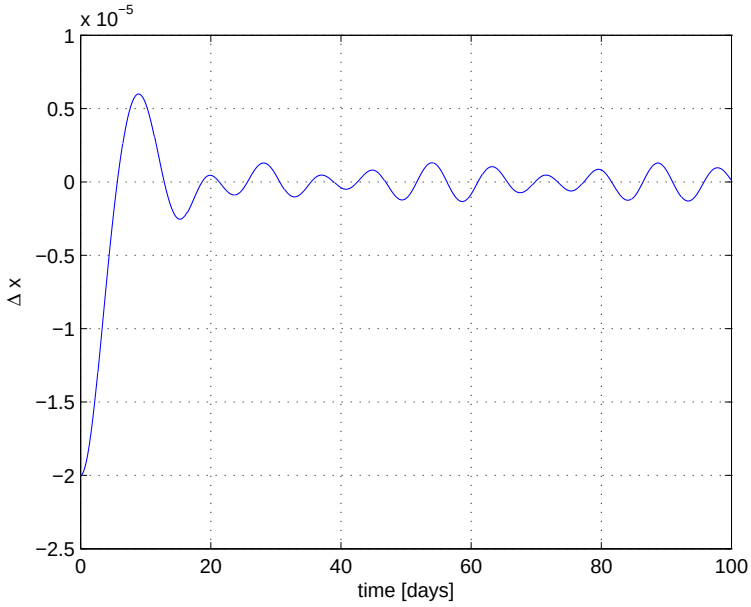

Figure 6.3: Linear Feedback Control on Sail x-Position.

To remedy this we apply a proportional-derivative controller to the position deviation and the rate at which the sailcraft is receding from the sub-L_1 point. Let's suppose that the current sail position is x and the sub-L_1 point is at x_{L_1}, then if $x > x_{L_1}$ the angle α must be increased to reduce the force along the x-axis and move the sail in the direction of the sun. If $x < x_{L_1}$ the opposite should be done. Now if the sail is already at the required equilibrium and $\dot{x} > 0$, then α must be increased, and if $\dot{x} < 0$, then α must be decreased. Then the controller will have the form

$\delta\alpha = c_1(x - x_{L_1}) + c_2\dot{x}$, where c_1 and c_2 are the PD-controller constant gains.

The PD-controller will help bring the sail to the sub-L_1 point. Once the sail is there, it will experience accelerations away from the equilibrium due to the coupling of the dynamics. To reject these disturbances α needs to be corrected at every instant in the orbit to account for the acceleration arising from the r and θ coordinates. This can be done by finding an α that yields a zero net acceleration in the x-direction. From Eq. (6.8), it is possible to find this α by solving:

$$\begin{aligned}\cos^3\alpha_1 &= -\left[2\dot{r}\cos\theta - 2r\dot{\theta}\sin\theta + x_{L_1} - \frac{(1-\mu)(x_{L_1}+\mu)}{|\mathbf{r}_1(x_{L_1})|^3}\right. \\ &- \left.\frac{\mu}{|\mathbf{r}_2(x_{L_1})|^3}(x_{L_1}+\mu-1)\right]\frac{|\mathbf{r}_1(x_{L_1})|^2}{\beta'(1-\mu)}. \end{aligned} \tag{6.47}$$

Even though this equation is cubic, $\cos^3\alpha$ is one-to-one in the domain of $\alpha \in [0, \pi/2]$, thus there will always be a real solution. The active PD-control law that stabilizes the sail in the x-direction about the sub-L_1 point is then:

$$\alpha = \alpha_1 + c_1(x - x_0) + c_2\dot{x}, \tag{6.48}$$

where α_1 is the real solution of Eq. (6.47).

Figure 6.4 shows the sail's trajectory and x-position using this controller with $c_1 = 3000$ and $c_2 = 500$ with the sail starting at a distance of 2×10^{-5}, in the normalized units, sunward of the sub-L_1 point.

In order to maintain the sail exactly at x_{L_1}, α has to be adjusted at every point in the orbit. Continuous active modulation is necessary to avoid oscillations in the x-direction and may not always be feasible. Although a completely constant sun-sail angle is not practical, since the controller needs to correct from deviations, the part that is dependent on the orbit position can be neglected on the controller. Thus, the controller still is given by Eq. (6.48) with α_1 satisfying:

$$\begin{aligned}\cos^3\alpha_1 &= -\left[x_{L_1} - \frac{(1-\mu)(x_{L_1}+\mu)}{|\mathbf{r}_1(x_{L_1})|^3}\right. \\ &- \left.\frac{\mu}{|\mathbf{r}_2(x_{L_1})|^3}(x_{L_1}+\mu-1)\right]\frac{|\mathbf{r}_1(x_{L_1})|^2}{\beta'(1-\mu)}. \qquad (6.49)\end{aligned}$$

Notice that α_1 is constant for this case and the new controller has a similar form and performance as the linear feedback controller. Hence, it is expected that the sail x-position oscillates about x_{L_1}. The amplitude of the oscillations are dependent on the PD gains.

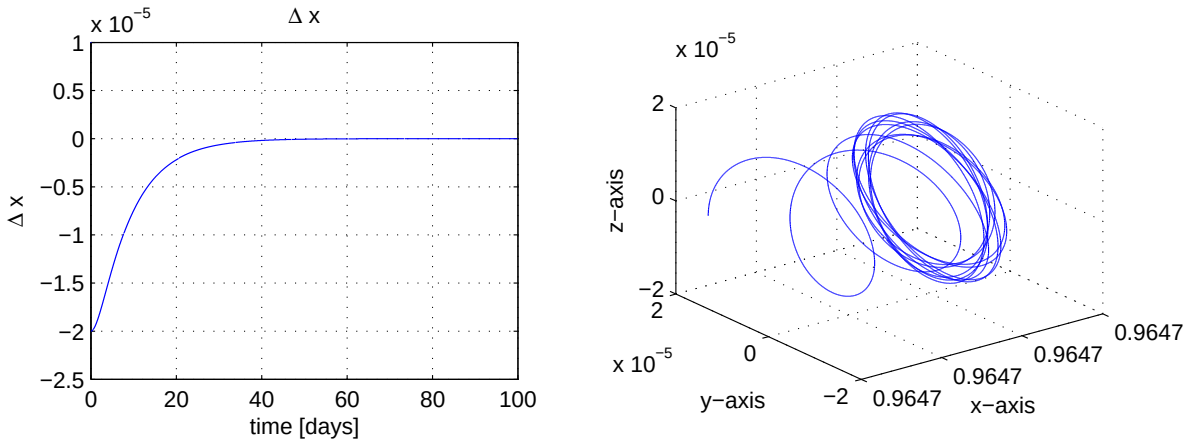

Figure 6.4: Active Proportional Derivative Control on Sail x-Position.

6.5.2 Control of Sail Orbit Radius

Once the sail is stabilized along the x-direction, $\dot{x}$ becomes zero (or sufficiently small) and consequently the dynamics in the r and θ coordinates decouple from the varying x coordinate. The dynamical equations governing this motion reduce to:

$$\ddot{r} = r\cos^2\theta - \left(\frac{1-\mu}{|\mathbf{r}_1|^3} + \frac{\mu}{|\mathbf{r}_2|^3}\right)r + r\dot{\theta}^2 - \frac{\beta(1-\mu)}{|\mathbf{r}_1|^2}\cos^2\alpha\sin\alpha\cos\overline{\delta}, \qquad (6.50)$$

$$\ddot{\theta} = -\sin\theta\cos\theta - 2\frac{\dot{r}\dot{\theta}}{r} - \frac{1}{r}\frac{\beta(1-\mu)}{|\mathbf{r}_1|^2}\cos^2\alpha\sin\alpha\sin\overline{\delta}, \qquad (6.51)$$

where the new control variable is just $\overline{\delta} = \delta - \theta$. Another controller is needed to maintain the sail at the required orbit radius. The sail radius about the sub-L_1 point can differ from the nominal radius if deviations in the orbit insertion arise, and can be quite large. In figure 6.4 we can see the excursion in the radius r for the above example. Rather than controlling the orbit through r and θ directly, a simpler control law can be defined if the effective kinetic energy about the sub-L_1 point of the orbit is used.

The sail kinetic energy about the sub-L_1 point is given by:

$$E = \frac{1}{2}\left(r^2\dot{\theta}^2 + \dot{r}^2\right). \tag{6.52}$$

It is desired to achieve a final orbit with radius r_d. This orbit has an energy $E_0 = r_d^2\dot{\theta}_d^2/2$, which is called the reference energy. The error between the actual and reference kinetic energy about the sub-L_1 point orbit, which will be used to track the deviation from the actual to the desired sail orbit, is $\tilde{E} = E - E_0$. The sail orbit is controlled by defining a proportional controller of the form:

$$\overline{\delta} = -c_e \sin^{-1}\frac{\tilde{E}}{r_d}, \tag{6.53}$$

where c_e is a constant gain and r_d is used as a scaling factor. Note that E_0 is not constant but is a function of α:

$$E_0 = \frac{1}{2}r_d^2\dot{\theta}^2 = \frac{1}{2}r_d|a_t| = \frac{1}{2}r_d\frac{\beta'(1-\mu)}{|\mathbf{r}_1|^2}\cos\alpha\sin\alpha. \tag{6.54}$$

Figure 6.5 shows the results of using this controller with $c_e = 10$. The sail was started at a radius 30% larger than the nominal and sunward to the sub-L_1 point. It

can be seen that the controller is able to track the nominal energy. However, since the nominal energy is not constant, the sail orbit oscillates about the nominal radius with very small deviations. In the same figure, the steady state sail orbit is shown to be a closed loop. The period of the orbit about the sub-L_1 point is of approximately 6.6 days.

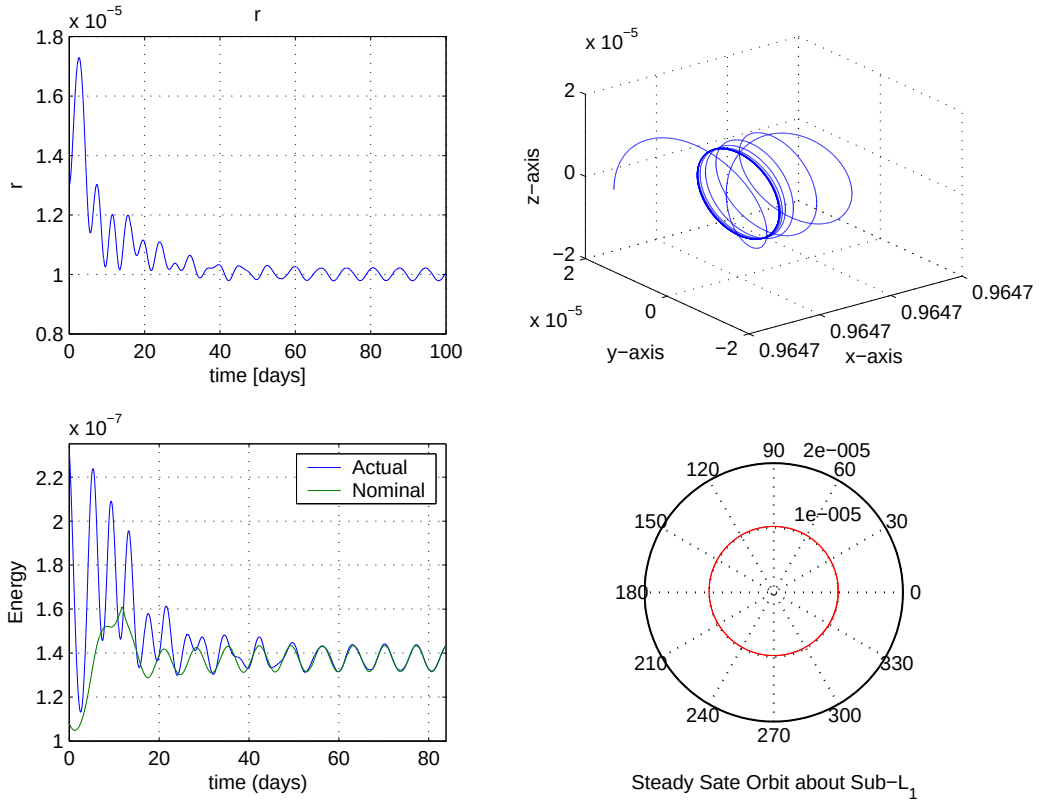

Figure 6.5: Energy Controlled Sail.

6.6 Control about a Sub-L_1 Halo Orbit

In this section the controller is modified to track a halo orbit. The point that the sail is stabilized about is not fixed, but is a moving point in the halo orbit. The controller is adapted to track this moving point along the reference trajectory by including information of the velocity of the moving point at any time along the trajectory. The velocity of the moving point along the x-axis is used to stabilized the

sail at the correct velocity while its x location is being tracked. The velocities of the moving point, $\dot{y}_r$ and $\dot{z}_r$, along the y and z axes are used to obtain the kinetic energy of the moving point E_r for controlling the orbiting radius along the trajectory. It is assumed that the coupling between x-dynamics and y or z dynamics are small and hence are neglected. With this assumption, the modified version of the controller in Eq. (6.48) for a moving point is:

$$\alpha = \alpha_1 + c_1(x - x_r(t)) + c_2(\dot{x} - \dot{x}_r(t)), \tag{6.55}$$

where $x_r(t)$ and $\dot{x}_r(t)$ are the reference position and reference velocity along the x-coordinate at time t, respectively.

Figure 6.6 depicts the geometry of a sail around a trajectory in the yz-plane. The modified controller given in Eq. (6.53) for this situation is:

$$\overline{\delta} = \delta - \theta - \delta_u, \tag{6.56}$$

where

$$\tan\delta = \frac{z - z_r}{y - y_r}, \tag{6.57}$$

$$\tan\theta = \frac{z}{y}, \tag{6.58}$$

$$\sin\delta_u = \frac{E_r - E_0}{k_2 r_0}. \tag{6.59}$$

Note that when this controller is applied to a fixed equilibrium point it reduces to the controller developed in the previous section. For an equilibrium point y_r and z_r are zero, hence δ and θ are the same. Also the velocity of the equilibrium point is zero, thus its kinetic energy, E_r, is also zero.

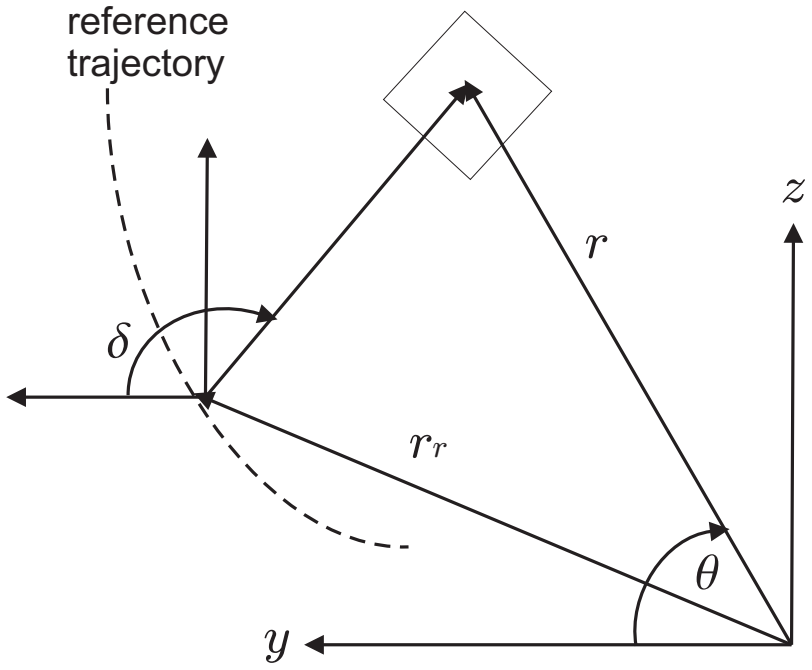

Figure 6.6: Sail about a General Trajectory.

The results are applied to a halo orbit, generated as discussed in section 6.3, about a sub-L_1 point and the results are shown in Figures 6.7- 6.8. Figure 6.7 shows how the controlled sail is orbiting a moving point in the halo orbit. Figure 6.8 shows the halo orbit and the sail actual trajectory about it. The period of the sail orbit relative to the moving point is of approximately 15.9 hrs. This shows proof of concept for the approach, but additional studies are needed.

6.7 Sail Propulsive Model Estimation

Our whole approach is predicated on the possibility that the sail propulsive model being used in the sail controller differs from some ideal propulsive model. However, initially only an estimate of the propulsive sail model may be known rather than the actual propulsive model. If the estimated propulsive model is not too far off from the actual model, then the controller will still work, but it may not settle into the required position but shift into a new equilibrium instead. Specifically, the x-

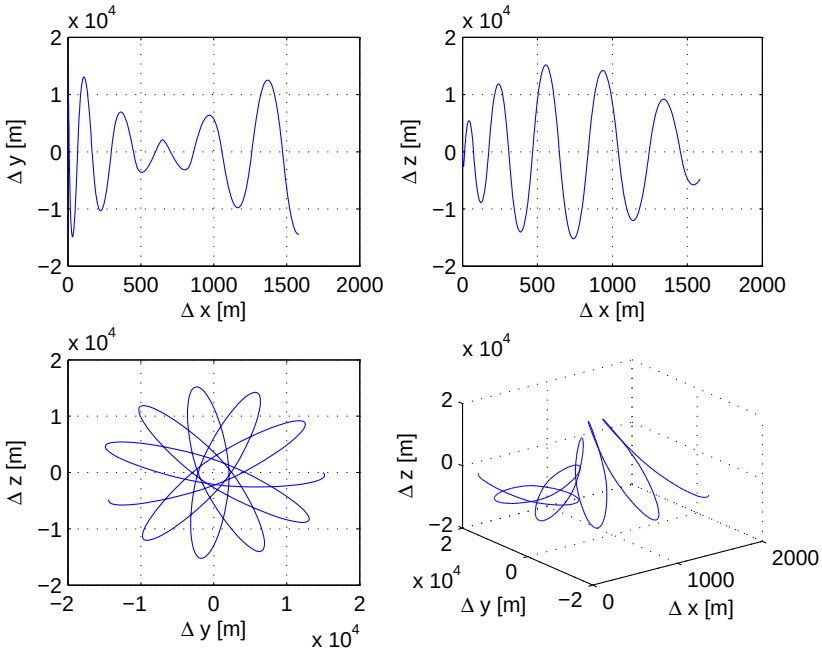

Figure 6.7: Relative sail orbit with respect to moving point on halo orbit. Time of propagation is 3.65 days.

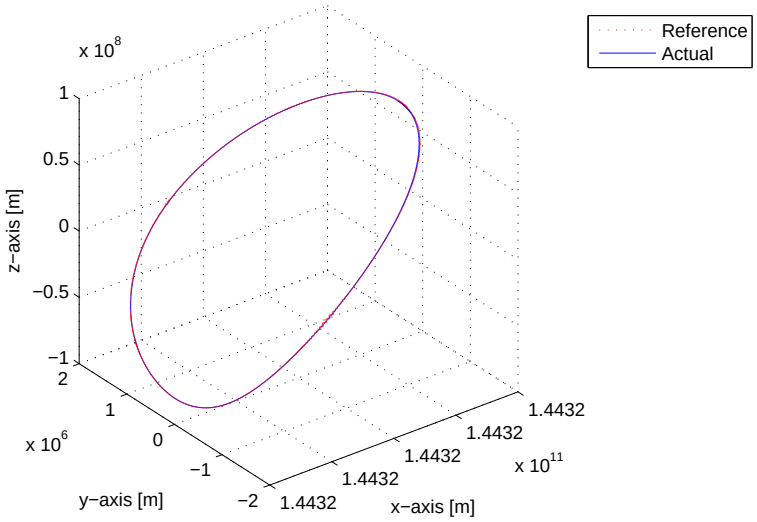

Figure 6.8: Controlled sail about Halo Orbit about sub-L_1 point.

position will be affected by the uncertainty in the propulsive model. For simplicity, it is assumed that the sail is desired to be stationed at a sub-L_1 point using the above methodology. Using the difference between the new equilibrium and the required sub-L_1 point it is possible to refine the estimate of the propulsive model. For achieving this, a formalism for updating the propulsive parameters can be obtained from the control laws. The objective is to find the sensitivity of changes in the x-equilibrium with respect to changes in the propulsive model, which for the ideal sail is the k parameter. This sensitivity can be written as:

$$\frac{\partial x}{\partial k} = \frac{\partial x}{\partial \alpha}\frac{\partial \alpha}{\partial k}, \tag{6.60}$$

each of the partial derivatives in the right-hand side of the equation can be computed from the control laws, Eqs. (6.48)-(6.49). Note that α is time varying, nonetheless, an average value can be used to approximate the partial derivative. Thus, from the average value of α in Eq. (6.49), the partial derivative of $\overline{\alpha}$ with respect to k is

$$\begin{aligned}\frac{\partial \overline{\alpha}}{\partial k} &= -\left[x_{L_1} - \frac{(1-\mu)(x_{L_1}+\mu)}{|\mathbf{r}_1(x_{L_1})|^3} - \frac{\mu}{|\mathbf{r}_2(x_{L_1})|^3}(x_{L_1}\right. \\ &+ \left.\mu - 1)\right]\frac{|\mathbf{r}_1(x_{L_1})|^2}{\beta(1-\mu)} \cdot \frac{1}{k^2 3\cos^2\overline{\alpha}\sin\overline{\alpha}},\end{aligned} \tag{6.61}$$

the other partial derivative, obtained from Eq. (6.48), is simply

$$\frac{\partial x}{\partial \overline{\alpha}} = \frac{1}{c_1}. \tag{6.62}$$

Thus, once the sail settles into a constant or nearly constant distance from the sun along the x-direction, the difference between the current and desired position can be used to update k through:

$$\Delta k \approx \frac{\Delta x}{\partial x/\partial k}. \tag{6.63}$$

Several iterations are in general necessary before converging into the the actual value of k. This current approach shows the feasibility of an estimation method and is not optimal in general.

Figure 6.9 shows the application of this idea to two cases. In the first case the controller assumes a $k = 1.1$ while the actual is 1.05 and the sail is starts behind the sub-L_1 point at a distance of 2×10^{-5}, in the normalized units. In the second case the actual k is 1.15 and the controller is initialized with $k = 1.1$ with the sail initially located at the same distance as the first case but sunward of the sub-L_1 point. In both of these cases, the controller tries to stabilize the sail x-position. When the controller senses that it is converging to a different x-location, it uses this information to update k. After 120 days, $k = 1.0493$ and $k = 1.1506$ for the first and second cases, respectively.

The estimation can also be done with the second PD-controller presented and shown by the simulation in figure 6.10. The same two above cases for the implementation of the adaptive controller were used. The sail was placed at distance of 2×10^{-5}, in the normalized units, sunward and behind of x_{L_1}. During the simulation, the k parameter is estimated to a value close to the actual, however, since the sail x-position does not settle into a constant value, the estimation is not perfect and the k parameter does not converge exactly. Despite this, the sail is driven close to the desired location with this control implementation.

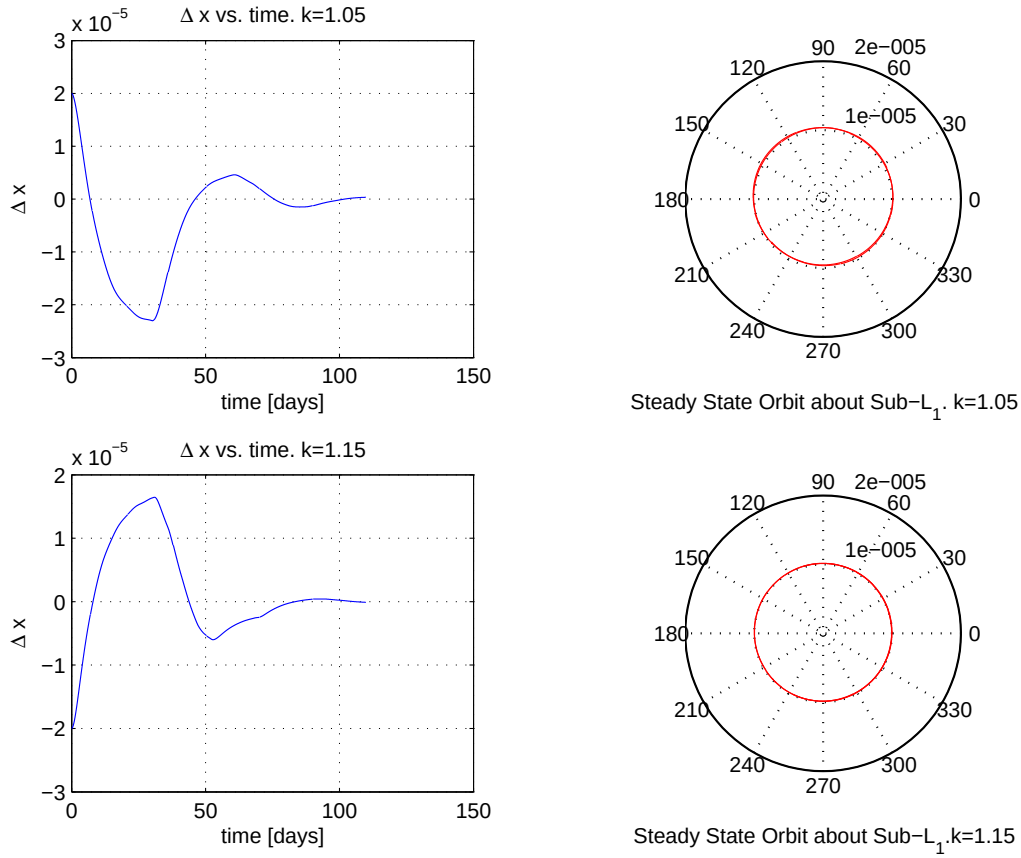

Figure 6.9: Adaptive controller.

6.8 Sail Control Under Degradation

The sail membrane will suffer from degradation due to solar radiation and the space environment [20]. The membrane degradation will result in a loss of propulsion forces acting on the sail. In order to maintain the sail orbiting the sub-L_1 point this effect must be accounted for in E_0. It is possible to keep a constant radius about the equilibrium, however, this control law would fail when the force acting on the sail becomes insufficient for maintaining the x-position of the equilibrium. A better approach is to make the radius decrease as the sail degrades. Hence, the sail will eventually settle into the sub-L_1 point when the sail performance degrades to its minimum at $\beta' = \beta$. For such approach, the required energy satisfies:

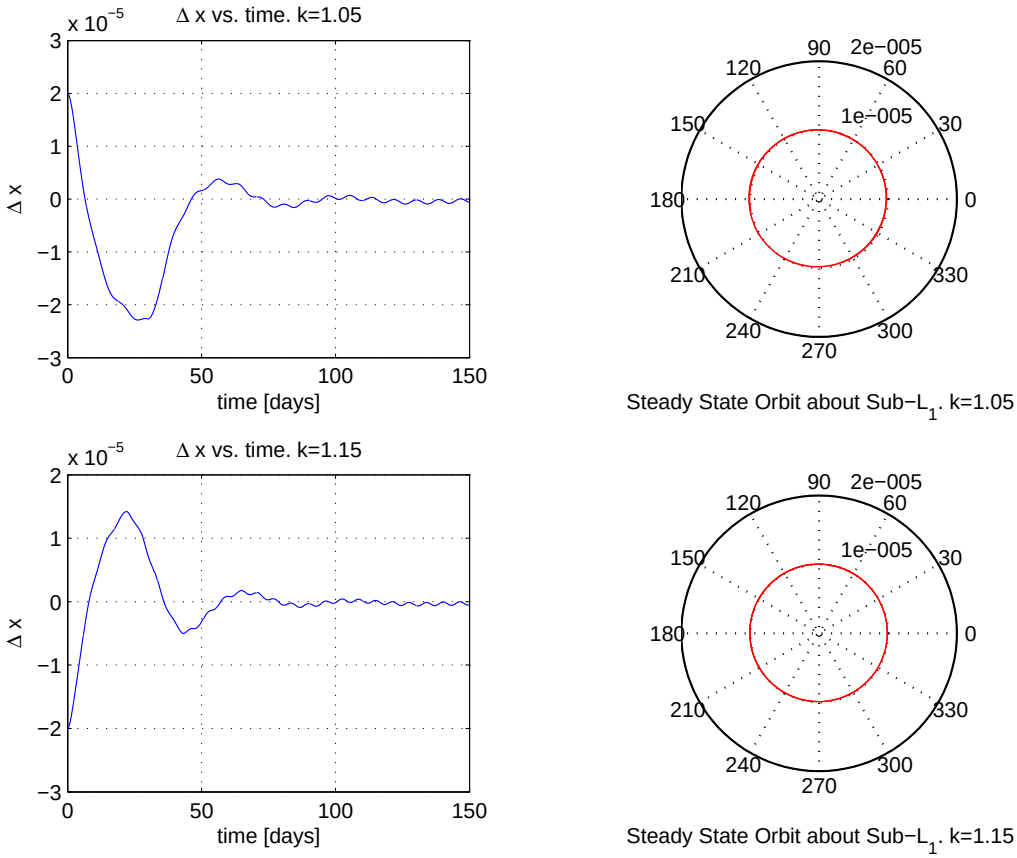

Figure 6.10: Adaptive controller for the simple PD-Controller.

$$E_0 = \frac{1}{2} r_d^2 \dot{\theta}^2 = \frac{1}{2} r_{d0}^2 k^2 \dot{\theta}^2, \tag{6.64}$$

where k is a function of time, and the orbit radius satisfies $r_d(k(0)) = r_{do}$ (the initial value of the orbit radius) and $r_d(1) = 0$. It is possible to choose how r_d changes with degradation. For instance, if r_d varies linearly with k, then:

$$E_0 = \frac{1}{2} \left(\frac{k(t) - 1}{k(0) - 1} \right)^2 r_{d0}^2 \dot{\theta}^2, \tag{6.65}$$

where $k(t)$ is the value of k at time t, and $k(0)$ is the initial value of k. When $k = 1$, the sail radius is zero and the sail is at the sub-L_1 point at which the reference energy

is zero. When $k(t) < 1$, the sail force is not sufficient to keep it at the equilibrium and a mission redesign must occur. Figure 6.11 shows a simulation of a solar sail under degradation. The sail was initially positioned sunward of the equilibrium. The controller stabilized the sail at the required x-position and the radius was decreased as the sail surface degraded.

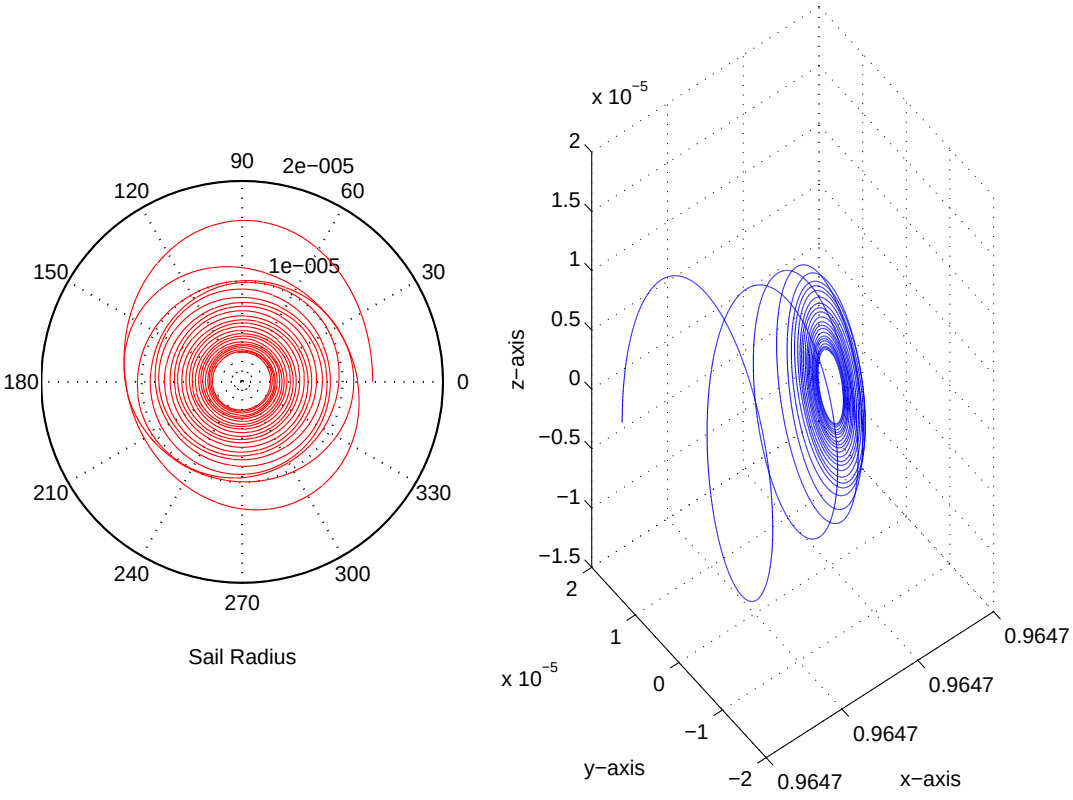

Figure 6.11: Solar sail under degradation.

A final test is now given which involves simultaneous control, estimation, and degradation of the sail. Here the sail is considered to undergo surface degradation and at the same time we try to estimate its value to be used in the controller. Initially, the sail is located 2×10^{-5} distance units sunward of the equilibrium and with a larger radius than the nominal. For simulation purposes, the sail degrades linearly with time. Initially, the actual value of β' is 0.115 or $k(0) = 1.15$. The initial estimate of k used in the controller is 1.1. After 150 days k decays to 1.0897 while the

estimated value is 1.092. Initially the sail overshoots x_{L_1}, but as the estimation of k becomes closer to the actual value the sail approaches the equilibrium's x-position while the orbiting radius is reduced as the sail propulsion decays. Figure 6.12 shows a simulation of the sail trajectory for this case.

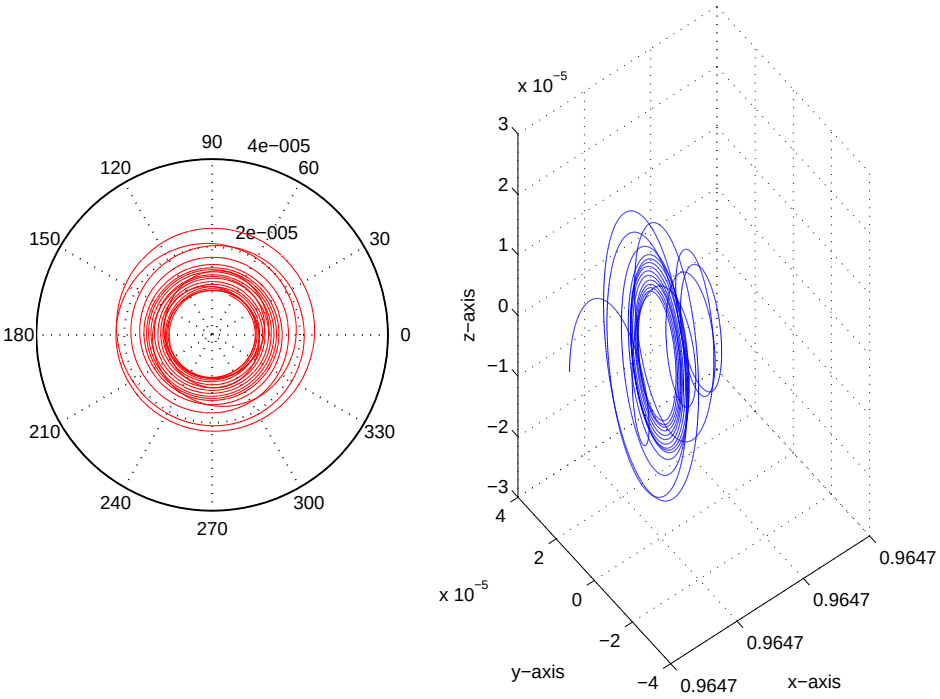

Figure 6.12: Solar Sail Under Degradation and Uncertainties.

6.9 Control Implementation

So far in our discussion, we have neglected the actual implementation of control laws in the sail environment. We now show, through explicit discussion, that our methodology can be implemented into a standard sail design.

There are two ways in which the controller can be implemented. The sail can be made to spin with an average angular velocity and use the attitude control system to modulate the angular velocity needed to follow the nominal orbit. Thus, one of the sail body fixed axis is always pointing outward from the equilibrium point. In this

case we choose the sail Y body-fixed axis to point away from the center of the sub-L_1 relative orbit. The angle α is controlled by exerting moments about the sail X-axis while δ is controlled by rotating the about sun-sail line. Another option is to change the sail attitude at every point in the orbit without exerting any moments about the sail normal axis. For this approach, α and δ are effected by a combination of moments about the sail X and Y body-fixed axes. Both of these approaches control the angle α and δ to keep the sail in a quasi-circular orbit. In this paper we only consider the spinning case and we assumed that the sail behaves as a rigid body with moments of inertia axes coincident with the sail body-fixed axes.

The dynamics for a spinning rigid body are governed by Euler equations. Given a set of required angular velocities and their rates, the torques needed to achieved them are given by:

$$M_X = I_X\dot{\omega}_X + (I_Z - I_Y)\omega_Y\omega_Z, \tag{6.66}$$

$$M_Y = I_Y\dot{\omega}_Y + (I_X - I_Z)\omega_X\omega_Z, \tag{6.67}$$

$$M_Z = I_Z\dot{\omega}_Z + (I_Y - I_X)\omega_X\omega_Y, \tag{6.68}$$

Where M_i, I_i, and ω_i are a moment, a moment of inertia, and an angular velocity about the sail body-fixed i-axis, respectively. We assume that the sail Z-axis is coincident with the sail normal and that I_Z is the sail maximum moment of inertia. The angular velocities, in the sail body-fixed frame and with the sail Y body-fixed axis pointing outward from the sub-L_1 equilibrium point, can be obtained from the sail angle rates:

$$\omega_X = \dot{\delta}\sin\alpha, \tag{6.69}$$

$$\omega_Y = \dot{\alpha}, \tag{6.70}$$

$$\omega_Z = -\dot{\delta}\cos\alpha. \tag{6.71}$$

Recall that $\delta = \theta + \overline{\delta}$. The angular rates are obtained from the controller commands and must be in radians per second. Taking a time derivative yields

$$\dot{\omega}_X = \ddot{\delta}\sin\alpha + \dot{\delta}\dot{\alpha}\cos\alpha, \tag{6.72}$$

$$\dot{\omega}_Y = \ddot{\alpha}, \tag{6.73}$$

$$\dot{\omega}_Z = -\ddot{\delta}\cos\alpha - \dot{\delta}\dot{\alpha}\sin\alpha. \tag{6.74}$$

For a general sail, the moments needed are:

$$M_X = I_X(\ddot{\delta}\sin\alpha + \dot{\delta}\dot{\alpha}\cos\alpha) - (I_Z - I_Y)\dot{\alpha}\dot{\delta}\cos\alpha, \tag{6.75}$$

$$M_Y = I_Y\ddot{\alpha} - (I_X - I_Z)\dot{\delta}^2\cos\alpha\sin\alpha, \tag{6.76}$$

$$M_Y = -I_Z(\ddot{\delta}\cos\alpha - \dot{\delta}\dot{\alpha}\sin\alpha) + (I_Y - I_X)\dot{\alpha}\dot{\delta}\sin\alpha. \tag{6.77}$$

These are the moments that need to be supplied to the sail by the attitude control system in order to follow the control commands. The moments can be generated by having control vanes [34], movable sail quadrants, or any other type of attitude control [34, 35]. Figure 6.13 shows the moments required to maintain the sail for the Solar Polar Imager mission (SPI) [36] in a circular orbit about a sub-L_1 point. The mass of the sail is 450 kg and its principal moments of inertia are 321490 kg m^2, 321490 kg m^2, and 642876 kg m^2, along the X, Y, and Z axes[36], respectively.

For a sun-sail-line angle α that is almost constant, such as is the case of the last PD-controller developed, it can be assumed that $\ddot{\alpha} = 0$ and $\dot{\alpha} = 0$. Then, the control torques needed for the spinning the sail simplify to:

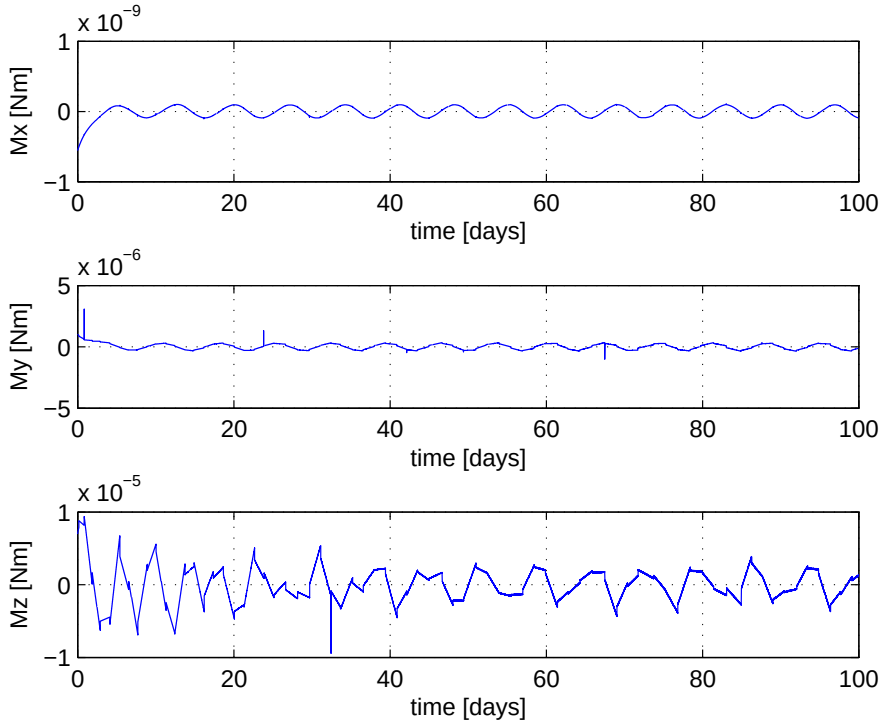

Figure 6.13: Control moments required for station-keeping SPI sail.

$$M_X = I_X \ddot{\delta} \sin\alpha, \tag{6.78}$$

$$M_Y = -(I_X - I_Z)\dot{\delta}^2 \cos\alpha \sin\alpha, \tag{6.79}$$

$$M_Z = -I_Z \ddot{\delta} \cos\alpha. \tag{6.80}$$

When the sail reaches steady-state $\ddot{\delta} \to 0$ and $\dot{\delta} \to$ constant. Thus the steady state moments are:

$$M_X = 0, \tag{6.81}$$

$$M_Y \approx constant, \tag{6.82}$$

$$M_Z = 0. \tag{6.83}$$

Thus, the long term control of the sail attitude is effected by applying a constant

torque about the sail y-axis, which point away from the orbit center. Specific implementation of such control laws are not considered in this paper, but can be found in References [34, 35] and [22].

CHAPTER VII

Conclusions

This dissertation studies the modeling of solar sails of arbitrary shape, the estimation of force and moment coefficients based on navigation data, and trajectory control. The goal is to develop an analytic methodology to capture all the features present in a solar sail surface to accurately describe the force and moment generated by the sail as they are highly dependent in the sail shape. Having a precise analytic model of a solar sail is advantageous over a finite element model as the first can be easily incorporated in existing navigation tools. We achieve this objective by deriving the generalized solar sail model (GSM), which captures the force and moment acting on a solar sail of general shape using a series of tensors defined as surface integrals. Once the GSM is defined, it is used to compare the performance of different sail geometries. Also, since both the force and moment acting on a solar sail are linear in the GSM coefficients, the GSM is used to develop a linear-estimation algorithm from navigation or tested data. Then, robust control laws are developed using the ideal sail model. These control laws are used to station a solar sail at a sub-L_1 point or to track a halo orbit in the vicinity of a sub-L_1 point. Detailed results and future topics of research are given in the following sections.

7.1 Main Results in this Dissertation

In Chapter II, the dynamics of both the restricted two-body problem and the circular restricted three-body problem were presented. Then, a brief derivation of the models for the sun's solar radiation pressure were given, which is the source of the force and moments experienced by the sail. Next, the classical flat solar sail models were presented for the ideal and non-ideal cases. The flat sail models are useful during initial mission design studies, however, a more precise model is necessary for a final mission trajectory and actual sail navigation.

In Chapter III, an analytic model for solar sails of arbitrary shape is developed. Equations for the force and moment are derived in terms of tensors, which are independent of the sail attitude. Thus, the resulting equations can be used in all orientations of the sail. With the force and moment defined, it is shown how the center of pressure can be calculated. It is shown that solar sails with symmetries in their geometries require fewer coefficients for capturing the force and moment. The number of independent parameters needed depends on the type of symmetry.

In Chapter IV, applications of the GSM to several examples are presented. Four sails with different geometries are presented. It is shown how the force and moment tensor are computed for each of these sails once their specific shape is defined. Then, the force and moment generated by these sails are compared and their differences are pointed out. Also, first and second order force partial derivatives are presented. The analytic nature of the GSM equations allows the derivation of partial derivatives, which are required in optimization algorithms and in other studies. It is also shown that the GSM equations can be used in previous studies where the flat sail models had been used before. Specifically, a guidance law and attitude for maximum propulsive

force are developed for a square, billow sail. Finally, NASA's S5 project is discussed, as well as how the GSM equations form a central part in this software package.

In Chapter V, an estimation algorithm for the GSM force and moment coefficients is developed. The force and moment equations are linear in the tensors coefficients, which are manipulated into a product of a matrix and vector to facilitate the estimation. It is shown that the accuracy of the estimation results is dependent on the attitudes at which the measurements are taken. Several attitude samplings are discussed and their effect on the covariances of the estimates is also discussed. The simulated data used in the estimation examples are generated with a sinusoid sail.

In Chapter VI, the solar sail ideal flat model is used to develop control laws to station a sail about a sub-L_1 point or to track a neighboring halo orbit. The equations of motion of the circular restricted three-body problem and the equations for the sail propulsion are transformed into cylindrical coordinates to develop the controllers. Control of the sail location along the x-axis and control of the sail orbit about the equilibrium point require two independent controllers. A linear feedback controller and a proportional-derivative controller are developed to control the sail distance from the sun. An energy-based feedback controller is presented to control the sail orbit about the chosen equilibrium point. These controllers are modified to place the sail about a halo orbit. A simple adaptive control technique is used to estimate the sail performance when the sail optical parameters degrade.

The results presented in this dissertation open a new way of modeling and flying solar sails. Modeling forces and moments on solar sails are no longer restricted to simple analytical sail models or finite-element models. The generalized sail model introduces a new way of modeling solar sails and estimating parameters from navigation data. Excess thrust controllers allow the tracking of nominal trajectories for

sail with higher performance that the mission requires.

7.2 Future Research

Several of the topics presented in this dissertation can be expanded, and should be studied further in the future. A list of topics include:

1. Analysis of sail shapes varying with solar sail attitude.

   In this dissertation, the generalized sail model equations were developed under the assumption that the sail shape remains constant with sail attitude. It is known that the sail shape is dependent on the sail attitude, however, no data exists on the magnitude of the deformations. Also, due to the lightweight and extended sail structure the sail may have oscillating modes that will affect the sail shape. Further studies should be made when more data on this is available.

2. Studies of the effect of sail self-shadowing on sail performance.

   Another assumption in this dissertation is that all of the sail surface is illuminated all the time. A situation that may invalidate this assumption are billowed sails at high α angles. Another more common situation is when the sail attitude control system uses an articulated boom with a mass to change the sail center of mass and generate a torque. When the boom is moved to change the center of mass, part of the sail will have a shadow over it. Also, the shadow cast on the sail surface will be time varying.

3. Refinement of the trajectory control laws.

   In this dissertation several controllers were developed using the ideal flat sail model. However, GSM allows to obtain more accurate control laws, which take into account the sail shape. Further research on developing controller using

GSM should be performed. Also, the control laws developed for tracking a halo orbit require further studies to achieve a reasonable rotation rate about the moving point in the halo orbit.

APPENDIX A

S5 MATLAB SOLAR RADIATION PRESSURE

The following Matlab® code was used in the development of the the Solar Radiation Pressure module of the S5 project. The main program that calculates the total force and moment acting on a solar sail, due to the sail itself and control vanes, is first presented. Then, the auxiliary subroutines necessary are also presented.

A.1 Force and Moment

```
function [F,T]=srp(psi,q,r1,flag)
global a2 a3 rho s
%Reading Sail Properties load prop.dat
%Sail Parameters
%Optical Parameters
rho=prop(1); %Reflectivity
s=prop(2); %Fraction of specular Reflection
Bf=prop(3); %Front Surf. Non-Lambertian Coefficient
Bb=prop(4); %Back Surf. Non-Lambertian Coefficient
emb=prop(5); %Back Emissivity
emf=prop(6); %Front Emissivity
```

```
As=prop(7); %Sail Area [m2̂]
va=prop(8); %Vane Area
momarm=prop(9); %Moment Arm
a2=Bf*(1-s)*rho+(1-rho)*(emf*Bf-emb*Bb)/(emf+emb);
a3=1-rho*s;
% Loading sail GSM Force and Moment Tensors
load coefs06.mat
%Matrix Transformation
%Inertial To Body-Fixed Frame
R=quaternion(q); % Subroutine
% Solar Pressure
r=norm(r1);
P=solp(r);
r0=R*r1/r;
% Location of Vanes CP in Body-Fixed Frame
arm=momarm*[1 0 -1 0; 0 1 0 -1; 0 0 0 0];
if flag <= 2
%Coordinates of Vane Normal Vectors
%in Sail Body-Fixed Frame
Rv=vanenorm(psi); % Subroutine
%Calling localcoord m-file for
%Calculation of normal and tangential vectors
[n,t]=localcoord(R,r1,Rv); % Subroutine
for i=1:5
%Calculation of Normal-to-Sun-Line angle
```

```
%for sail and control vanes
alpha(i)=acos(-dot(n(:,i)',r1)/r);
%Forces on sail
%Force: Normal Component
if (i==1)
A=As;
else
A=va;
end
%Force: Normal Component
Fn(i)=-P*A*((1+rho*s)*(cos(alpha(i)))^2+Bf*(1-s)*rho*cos(alpha(i))+
(1-rho)*(emf*Bf-emb*Bb)/(emf+emb)*cos(alpha(i)));
%Force: Tangential Component
Ft(i)=P*A*(1-rho*s)*cos(alpha(i))*sin(alpha(i));
%Resultant Force in Inertial Frame. Force in Newtons
fm(:,i)=Fn(i)*n(:,i)+Ft(i)*t(:,i);
end
%Total Force in Inertial frame
Fbf=R*fm;
if flag == 1
F=sum(fm')';
elseif flag == 2
%Forces in Sail-Body-Fixed
F=sum(Fbf')';
end
```

```
%Calculation of torques
for i=1:4
k=1+i;
tor(:,i)=cross(arm(:,i),
Fbf(:,k));
end
T=sum(tor')';
elseif flag >=3
f1=-a3*dot(J1,r0)*r0;
f2=a2*dr2(J2,r0);
f3=-2*rho*s*dr3d(J3,r0);
F1=P*(f1+f2+f3);
[Fv, Mv]=FTvanes(psi,r0); % Subroutine
Fv=P*Fv; F2=sum(Fv')';
Fbf=F1+F2;
if flag==3
F=R'*Fbf;
elseif flag==4
F=Fbf;
end
%Calculation of Sail Internal Torque
m1=a2*dr2(K2,r0);
m2=-2*rho*s*dr3d(K3,r0);
m3=-a3*cross(dr2b(L,r0),r0);
M=P*(m1+m2+m3);
```

```
Mv=P*sum(Mv')';
for i=1:4
tor(:,i)=cross(arm(:,i),
Fv(:,i));
end
T1=sum(tor')';
T=M+Mv+T1;
end
```

A.2 Vanes Normal Vectors in the Sail-Body Fixed Frame

```
function vnor= vanenorm (psi)
% This routine uses the vane defection angles ,psi, with respect
% to the sail to calculate the normal vector of each vane for the
% case of a flat vanes.
zva=[0 0 1];
%Rotation about X. Vane 1
R1=[1 0 0; 0 cos(psi(1)) sin(psi(1)); 0 -sin(psi(1)) cos(psi(1))]'*zva;
%Rotation about Y. Vane 2
R2=[cos(psi(2)) 0 -sin(psi(2)); 0 1 0; sin(psi(2)) 0 cos(psi(2))]'*zva;
%Rotation about X. Vane 3
R3=[1 0 0; 0 cos(-psi(3)) sin(-psi(3)); 0 -sin(-psi(3)) cos(-psi(3))]'*zva;
%Rotation about Y. Vane 4
R4=[cos(-psi(4)) 0 -sin(-psi(4)); 0 1 0; sin(-psi(4)) 0 cos(-psi(4))]'*zva;
vnor=[R1 R2 R3 R4];
```

A.3 Force and Moment due to Control Vanes

```
function [Fv, Mv]=FTvanes(psi,r0)
%This File computes the force and moment
%for each of the sail vanes given their angular
% deflection with respect to the sail, which is in terms
%in the vector psi=[psi(1), psi(2), psi(3), psi(4)]
global a2 a3 rho s
load coefv06.mat
%Rotation about X. Vane 1
R1=[1 0 0; 0 cos(psi(1)) sin(psi(1)); 0 -sin(psi(1)) cos(psi(1))];
%Rotation about Y. Vane 2
R2=[cos(psi(2)) 0 -sin(psi(2)); 0 1 0; sin(psi(2)) 0 cos(psi(2))];
%Rotation about X. Vane 3
R3=[1 0 0; 0 cos(-psi(3)) sin(-psi(3)); 0 -sin(-psi(3)) cos(-psi(3))];
%Rotation about Y. Vane 4
R4=[cos(-psi(4)) 0 -sin(-psi(4)); 0 1 0; sin(-psi(4)) 0 cos(-psi(4))];
for i=1:4
%Rotation about Z-BFF axis to account
%for vane-sail axis alignments
ang=(i-2)*pi/2;
Rz=[cos(ang) sin(ang) 0 -sin(ang) cos(ang) 0 0 0 1];
if i==1
%Force and Torque on Vane 1
rv1=Rz*R1*r0;
```

```
fv1=-a3*dot(Jv1,rv1)*rv1;

fv2=a2*dr2(Jv2,rv1);

fv3=-2*rho*s*dr3d(Jv3,rv1);

Fv1vff=fv1+fv2+fv3;

Fv1=R1'*Rz'*Fv1vff;

mv1=a2*dr2(Kv2,r0);

mv2=-2*rho*s*dr3d(Kv3,r0);

mv3=-a3*cross(dr2b(Lv,r0),r0);

Mv1vff=(mv1+mv2+mv3);

Mv1=R1'*Rz'*Mv1vff;

elseif i==2

%Force and Torque on Vane 2

rv2=Rz*R2*r0;

fv1=-a3*dot(Jv1,rv2)*rv2;

fv2=a2*dr2(Jv2,rv2);

fv3=-2*rho*s*dr3d(Jv3,rv2);

Fv2vff=fv1+fv2+fv3;

Fv2=R2'*Rz'*Fv2vff;

mv1=a2*dr2(Kv2,r0);

mv2=-2*rho*s*dr3d(Kv3,r0);

mv3=-a3*cross(dr2b(Lv,r0),r0);

Mv2vff=(mv1+mv2+mv3);

Mv2=R2'*Rz'*Mv2vff;

elseif i==3

%Force and Torque on Vane 3
```

```
rv3=Rz*R3*r0;
fv1=-a3*dot(Jv1,rv3)*rv3;
fv2=a2*dr2(Jv2,rv3);
fv3=-2*rho*s*dr3d(Jv3,rv3);
Fv3vff=fv1+fv2+fv3;
Fv3=R3'*Rz'*Fv3vff;
mv1=a2*dr2(Kv2,r0);
mv2=-2*rho*s*dr3d(Kv3,r0);
mv3=-a3*cross(dr2b(Lv,r0),r0);
Mv3vff=(mv1+mv2+mv3);;
Mv3=R1'*Rz'*Mv3vff;
elseif i==4
%Force on Vane 1
rv4=Rz*R4*r0;
fv1=-a3*dot(Jv1,rv4)*rv4;
fv2=a2*dr2(Jv2,rv4);
fv3=-2*rho*s*dr3d(Jv3,rv4);
Fv4vff=fv1+fv2+fv3;
Fv4=R4'*Rz'*Fv4vff;
mv1=a2*dr2(Kv2,r0);
mv2=-2*rho*s*dr3d(Kv3,r0);
mv3=-a3*cross(dr2b(Lv,r0),r0);
Mv4vff=(mv1+mv2+mv3);;
Mv4=R1'*Rz'*Mv4vff;
end
```

```
end
%Total force produced by vanes
Fv=[Fv1 Fv2 Fv3 Fv4];
%Total moment produced by vanes
Mv=[Mv1 Mv2 Mv3 Mv4];
```

A.4 Normal and Transverse Vectors

```
function [n,t] = localcoord(R,r,Rv)
% This file computes the sail normal and transverse
% vectors given a rotation matrix R that transforms
% the sail inertial coordinates into a body-fixed, the
% sail position vector r, and the the matrix Rv, which contains
% the the vanes' normal vectors
n1=[R(3,1) R(3,2) R(3,3)]';
R2=R'*Rv; n2=[n1 R2];
r1=r/norm(r);
%Computing Tangential vector in Inertial Coordinates
for i=1:5
n(:,i)=n2(:,i)/norm(n2(:,i));
om1=cross(n(:,i)',r1);
if (norm(om1)==0)
t(:,i)=[1 0 0]';
else om=om1/norm(om1);
t(:,i)=cross(om,n(:,i))';
end
```

```
end
```

A.5 Sail Attitude

```
function [R] = quaternion(q)
% This code take the sail attitude information in quaternion
% and returns a a rotation matrix R from inertial to sail
% body fixed coordinates
q0=[q(1); q(2); q(3)];
S=[0 -q(3) q(2); q(3) 0 -q(1); -q(2) q(1) 0];
%Transformation of quaternion to inertial-to-body-fixed
%Rotation Matrix
R=(q(4)^2-q0'*q0)*eye(3)+2.*q0*q0'-2.*q(4)*S;
```

A.6 Solar Radiation Pressure

```
function p= solp(r)
% This program computes the sun's solar radiation
% pressure , p, at a distance r form the sun
%Reading Physical Constants
load physconst.dat
%Natural Parameters
Rs=physconst(1); %Sun Radius (m)
Io=physconst(2); %Sun's Specific Intensity (W/m^2)
c=physconst(3); %Speed of Light (m/s)
% Solar Pressure
%Takes into account Solar disk
```

```
Fr=2/3.*(r/Rs).^2.*(1-(1-(Rs./r).^2).^(3/2));

Pr=1/c*Io*pi.*(Rs./r).^2;

p=Pr.*Fr;
```

BIBLIOGRAPHY

[1] H. Baoyin and C.R. McInnes. Solar sail halo orbits at the sun-earth artificial l_1 point. *Celestial Mechanics and Dymanical Astronomy*, 2006(94):155–171, 2006.

[2] B. Dachwald. Optimal solar-sail trajectories for missions to the outer solar system. *Journal of Guidance, Control, and Dynamics*, 28(6):1187–1193, 2005.

[3] B. Dachwald. Solar sail trajectory optimization for intercepting, impacting, and deflecting near-earth asteroids. In *AIAA Guidance, Navigation, and Control Conference and Exhibit*, August 15-18, 2005. San Francisco, CA.

[4] J.M.A. Danby. *Fundamentals of Celestial Mechanics*. Willmann-Bell, Inc., Richmond, VA, 1992.

[5] B. Derbes and D. Lichodziejewski. Sail coordinate systems and format for reporting propulsive perfomance. In *The 14th AAS/AIAA Space Flight Mechanics Meeting*, February 8-12, 2004. Maui, Hawaii.

[6] B. Derbes and G. Veal. Team encounter solar sails. In *The 45th AIAA/ASME/ASCE/AHS/ASC Structures, Structural Dynamics and Materials Conference*, April 19-22, 2004. Palm Springs, California.

[7] J. Ellis, Lisano M., P. Wolff, J. Evans, J. Bladt, D.J. Scheeres, L. Rios-Reyes, and D. Lawrence. A solar sail integrated simulation toolkit. In *The 14th AAS/AIAA Space Flight Mechanics Meeting*, February 8-12, 2004. Maui, Hawaii.

[8] C. Garner and M. Leipold. Developments and activities in solar sail propulsion. In *36th AIAA/ASME/SAE/ASEE Joint Propulsion Conference and Exhibit*, July 16-19, 2000. Huntsville, Alabama.

[9] V.M. Gotlib, et. al. Cosmos 1: The worlds first solar sail spacecraft. In *The 14th AAS/AIAA Space Flight Mechanics Meeting*, February 8-12, 2004. Maui, Hawaii.

[10] D.T. Greenwood. *Principles of Dynamics*. Prentice Hall, New Jersey, 1988.

[11] R.J. Hale. *Introduction to Space Flight*. Prentice Hall, New Jersey, 1994.

[12] A.F. Heaton. Solar sail gnc model comparisons. In *AIAA Guidance, Navigation, and Control Conference and Exhibit*, 2004. Providence, Rhode Island.

[13] K.R. Koch. *Parameter Estimation and hypothesis Testing in Linear Models*. Springer, New York, 1999.

[14] R.E. Larson, R.P. Hostetler, and B.H. Edwards. *Calculus with Analytic Geometry*.

[15] D.A. Lawrence and S.W. Piggott. Integrated trajectory and attitude control for a four-vane solar sail. In *AIAA Guidance, Navigation, and Control Conference and Exhibit*, August 15-18, 2005. San Francisco, CA.

[16] D.A. Lawrence and S.W. Piggott. Solar sail trajectory control for sub-l1 station-keeping. In *AIAA Guidance, Navigation, and Control Conference and Exhibit*, August 16-19, 2004. Providence, RI.

[17] D. Lichodziejewski, B. Derbes, K. Belvin, K. Slade, and T. Mann. Development and ground testing of a compactly stowed scalable inflatably deployed solar sail. In *The 45th AIAA/ASME/ASCE/AHS/ASC Structures, Structural Dynamics and Materials Conference*, April 19-22, 2004. Palm Springs, California.

[18] D. Lichodziejewski, B. Derbes, K. Slade, and T. Mann. Vacuum deployment and testing of a 4-quadrant scalable inflatable rigidizable solar sail system. In *The 46th AIAA/ASME/ASCE/AHS/ASC Structures, Structural Dynamics and Materials Conference*, April 18-21, 2005. Austin, Texas.

[19] M. Lisano, D. Lawrence, and S. Piggot. Solar sail transfer trajectory design and stationkeeping control for missions to the sub-l1 equilibrium region. In *15th AAS/AIAA Space Flight Mechanics Meeting*, January 23-27, 2005. Copper Mountain, Colorado.

[20] F. Lura and D. Hagelschuer. Experiments in the test facility kobe for the investigation of degradation effects of thin foil samples for a solar sail mission concerning the simultaneous influence of space environment properties. In *22nd Space Simulation Conference*, 2002. Ellicott City, MD.

[21] C.R. McInnes. *Solar Sailing: Technology, Dynamics and Mission Applications*. Springer-Praxis, Chichester, UK, 1999.

[22] E. Mettler and Ploen S.R. Solar sail dynamics and control using a boom mounted bus articulated by a bi-state two-axis gimbal and reaction wheels. In *AIAA/AAS Astyrodynamics Specialist Conference and Exhibit*, 5-8 August 2002. Monterrey, California.

[23] J.R. Meyer-Arendt. *Introduction to Classical and Modern Optics*. Prentice Hall, New Jersey, 1989.

[24] O.M. Mori, Y. Tsuda, M. Shida, and J. Kawaguchi. Dynamic and static deployment motions of spin type solar sail. In *The 18th International Symposium on Space Flight Dynamics*, October 11-15, 2004. Munich, Germany.

[25] D.M. Murphy and B.D. Macy. Demonstration of a 10-m solar sail system. In *The 45th AIAA/ASME/ASCE/AHS/ASC Structures, Structural Dynamics and Materials Conference*, April 19-22, 2004. Palm Springs, California.

[26] L. Rios-Reyes and D.J. Scheeres. Applications of the generalized model for solar sails. In *AIAA Guidance, Navigation, and Control Conference and Exhibit*, 2004. Providence, Rhode Island.

[27] L. Rios-Reyes and D.J. Scheeres. Generalized model for solar sails. *Journal of Spacecraft and Rockets*, 42(1):182–285, 2005.

[28] L. Rios-Reyes and D.J. Scheeres. Robust solar sail trajectory control for large pre-launch modeling errors. In *AIAA Guidance, Navigation, and Control Conference*, August 15-18, 2005. San Francisco, CA.

[29] L. Rios-Reyes and D.J. Scheeres. Generalized models for solar sails. In *The 14th AAS/AIAA Space Flight Mechanics Meeting*, February 8-12, 2004. Maui, Hawaii.

[30] L. Rios-Reyes and D.J. Scheeres. Solar sail navigation: Estimation of force, moment, and optical parameters. In *The 16th AAS/AIAA Space Flight Mechanics Meeting*, January 22-26, 2006. Tampa, FL.

[31] L. Rios-Reyes and D.J. Scheeres. Solar sail navigation with the generalized sail model. In *The 15th Workshop on JAXA Astrodynamics and Flight Mechanics,*, July 25-26, 2005. ISAS/Jaxa, Japan.

[32] D.N. Sharma and D.J. Scheeres. Solar system escape trajectories using solar sails. *Journal of Spacecraft and Rockets*, 41(4):684–687, 2004.

[33] S. Takeuchi. Deployment experiment result of solar sail using sounding rocket. In *55th International Astronautical Congress of the International Astronautical Federation, the International Academy of Astronautics, and the International Institute of Space Law*, October 4-8, 2004. Vancouver, Canada.

[34] B. Wie. Solar sail attitude control and dynamics, part 1. *Journal of Guidance, Control, and Dynamics*, 27(4):526–535, 2004.

[35] B. Wie. Solar sail attitude control and dynamics, part 2. *Journal of Guidance, Control, and Dynamics*, 27(4):536–544, 2004.

[36] B. Wie and D. Murphy. Propellantless aocs design for a 160-m, 450-kg sailcraft of the solar polar imager mission. In *41st AIAA Joint Propulsion Conference*, July 10-13, 2005. Tucson, AZ.

[37] J.L. Wright. *Space Sailing*. Gordon and Breach Science Publishers, Philadelphia, Pennsylvania, 1992.

[38] J.L. Wright and J. Warmke. Solar sail mission applications. In *AIAA/ASS Astrodynamics Conference*, August 18-20, 1976. San Diego, CA.